RHENIUM(I) TRICARBONYL SCHIFF BASE COMPLEXES: A MECHANISTIC STUDY

by

MAMPOTSO SELINA TSOSANE

A dissertation submitted to meet the requirements for the degree of

MAGISTER SCIENTIAE

in the

DEPARTMENT OF CHEMISTRY

FACULTY OF NATURAL AND AGRICULTURAL SCIENCES

at the

UNIVERSITY OF THE FREE STATE

SUPERVISOR : Dr. ALICE BRINK

CO-SUPERVISOR : Prof. HENDRIK G. VISSER

Prof. ANDREAS ROODT

June 2016

ACKNOWLEDGEMENTS

Above all, I would like to humble myself and thank GOD Almighty for the love, mercy, support, strength and wisdom. My very existence is owed to you, Lord. Heavenly Father, thank you for everything I am and have. I never would have made if it wasn't for your love and mercy. Thank you.

An infinite amount of gratitude is extended to Prof. Andreas Roodt for the opportunity, you believed in me when no one did. I thank you from the deepest part of heart. Thank you for your wisdom and always having a big smile on your face. Thank you for sending me to Switzerland as part of my research. May God's love and mercy be with you always. Thank you.

I thank all my supervisors, Dr. Alice Brink (fantastic supervisor) and Prof. Hendrik G. Visser, for your amazing assistance towards my research. Thank you for encouragement and always making time for me. Thank you.

A humble gratitude is extended to Prof. Roger Alberto of the University of Zürich, Switzerland. Thank you for sharing your knowledge with me. I am truly honoured to have met such an intelligent and highly extinguished scientist. Thank you for making my two-month visit to your facility possible and amazing. Thank you for allowing me to work in your group with such intelligent scientists. I would like to thank Angelo Frei, Dr. Hendrik Braband, Dr. Micheal Benz and the lovely secretary Ramona. Thank you.

If it wasn't for Dr. Nicola Bernard, I never would have persuaded my masters. Thank you for inspiring me and the opportunity by allowing me to work for you as your assistant in your research. I would like to thank Renier, Carla, Tom and Pennie for your assistance towards crystal data collection, kinetic data collection, Schlenk experiments and the laughter. Thank you.

Acknowledgements

To my loved ones and family, Nthakoana Julia Tsosane and Motlalentoa Joseph Tsosane (my parents), thank you for your support. Especially my mother, you didn't have much but the little that you had you gave me with an open heart. I thank you so much for your strength and love. To my fiancé (Tshepo) and beloved twins lost in the miscarriage, thank you for giving me strength, I LOVE YOU. Thank you.

To my mother:

"Love is patient, love is kind. It always protects, always trusts,

always hopes, always perseveres and love never fails."

1 Cor 13:4-8.

"Apply your heart to instruction and your ears to words of knowledge"

TABLE OF CONTENTS

ABBREVIATIONS

5Me-Sal-Cyhex	5-methyl-(2-cyclohexyliminomethyl)phenol
PET	Positron emission tomography
SPECT	Single-photon emission computed tomography
NMR	Nuclear magnetic resonance
IR	Infra-red
UV-Vis	Ultravoilet visible
XRD	X-ray diffraction
fac	Facial
L,L'-bid	Bidentate ligand with *L,L'* donor atoms
BAM	Biologically active molecule
BBB	Blood brain barrier
HMPAO	Hexamethylpropyleneamineoxime
BATO	Boronic adducts of technetium oxime
MIBI	Methoxyisobutylisocyanide
dmpe	1,2-bis(dimethylphosphino)ethane
MDP	Methylenediphosphonate
HMDP	Hydroxymethylenediphosphonate
CNS	Central nervous system
BFCA	Bifunctional chelating agent
DMSA	Dimercaptosuccinic acid
MAG_3	Mercaptoacetylglycylglycylglycine
NOBIN	1-amino-1'-hydroxylbinaphthyl
HIV	Human immunodeficiency virus

Abbreviations

AIDS	Acquired immune deficiency virus
HPLC	High performance liquid chromatography
DCM	Dichloromethane
MeOH	Methanol
TBA	Tetra(*n*-butyl)ammonium
THF	Tetrahydrofuran
MeCN	Acetonitrile
Cyhex	Cyhexyl
CD_3OD	Deuterated methanol
$CDCl_3$	Deuterated chloroform
TMS	Tetramethylsilane
Z	Number of molecules in a unit cell
Å	Angstrom
ppm	Parts per million
υ_{CO}	C = O stretching frequency on IR
π	Pi
α	Alpha
β^-	Beta
β^+	Positron
γ	Gamma
λ	Wavelength
σ	Sigma
θ	Theta
^{o}	Degrees
$R^{\neq}$	Activated transition state
keV	Kilo electron volts
MeV	Mega electron volts

Abbreviations

ΔH	Enthalpy of activation
ΔS	Entropy of activation
CO	Carbonyl group
k_{obs}	Observed pseudo first-order rate constant
h	Planck's constant
k_B	Boltzmann's constant
k_1	Rate constant for forward reaction
k_{-1}	Rate constant for reverse reaction
K_1	Equilibrium constant

ABSTRACT

Both technetium and rhenium have been studied extensively over the years, due to their ability to coordinate with mono- and bidentate ligands to form metal(I) tricarbonyl complexes, *fac*-[$M(CO)_3(X)(L,L'\text{-Bid})$] (M = Tc(I) and Re(I), L,L'-bid = bidentate ligand and X = MeOH, H_2O or Br). The interest in these complexes is based on the diagnostic properties of technetium and therapeutic properties of rhenium in the study of radiopharmaceuticals. These complexes possess characteristics that can be utilized for the application in nuclear medicine.

The aim of this study was based on the study of the chemistry of technetium and rhenium to gain more information about their ability to coordinate with potential ligands such as Schiff base ligands. From this, a Schiff base ligand such as 5-methyl-(2-cyclohexyliminomethyl)phenol – 5Me-Sal-Cyhex was synthesized and characterized. This was successfully coordinated to *fac*-$[M(CO)_3]^+$ core to form metal(I) tricarbonyl complexes.

The synthesis and characterization of the *N,O*-bidentate ligand or Schiff base ligand and all metal complexes are reported in Chapter 3. All rhenium products obtained were characterized by UV/Vis, NMR (^1H and ^{13}C) and IR.

The rhenium complexes, *fac*-$[Re(CO)_3(X)(N,O\text{-Bid})]$, were synthesized with variety of monodentate ligands (X = MeOH, imidazole, pyridine and pyrazole) coordinated on the sixth position. Three crystal structures of 5-methyl-(2-cyclohexyliminomethyl)phenol – 5Me-Sal-Cyhex, *fac*-$[Re(CO)_3(MeOH)(5Me\text{-}Sal\text{-}Cyhex)]$ and *fac*-$[Re(CO)_3(Imid)(5Me\text{-}Sal\text{-}Cyhex)]$ were obtained from the characterization performed by X-ray diffraction. These complexes crystallised in the orthorhombic and monoclinic crystal systems in the respective space groups of $P2_12_12_1$, $C2/c$ and $P2_1/n$.

Technetium(I)-99 tricarbonyl complexes, *fac*-$[^{99}Tc(CO)_3(MeOH)(5Me\text{-}Sal\text{-}Cyhex)]$ and *fac*-$[^{99}Tc(CO)_3(MeCN)(5Me\text{-}Sal\text{-}Cyhex)]$ were synthesized and characterized by HPLC to determine the reaction completion and chemical similarity between rhenium and radioactive technetium-99.

A kinetic investigation was performed on the formation reaction between 5Me-Sal-Cyhex and $[NEt_4]_2[Re(CO)_3(Br)_3]$. It was observed that the formation reaction would unsuccessfully

be determined due to the small absorbance changes over time. A model *N,N'*-bidentate ligand system (ethylenediamine) was therefore selected to study the formation reaction. The UV/Vis analysis showed two reactions that occur during the formation reaction between ethylenediamine and ReAA. Since the first fast reaction has the half-life, $t_{1/2}$ = <5 seconds, the stopped flow kinetic investigation is required. The second slow formation reaction between ethylenediamine and ReAA was monitored at 14.8^{o}C, 25.2^{o}C, 35.0^{o}C and 45.0^{o}C. Rate constants and activation parameters ($\Delta H^{\neq}$ = 28 ± 0.05 kJ mol^{-1} and $\Delta S^{\neq}$ = -188 ± 0.17 J K^{-1} mol^{-1}) of the formation reaction between ethylenediamine and $[NEt_4]_2[Re(CO)_3(Br)_3]$ were obtained. The negative $\Delta S^{\neq}$ value is indicative of an associative-type mechanism.

In addition to the above UV/Vis study, ^{1}H NMR analysis was performed which confirmed the mechanistic and kinetic observations of the reaction between ethylenediamine and ReAA that forms in over 13 hour period. From the ^{1}H NMR investigation, it was observed that the formation reaction between ethylenediamine and ReAA occurs via two reactions, defined as a first fast and second slow reaction.

OPSOMMING

Beide tegnesium en renium is breedvoerig oor die jare bestudeer as gevolg van hulle vermoë om met mono- en bidentate ligande te koördineer om metaal(I) trikarbonielkomplekse, *fac*-[$M(CO)_3(X)(L,L'\text{-Bid})$] (M = Tc(I) en Re(I), L,L'-bid = bidentate ligand en X = MeOH, H_2O of Br^-), te vorm. Die belangstelling in hierdie komplekse is gebaseer op die diagnostiese eienskappe van tegnesium en terapeutiese eienskappe van renium in die bestudering van kerngenees middels. Hierdie komplekse beskik oor eienskappe wat gebruik kan word in die toepassing van kerngeneeskunde.

Die doel van hierdie ondersoek is gegrond op die bestudering van die chemie van tegnesium en renium ten einde meer inligting in te win oor hulle vermoë om met potensiële ligande soos Schiff-basis te koördineer. Vir hierdie projek is 'n Schiff-basis ligand, 5-metiel-(2-sikloheksieliminometiel)fenol – 5Me-Sal-Cyhex (5Me-Sal-Siheks) – vervaardig en gekarakteriseer. Dit is suksesvol aan die *fac*-$[M(CO)_3]^+$ entiteit gekoördineer om metaal(I) trikarboniel komplekse te vorm.

Die sintese en karakterisering van die *N,O*-bidentate ligand, of Schiff-basis, asook alle metaalkomplekse word in die studie gerappoteer. Alle gesintetiseerde renium produkte is met behulp van UV/Vis, KMR (^1H en ^{13}C) en IR spektroskopie gekarakteriseer.

Die reniumkomplekse, *fac*-$[Re(CO)_3(X)(N,O\text{-Bid})]$, is gesintetiseer met 'n verskeidenheid monodentate ligande (X = MeOH, imidasool, piridien en pirasool) in die sesde posisie gekoördineer. Drie kristalstrukture van 5-metiel-(2-sikloheksieliminometiel)fenol – 5Me-Sal-Cyhex, *fas*-$[Re(CO)_3(MeOH)(5Me\text{-}Sal\text{-}Cyhex)]$ en *fas*-$[Re(CO)_3(Imid)(5Me\text{-}Sal\text{-}Cyhex)]$ is gekaratireseer deur middel van X-straal diffraksie. Hierdie komplekse het in die ortorombiese en monokliniese kristalstelsels gekristalliseer, in die ruimtegroepe $P2_12_12_1$, $C2/c$ en $P2_1/n$, onderskeidelik.

Tegnesium(I)-99 trikarboniel komplekse, *fas*-$[^{99}Tc(CO)_3(MeOH)(5Me\text{-}Sal\text{-}Cyhex)]$ en *fas*-$[^{99}Tc(CO)_3(MeCN)(5Me\text{-}Sal\text{-}Cyhex)]$ is gesintetiseer en gekarakteriseer deur middel van hoëdrukvloeistofchromatografie (HDVC) om die verloop van die reaksie en chemiese ooreenkomste tussen renium en radioaktiewe tegnesium-99 te bepaal.

Opsomming

`n Kinetiese ondersoek is uitgevoer op die vormingsreaksie tussen 5Me-Sal-Siheks en $[NEt_4]_2[Re(CO)_3(Br)_3]$; dit is waargeneem dat die vasstelling van die vormingsreaksie onsuksesvol was danksy die klein verandering in absorbansie oor tyd. `n Model *N,N'*-bidentate ligandstelsel (etileendiamien) is dus gekies om die vormingsreaksie te bestudeer. Die UV/Vis analise het aangedui dat twee reaksies plaasvind gedurende die vormingsreaksie tussen etileendiamien en ReAA. Aangesien die eerste, vinnige reaksie `n halfleeftyd van $t_{1/2}$ < 5 sekondes het, was die gestopte vloei kinetiese ondersoek genoodsaak. Die tweede, stadige vormingsreaksie tussen etileendiamien en ReAA is by 14.8^{o}C, 25.2^{o}C, 35.0^{o}C en 45.0^{o}C gemonitor. Tempokonstantes en aktiveringsparameters ($\Delta H^{\neq}$ = 28 ± 0.05 kJ mol^{-1} en $\Delta S^{\neq}$ = -188 ± 0.17 J K^{-1} mol^{-1}) van die vormingsreaksie tussen etileendiamien en $[NEt_4]_2[Re(CO)_3(Br)_3]$ is verkry. Die negatiewe waarde vir $\Delta S^{\neq}$ is aanduidend van `n assosiatiewe tipe meganisme.

Bykomend tot die bogenoemde UV/Vis studie is `n $^{1}$H KMR analise uitgevoer wat die meganistiese en kinetiese waarnemings van die reaksie tussen etileendiamien en ReAA, wat oor `n 13 uur tydperk vorm, bevestig het. Uit die ^{1}H KMR ondersoek blyk dit dat die vormingsreaksie tussen etileendiamien en ReAA plaasvind deur twee reaksies, gedefinieer as `n vinnige eerste, en tweede stadige reaksie.

1 INTRODUCTION AND AIM

1.1 INTRODUCTION

Radiopharmaceuticals are drugs that contain radionuclides or radioactive isotopes and are used in nuclear medicine for diagnostic and / or therapeutic applications. Several metals are utilised in the development of radiopharmaceuticals and they are selected depending on the proposed medical applications. For diagnostic application, ^{99m}Tc, ^{111}In, $^{62/64}$Cu and $^{67/68}$Ga are preferred.[1] Particularly, technetium and rhenium, are investigated in this study to better describe the production of radiopharmaceuticals. Technetium is used as a diagnostic imaging agent for brain, kidney, bone, heart and liver, while rhenium is used as a therapeutic agent. It is also often used as a model for technetium due to its similar chemical properties and non-radioactive isotope. Technetium is an element of atomic number of 43 and it possesses rich coordination chemistry.[2] It has several nuclides to consider, however the two nuclides, ^{99}Tc, and its metastable nuclear isomer, ^{99m}Tc, are extensively investigated.

Technetium is produced as a major fission product in the nuclear reactor, where the fission yield of ^{99}Tc is approximately 6.1%, i.e 2.5 g of ^{99}Tc per day from the 100 MeV nuclear reactor. ^{99}Tc is a long-lived isotope with half-life of 2.12 x 10^5 years and it is a β^- emitter without γ-radiation. The metastable nuclear isomer of ^{99}Tc, ^{99m}Tc ($t_{1/2}$ = 6.02 h, 100% γ, IT, E_{max} = 140 KeV), is the radionuclide which is utilised in diagnostic imaging since it possess physical properties that are almost ideal for nuclear medicine.[3]

Rhenium is an extremely rare element of atomic number of 75 and it possesses extensive coordination chemistry. Rhenium occurs naturally as a mixture two isotopes, ^{185}Re (37.40%) and ^{187}Re (62.60%).[4] It also consists of two isotopes used in the development of radiopharmaceuticals, namely ^{186}Re and ^{188}Re. The beta decay of ^{188}W (half-life = 69 days), in a generator system (^{186}W (2n, γ) ^{188}W (β^-) $\longrightarrow$ ^{188}Re), produce the β^- emitter ^{188}Re. ^{188}Re can also be obtained with relatively high specific activity by direct production in a nuclear

[1] S. Liu, D.S. Edwards, *Top Curr. Chem.*, 2002, **222**, 259.
[2] T, Parera, P.A. Marzilli, F.R. Fronczek, L.G. Marzilli, *Inorg. Chem.*, 2010, **49**, 2123.
[3] S. Jurrison, D. Berning, W. Jia, D. Ma, *Chem. Rev.*, 1993, **93**, 1137.
[4] G. Rouschians, *Chem. Rev.*, 1974, **74**, 531.

reactor with the radiation of enriched ^{187}Re. The isotope, ^{188}Re, has half-life of 16.9 hours and E_{max} = 2.1 MeV.[4,5] This isotope has favourable properties since it can be obtained by utilizing the generator system, ^{188}W/^{188}Re. Another isotope of rhenium is ^{186}Re ($t_{1/2}$ = 89 h, E_{max} = 1.1 MeV) and also a β^- emitter that decays to stable ^{186}Os.[4,5] ^{186}Re is not easily obtained from a generator system and can be directly produced in a nuclear reactor. This isotope is less favourable since it is not easily synthesized.

1.2 AIM OF THIS STUDY

Radiopharmaceuticals may be developed from many transition metals such as ^{188}Re, ^{67}Cu, ^{99m}Tc, in order to produce effective drugs with high ability of delivering radiation to specific sites or infected cells. To develop such radiopharmaceuticals, many aspects and factors should be considered. [6] These factors as well as literature examples, are well described in Chapter 2. One of the primary objectives of this study is based on the synthesis and the characterization of metal(I) tricarbonyl complexes, *fac*-[M(CO)$_3$(X)(*N,O*-Bid)] (*N,O*-Bid = bidentate ligands containing *N,O* donor atoms) with focus on rhenium and technetium transition metals. This is possible due to the fact that the *fac*-[M(CO)$_3$]$^+$ core has the ability to coordinate various type of ligands. The metal(I) tricarbonyl complex, *fac*-[M(CO)$_3$(X)$_3$]$^{2-}$ (M = Tc(I) or Re(I), X = Cl, Br), can be prepared through a one-step synthesis from the oxometallates, [MOCl$_4$]$^-$ and [MO$_4$]$^-$. This complex contains halide ligands which can easily be substituted by *N,N', O,O'* or *N,O*-bidentate ligands (Bid) or solvent (X) molecules as monodentate ligands to yield *fac*-[M(CO)$_3$(X)(Bid)] type complexes.

In this study, *N,O* and *N,N'* bidentate ligands of interest were used based on the coordination of a Schiff base synthesized ligand to a metal complex. Schiff base ligands have known coordination capability to various transition metal complexes and are easy to manipulate. The characteristics of these ligand types are discussed in detail in Chapter 2.[7] This study also investigates the kinetic behaviour of the formation between the rhenium(I) tricarbonyl complex and the bidentate ligands of interest. The understanding of the mechanistic behaviour of the radiopharmaceutical formation is critical for the development of new model

[5] U. Abram, R. Alberto, *J. Braz. Chem. Soc.*, 2006, **17**, 1486.
[6] P.S. Donnelly, *Dalton Trans.*, 2011, **40**, 999.
[7] R. Alberto, R. Schibli, A. Egli, P.A. Schubiger, W.A. Herrmann, G. Artus, U. Abram, T.A. Kaden, *J. Organomet. Chem.*, 1995, **493**, 119.

complexes, as this may well affect future labelling time, efficiency and understanding. To briefly summarise, the aims of this study are listed as follows:

- The exploration of several ligand systems are conducted with primary focus on the salicylidene based *N,O* ligands systems. Ligand variations are explored and the coordination of the *N,O* ligands to rhenium and technetium tricarbonyl complexes are conducted/attempted. Ideal experimental conditions are evaluated in order to better understand formation of model complexes. Substitution of the available 6^{th} position on the tricarbonyl core is evaluated in addition to understand the reactivity of the metal complexes.
- Characterization of all the ligand and metal complexes in the solid and solution state are done with the use of methods such as ultraviolet-visible spectroscopy (UV-Vis), infrared spectroscopy (IR), nuclear magnetic resonance (NMR) (^{1}H and ^{13}C) and single crystal X-ray diffraction (XRD).
- An investigation on the mechanistic and kinetic formation of the rhenium(I) tricarbonyl complexes with particular *N,O* and *N,N'* bidentate ligand systems are undertaken. An improved understanding of the labeling parameters involved during the formation of various *fac*-$[M(CO)_3]^+$ complexes are explored.

In the following chapters, a detailed discussion of technetium and rhenium chemistry and its impact in the development and study of radiopharmaceuticals will be described in Chapter 2, followed by the experimental synthetic and spectroscopic results in Chapter 3. The solid state characterization as described using single crystal X-ray diffraction is discussed in Chapter 4. Finally, the mechanistic investigation of the formation of particular *fac*-$[M(CO)_3]^+$ complexes are explored in Chapter 5.

2 THEORETICAL STUDY

2.1 INTRODUCTION

Nuclear medicine is a medical interest of study that is used to diagnose and treat diseases.[1] Early detection of a disease allows treatment to commence sooner, thereby improving prognosis. In particular, nuclear medicine can be used to diagnose various kinds of diseases such as cancer and can be used to determine normal functionality of certain organs in the patient's body. For instance, it has been used to determine if the heart is an adequate pump of blood by monitoring blood volume of the patient. Further examples of the usefulness of nuclear medicine include the testing of functionality of brain cells, lungs and kidneys.[1]

Cancer is one of the most dangerous diseases worldwide that has the potential to gradually increase with age and growth of the world's population. According to American Cancer Society, an estimation performed by World Research Fund revealed that up to one-third of the cancer cases occur in economically developed countries like the US. These cancer cases are related to obesity, physical inactivity or poor nutrition.[2] In 2015, approximately 1 658 370 new cancer cases were expected to be diagnosed. The American Cancer Society estimated cancer cases in the US in 2015 are as follows; lung and bronchus (13% in women and 14% in men), breast (29% in women), prostate (26% in men) and colon and rectum (8% in both genders). The most common cancer types responsible for death were: lung (1.6 million, 19.4% of the total), liver (0.8 million, 9.1%) and stomach (0.7 million, 8.8%).[3]

CANSA (Cancer Association of South Africa) estimated that 23.4% of women are diagnosed with pregnancy-associated breast cancer and 19.2% of women not pregnant are diagnosed.[4] Statistics indicate that breast cancer in women is the most common cancer disease diagnosed.

---

[1] H.A. Ziessman, J.P. O'Malley, J.H. Thrall, *Nuclear Medicine*, Eds: F.H. Fahey, Elsevier Saunders Inc., Philadelphia, USA, 2014.
[2] R.L. Siegel, K.D. Miller, A. Jemal, *CA. Cancer. J. Clin.*, 2015, **65**, 5.
[3] World Health Organization (WHO), *GLOBOCAN 2012: Cancer Facts Sheets*, International Agency for Research on Cancer. http://globocan.iarc.fr/Pages/fact_sheets_cancer.aspx. Accessed on 20-01-2015 at 12h45 pm.
[4] M.C. Herbst, *CANSA Facts Sheet on the Top Ten Cancer per Population Group*, 2009, Health Sciences and Departmant of Occupational Health, http://www.cansa.org.za/files/2015/05/Fact-Sheet-Breast-Cancer-Pregnancy-Breastfeeding-May-2015.pdf released online on April 2015 and accessed on 20-01-2015 at 13h15 pm.

These staggering statistics suggest that it is significant for researchers to develop new drugs for early detection and treatment. Hence, nuclear medicine is an important medical modality that can be used in the study and development of new radiopharmaceuticals.

2.2 NUCLEAR MEDICINE AND RADIOPHARMACEUTICALS

The term, nuclear medicine, refers to a medicine or pharmaceutical containing a small amount of radioactive material or radioisotope.[5] The combination of a pharmaceutical containing a radioisotope is typically referred to as a radiopharmaceutical. Radiopharmaceuticals are drugs containing radionuclides which are used in the nuclear medicine discipline in the diagnosis and treatment of diseases. Typical radionuclides used for diagnosis are photon emitters: gamma (γ) or positron particles (β^+), whereas for therapeutic applications particle emitters, alpha (α), beta (β) or Auger (e^-) are used. Different methods may be used to introduce a radiopharmaceutical into a patient's body which include injection and swallowing or inhalation in small quantities. Ideally, a radiopharmaceutical is designed to be absorbed in a specific area in the body where a disease or an abnormality exists. After administering the radiopharmaceutical, medical technicians must be able to detect the radioactive isotope. This can occur using techniques such as planar scintigraphy, PET (positron emission tomography) and SPECT (single-photon emission computed tomography).[5,6]

2.3 NUCLEAR MEDICINE WITH PET AND SPECT

Nuclear medicine is primarily concerned with the medical diagnostic applications for imaging metabolism and other functionalities in the human body. Nuclear medicine imaging scans uses radioactive material called radiopharmaceuticals or radiotracers (or radioactive tracers).[7] A radioactive tracer is administered to the patient before the imaging process. The advantage of this technique is that substances move to the organ systems in selective ways. These substances need to be labelled with radioactive tracers (e.g. technetium-99m) to enable imaging of the distribution of such substance into the human body with the use of gamma

[5] S. Liu, *Advanced Drug Delivery Rev.*, 2008, **60**, 1347.
[6] S.A. Zuckman, G.M. Freeman, D.E. Trouter, W.A. Volkert, R.A. Holmes, D.G. Van Derveer, E.K. Barefeld, *Inorg. Chem.*, 1981, **20**, 2386.
[7] N.B. Smith, A. Webb, *Introduction to Medical Imaging: Physics, Engineering and Clinical Applications*, Cambridge University Press, 2010, p89.

cameras or PET scanners. For this process, three modalities are utilised, namely, planar scintigraphy, PET (positron emission tomography) and SPECT (single-photon emission computed tomography).[7]

2.3.1 POSITRON EMISSION TOMOGRAPHY (PET)

PET is an imaging technique where PET radioactive isotopes usually attached to different direction moieties, are administered to a patient. PET isotopes or radionuclides are generated in a cyclotron and have short half-lives. The short half-life of a PET radionuclide allows for increased detection sensitivity over a given period of time.[8] In PET analysis, the PET isotopes produce positrons during decay and PET relies on the annihilation of positrons. Positrons emitted during decay travel a certain distance in the surrounding medium before reaching thermal energy in order to be annihilated. These positrons have sufficient energy to penetrate the human tissue. The advantage of PET imaging over SPECT is that it exhibits high sensitivity, i.e, the ability to detect and record a high percentage of the emitted events which implicate detection in PET subsection.[8,9] The sensitivity results are as follows:

- the signal-to-noise ratio is improved and thus improves image quality
- possess shorter scans,
- shorter scans allow multiple scans to be conducted of a patient from different observation angles.

The different radionuclides which may be used for PET are given in **Table 2.1**.

Table 2.1: Radionuclides used in PET analysis.[15,16,17]

Radionuclide	β^+ positron Energy (keV)	$t_{1/2}$
^{18}F	634	110 min
^{64}Cu	656	12.7 hours
^{68}Ga	1880, 770	1.1 hours
^{124}I	3160	4.17 days
^{89}Zr	897	3.27 days

[8] T.J. McCathy, S.W. Scharz, M.J. Welch, *J. Chem. Ed*., 1994, **71**, 830.
[9] A. Rahmim, H. Zaidi, *Nucl. Med. Commun.*, 2008, **29**, 193.

2.3.2 PLANAR SCINTIGRAPHY

Planar scintigraphy is the simplest technique used in imaging to provide a two-dimensional projection image of tracer activity distribution in the human body. This technique is based on gamma radiation created in the decay process of a radionuclide. In comparing SPECT and planar scintigraphy, SPECT uses three-dimensional assessment of the isotope dispersed in the patient's body, whereas planar scintigraphy uses two-dimensional assessment. Planar scintigraphy of a complex or large structures within the skeletal system does not yield an accurate three-dimensional anatomic image, whilst use of SPECT mapping allows for special localization of the pathology in the mapped organ.[10,11]

2.3.3 SINGLE-PHOTON EMISSION COMPUTED TOMOGRAPHY (SPECT)

The SPECT techniques were created on the basis of a planar imaging, which involves gamma cameras collecting or taking a series of planar shots during rotations around the patient's body. SPECT is based on the molecular tracer principle that is established as a tool used in noninvasive imaging.[9] It uses gamma cameras and collimators to create projection data that are utilized for an estimation of the dynamic 3-D tracer distributions *in vivo.* Typical SPECT radiotracers involve small molecules labelled with a gamma-emitting isotope such as ^{123}I, ^{111}In or ^{99m}Tc **(Table 2.2)**. The ^{99m}Tc radioisotope is widely used for diagnosis and considered the workhorse of nuclear medicine.[12]

Table 2.2: Radionuclides of SPECT.[15,16,17]

Radionuclide	Energy (keV)	$T_{1/2}$
^{67}Ga	93, 185, 294	3.3 days
^{99m}Tc	140	6.02 hours
^{123}I	159	13.3 hours
^{111}In	171, 245	2.8 days

From the above, PET radionuclides emit positrons during decay and SPECT radionuclides are gamma-emitting isotope. The isotropic radiation which a specific radionuclide provides, affects the imaging technique that is utilized in the process of developing a radiopharmaceutical. Other factors that should be considered when designing a

[10] A. Oron, I. Arieli, T. Pritsch, E. Evan-Sapir, N. Halperin, G. Agar, *ISRN Orthopedics*, 2013, **2013**, 1.
[11] Z. Lee, M. Ljungberg, R.F. Muzic jr, M.S. Berridge, *J. Nucl. Med.*, 2001, **42**, 1077.
[12] R. Golestani, C. Wu, R.A. Tio, C.J. Zeebregts, A.D. Petrov, F.J. Beekman, R.A.J.O. Dierckx, H.H. Boersma, R.H.J.A. Slart, *Eur. J. Nucl. Med.*, 2010, **37**, 1766.

radiopharmaceutical are related to the chemical and biological properties of the potential drug-like molecule. These factors include, amongst others, the choice and properties of the specific radionuclide, the different half-life of radionuclides, energy, type of radiation, existence of other possible radiation sources, bifunction chelators, oxidation states, solubility and stability.[12]

2.4 DEVELOPING RADIOPHARMACEUTICALS

Factors that should be considered when designing a radiopharmaceutical are, for example, the choice of a radionuclide that must be made in relation to their use in diagnostic or therapeutic purposes. Different nuclear properties of a radionuclide are required depending on the specific application. For diagnostic applications the radiation must be able to penetrate the patient's body and be detected by an instrument external to the patient. For SPECT or PET imaging, $^{62/64}$Cu, ^{111}In, $^{67/68}$Ga and ^{99m}Tc are considered. Favourably ^{64}Cu and ^{68}Ga are used in PET imaging while ^{99m}Tc is used in SPECT imaging due to its ideal nuclear properties (6 hours and γ-ray emission energy of 140 keV).[13]

The radiopharmaceuticals used as therapeutic β-emitters are ^{177}Lu, ^{90}Y and $^{186/188}$Re.[13] One of the aspects considered in developing radiopharmaceuticals is the half-life of a radionuclide. The half-life should be sufficiently long to: synthesize and develop the radiopharmaceutical; allow the transportation of the drug to the hospital; accumulate in the target tissue and be optimally cleared from non-target organs. The half-life of a radionuclide should also be short enough to minimize radiation damage to the patient without changing the administration and the quality of the radiopharmaceutical. Radionuclides with longer half-lives, i.e. from one to a few weeks are effective for tumors while radionuclides with shorter half-lives, i.e. from a few hours to a few days are used for targeting scattered cells.[14] Important radionuclides used for imaging are given in **Table 2.3** with the properties of therapeutic radionuclides indicated in **Table 2.4**.

[13] P.S. Donnelly, *Dalton Trans.*, 2011, **40**, 999.
[14] J. Carisson, E.F. Aronson, S. Hietala, T. Stigbrand, *Radiother. Oncl.*, 2003, **66**, 107.

Table 2.3: Radionuclides used for imaging.[15,16,17]

Radionuclides	Half-life	Decay Mode	γ-Gamma Ray Energy (keV)	Production
^{61}Cu	3.3 hours	β^+ (62%), EC(38%)	283, 380	Cyclotron
^{62}Cu	9.76 min	β^+ (98%), EC (2%)	2910	Generator
^{64}Cu	12.8 hours	β^+ or β^-, EC (41%)	656	Cyclotron
^{67}Ga	3.3 days	EC (100%)	93, 184, 300	Cyclotron
^{68}Ga	68 min	β^+ (89%), EC (11%)	1880, 770	Generator
^{99m}Tc	6.0 hours	IT (100%)	140	Generator
^{111}In	2.8 days	EC (100%)	171, 247	Cyclotron
^{123}I	13.2 hours	EC (100%)	159	Cyclotron
^{125}I	60 days	EC (100%)	35	Reactor

*IT = Isomeric transition, EC = electron capture, m = metastable isomer.

Table 2.4: Different properties of therapeutic radionuclides.[15,16,17]

Radionuclides	Half-life	β (MeV) or γ Energy (keV)	Maximum penetration range (mm)	Source
^{67}Cu	2.58 days	β (0.54), γ (185)	1.8	^{68}Zn (p, 2p) ^{67}Cu
^{90}Y	2.67 days	β (2.28)	12.0	^{90}Sr/^{90}Y Generator
^{153}Sm	1.95 days	β (0.8), γ (103)	3.0	^{152}Sm (n, γ) ^{153}Sm
^{177}Lu	6.7 days	β (0.497), γ (208)	1.5	^{176}Lu (n, γ) ^{177}Lu
^{166}Ho	1.1 days	β (1.8), γ (81, 1.4)	8.0	Reactor or Generator
^{186}Re	3.77 days	β (1.08), γ (131)	5.0	^{186}Re (n, γ) ^{186}Re
^{188}Re	16.95 days	β (2.13), γ (155)	11.0	^{188}W/^{188}Re Generator

The structural and chemical properties of many radionuclides, particularly ^{99m}Tc and $^{186/188}$Re which form an important part in this research, approves the administration of a radiopharmaceutical to the patient and enhances the development of therapeutic and diagnostic radiopharmaceutical. The radiopharmaceuticals designed, consist of radionuclides that may be incorporated in the final molecule with labelling techniques of radiopharmaceuticals, namely the integrated approach or otherwise the bifunctional chelator approach.[18]

[15] R.B. Firestone, *Table of Isotopes*, Eds: V.S. Shirley, S.Y.F. Chu, J. Zipkin, Wiley, New York, USA, 1996.
[16] P.A. Schubiger, A. Smith, *Pharm. Acta. Helv.*, 1995, **70**, 203.
[17] E. Brown, J. Dairiki, R.E. Doebler, A.A. Shibab-Elden, L.J. Jardine, J.K. Tuli, A.B. Byrurn, *Table of Isotopes*, 7th Edition, Eds: C.M. Lederer, V.S. Shirley, Wiley, New York, USA, 1978.
[18] S. Jurrisson, D. Berning, W. Jia, D. Ma, *Chem. Rev.*, 1993, **93**, 1137.

2.5 LABELLING METHOD OF RADIOPHARMACEUTICALS

A number of labelling methods or techniques whereby a radionuclide is introduced/attached to the directing moiety, are utilized for biomolecules. Two methods used for the development of targeting biomolecules are the *integrated approach* or *bifunctional chelator approach* which will be described in more detail in the following paragraphs.

2.5.1 INTEGRATED APPROACH

The integrated approach **(Figure 2.1)** involves the replacement of part of a known high affinity receptor ligands with a metal chelate or requisite radionuclide chelate. In this approach the radionuclide is incorporated directly into the targeting moiety. This strategy is performed ideally by not altering the size, conformation and receptor binding affinity of the initial molecule. A disadvantage of possibly decreased receptor binding affinity exists as well as the requirement for more complicated target molecules that have to be synthesized.[19]

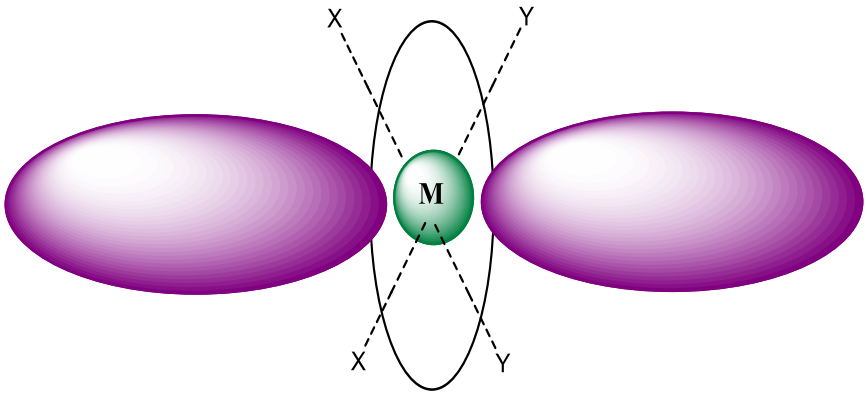

Figure 2.1: Integrated approach in a radiopharmaceutical design.[20]

[19] R.K. Hom, J.A. Katzenellenbogen, *Nucl. Med. Biol.*, 1997, **24**, 485.
[20] S. Liu, *Chem. Soc. Rev.*, 2004, **33**, 445.

2.5.2 BIFUNCTIONAL CHELATOR APPROACH

The bifunctional chelator approach **(Figure 2.2)** involves ligand systems connected to a chosen radiometal with a bifunctional chelator containing a functional group suitable for the linkage of the complex to a targeting molecule.[21] This approach uses high affinity receptor ligands as the targeting biomolecule. A linker, also known as a pharmacokinetic modifier, is used to bind chelators and targeting biomolecules. The linker also has the ability to improve lipophilicity by utilizing a hydrocarbon chain which may be important in the uptake of a new pharmaceutical.[21]

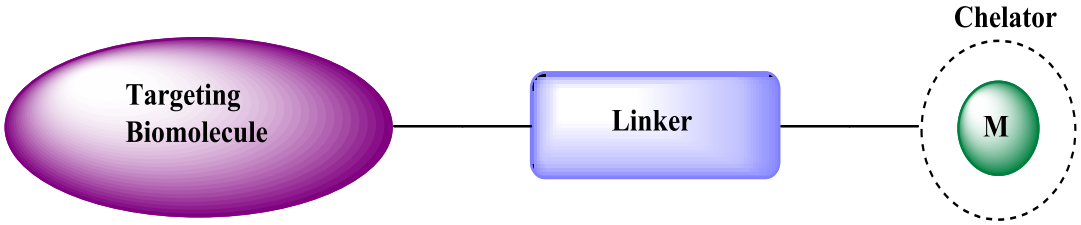

Figure 2.2: Bifunctional chelator approach in a radiopharmaceutical design.[20]

The bifunctional chelator is utilized to enhance the nature, oxidation state and stability of a radiometal.[21] Chelators containing functionality with certain varied physicochemical properties stabilizes the metal centre, particularly rhenium or technetium. Metal biomolecules often varies to substantial degree in properties, for example in dipole moment, in size and solubility from the uncoordinated biomolecule.

Certain limited ligands, also known as basic frameworks, are readily available either commercially or are reported synthetic procedures. They have the advantage of providing sufficient stability to the ^{99m}Tc core under physiological conditions. For example, tetradentate N,S,O chelators for the $[Tc(V)=O]^{3+}$ core are considered to be basic frameworks that may be used.[22,23] The [3+1] mixed ligand approaches allow smooth tuning of the ligand properties and the screening of the biological behaviour of the ligand systems. The well-known mixed ligand approach termed [3+1], by Pietzsch and co-workers contains a constant tridentate ligand linked to a biomolecule whilst the monodentate co-ligand such as water, imidazole and benzyl isocyanide is continuously changed or *vice versa*.[24] The lipophilic Tc(III) complexes which consist of umbrella-like tetradentate N,S,S,S ligands and a monodentate isocynanide

[21] M. Bartholoma, J. Valliant, K.P. Maresca, J. Babich, J. Zubieta, *Chem. Commun.*, 2009, **5**, 493.
[22] H.J. Pietzsch, A. Gupta, R. Syhre, P. Leibinitz, H. Spies, *Bioconj. Chem.*, 2001, **12**, 538.
[23] S.S. Jurrisson, J.D. Luxdon, *Chem. Rev.*, 1999, **99**, 2205.
[24] H.J. Pietzsch, H. Spies, S. Hoffmann, *Inorg. Chem. Acta.*, 1989, **165**, 163.

ligand have an excellent stability *in vitro* towards plasma components. Another kind of mixed ligand approach, the hynic approach, involve a process whereby biomolecules are linked to 6-hydrazinonicotinamide which acts as a monodentate ligand and the remaining coordination sites at the metal core are then occupied by a co-ligand such as tridentate ligands like dithiolates, HS-CH_2-CH_2-S-CH_2-CH_2-SH (SSS) as well as aza and oxa ligands (SNS and SOS).

The major advantage of the hynic approach is the variability of the co-ligands that can have an impact on the biological properties.[25,26,27] The more recent [2+1] by Mundwiler *et al.*[28], mixed ligand concept is based on *fac*-$[M(OH_2)_3(CO)_3]^+$ which showed substitution of three aqua ligands with one bidentate ligand and one monodentate ligand. A biomolecule can be linked or substituted either to the bidentate ligand ($[2_B+1]$ concept) or to the monodentate ligand ($[2+1_B]$ concept), shown in **Figure 2.3**. In the $[2_B+1]$ mixed ligand concept, the varied portion of any radiolabelled biomolecule is represented by a bidentate co-ligand.[29,30,31]

[25] H.J. Pietzsch, S. Seifert, R. Syhre, F. Tisato, F. Refosco, P. Leibinitz, H. Spies, *Bioconj. Chem.*, 2003, **14**, 136.
[26] H. Spies, M. Glaser, H.J. Pietzsch, F.E. Hahn, O. Kintzel, T. Luegger, *Angew. Chem.*, 1994, **106**, 1416.
[27] H. Spies, M. Glaser, *Inorg. Chim. Acta.*, 1995, **240**, 465.
[28] S. Mundwiler, M. Kündig, K. Ortner, R. Alberto, *Dalton Trans.*, 2004, 1320.
[29] S. Liu, D.S. Edwards, A.R. Harris, S.J. Heminway, J.A. Barrett, *Inorg. Chem.*, 1999, **38**, 1326.
[30] S. Liu, D.S. Edwards, A.R. Harris, *Bioconj. Chem.*, 1998, **9**, 583.
[31] S. Liu, D.S. Edwards, *Chem. Rev.*, 1999, **99**, 1.

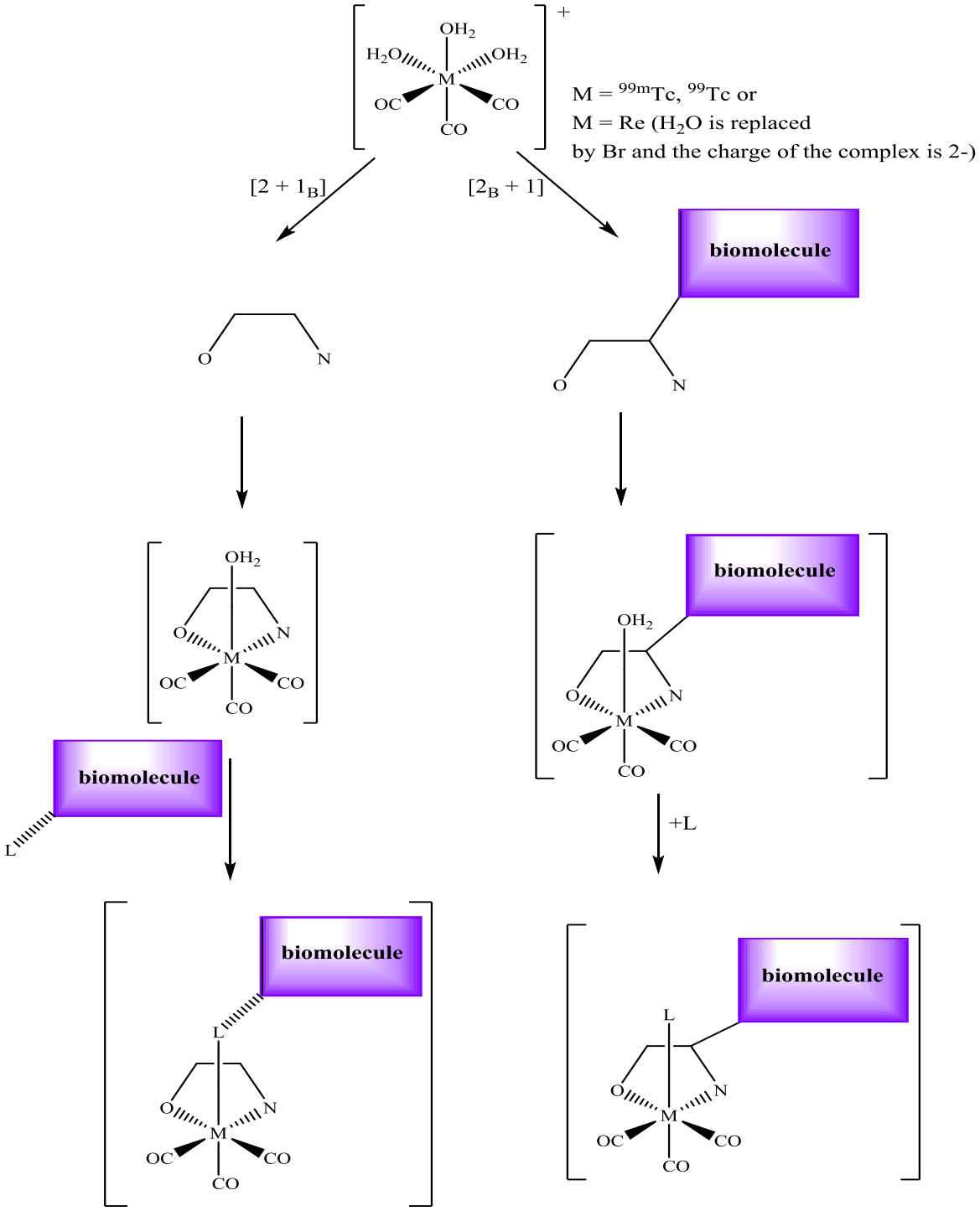

Figure 2.3: Schematic representation of the mixed ligand systems demonstrating the [2_B+1] (right) and [2+1_B] (left) concepts.[28]

The synthesis and characterization of the mixed ligand with technetium and rhenium complexes are based on the biologically active molecules originally produced. Since technetium and rhenium have good coordination ability and the complexes high stability, they were selected in this study for radiopharmaceutical design and application.

2.6 ^{99m}Tc CHEMISTRY

The element, 43, was named technetium in 1947 and discovered in 1937 by Carlo Perrier and Emilio Segré in a sample obtained from the Berkeley Radiation Laboratory, which is now called Lawrence Berkeley National Laboratory in California.[32,33] Technetium is an artificial element which can be obtained from the radioactive decay of molybdenum. The chemistry of this artificial element has been well explored despite the fact that technetium has no stable naturally occuring isotopes. Its coordination chemistry is progressively developed due to the extensive uses of technetium complexes in diagnostic applications in nuclear medicine.[34,35,36]

The ^{99}Tc nuclide is a long-lived isotope with β^- emission and a half-life of 2.12 x 10^5 years. ^{99m}Tc has been labelled the workhorse of diagnostic nuclear medicine.[37] Diagnostic nuclear medicine rely heavily on the use of ^{99m}Tc because of its nuclear properties (6.02 hours, E_γ = 140 keV), its availability from its parent, ^{99}Mo, in ^{99}Mo/^{99m}Tc generator and its relative low cost. The ^{99}Mo/^{99m}Tc generator which yields the necessary ^{99}Tc nuclide was developed in Brookhaven in the early 1960s. This consists of $[^{99}MoO_4]^-$ absorbed at the top of an alumina ion exchange column. The ^{99}Mo decay occur continuously to form ^{99m}Tc which is eluted with physiological saline (0.15 M NaCl) preferably over period of 7-10 days.[37,38]

[32] T. Parera, P. A. Marzilli, F. R. Fronczek, L. G. Marzilli, *Inorg. Chem.*, 2010, **49**, 2123.
[33] R. Alberto, *Top Curr. Chem.,* 2005, **252**, 1.
[34] C. Perrier, E. Segré, *J. Chem. Phys.*, 1937, **5**, 712.
[35] C. Perrier, E. Segré, *Nature*, 1947, **159**, 24.
[36] R. Alberto, *Comprehensive Coordination Chemistry II, Elsevier: Amsterdam,* 2004, 127.
[37] E. Segré, G.T. Seaborg, *Phys. Rev.*, 1938, **54**, 772.
[38] G. Andros, P.V. Haper, K.A. Lathrop, R.J. McCardle, *J. Clin. Endocrinol. Metab.*, 1965, **25**, 1067.

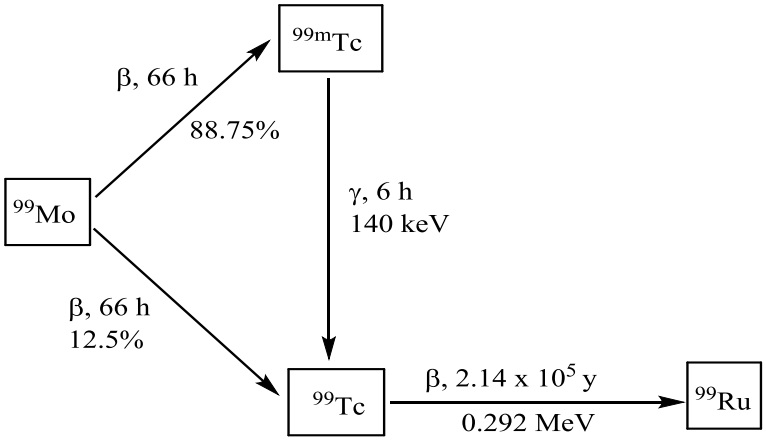

Figure 2.4: Decay sequence of ^{99m}Tc and ^{99}Tc.[39,40]

2.7 ^{99m}Tc RADIOPHARMACEUTICALS

Types of technetium imaging agents

- 1st generation Tc imaging agents **(a)** – have been used with great success to image organs such as the brain, heart, bone, liver and kidneys.
- 2nd generation Tc imaging agents **(b)** – The targeting potential lives in a biologically active molecule (BAM) covalently linked to a Tc – complex, e.g. a peptide.

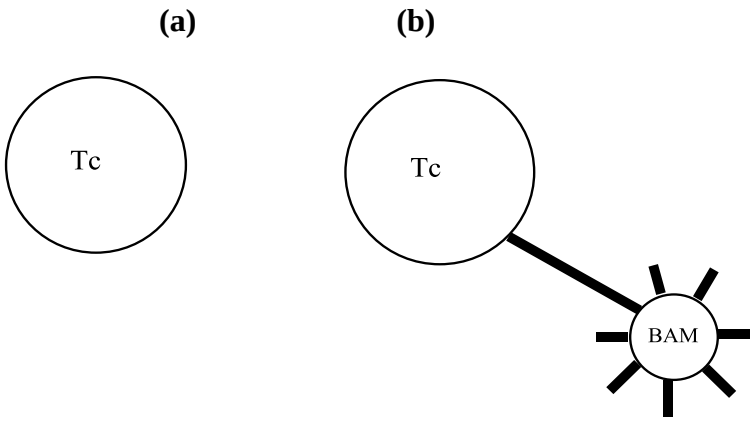

Figure 2.5: Targeting ^{99m}Tc type of imaging agents. a) 1st and b) 2nd generation.[40]

[39] U. Abram, R. Alberto, *J. Braz. Chem. Soc.*, 2006, **17**, 1486.
[40] J.R. Dilworth, S.J. Parrott, *Chem. Soc. Rev.*, 1998, **27**, 43.

2.8 FIRST GENERATION TECHNETIUM IMAGING AGENTS

The first generation Tc imaging agents were produced by the addition of permetallate before *in vitro* injection. They are typically administered to a patient in the condition depending on their physicochemical properties like the size of the complex and the charge. In 1961, the use

of technetium for imaging consisted of the use of $[^{99m}TcO_4]^-$ for the diagnosis of thyroid disfunction. This diagnosis was based on the principle that the pertechnetate anion, $[^{99m}TcO_4]^-$, has similar behaviour to iodide which is taken up by the thyroid. Many such technetium complexes were produced and lead to 'technetium essential' or the first generation Tc imaging agents.[40]

2.8.1 BRAIN IMAGING

Any agent to be used potentially on the brain must have the ability to transverse the blood-brain barrier (BBB). In order for metal complexes to be used they must possess lipophilic properties with an overall neutral charge.[40] The commercially successful Ceretec® uses the hexamethylpropyleneamineoxime (HMPAO hexametazime) ligand. The proligand, HMPAO, is coordinated to a TcO^{3+} core via four nitrogen atoms. The hydrogen bonding closes the ring of the functional oxime group and thus increases the stability of the lipophilic complex **(Figure 2.6)**. The complex, ^{99m}Tc-*d,l*-HMPAO **(Figure 2.6(a))** has been successfully used for brain perfusion imaging.[41,42,43] Its structural conformation influences the cerebral extraction and the *d,l*-isomer passes the blood-brain barrier (BBB) while the *meso*-form is excluded. However, the lipophilic *d,l*-HMPAO is transformed without any complications into a charged complex which would be unable to pass the blood-brain barrier (BBB).[44] The ethylcysteinate dimer (ECD) is a neutral, lipophilic tetradentate diaminedithiol ligand that is coordinated to a square pyramidal, Tc(V) oxo core, to form complex, ^{99m}Tc-ECD (Neurolite®) **(Figure 2.6(b))**. ^{99m}Tc-ECD also crosses the blood-brain barrier (BBB).

[41] C. K. Fair, D.E. Troutner, E.O. Schlemper, R.K. Murrmann *Acta. Cryst.,* 1984, **C40**, 1544.
[42] S. Jurisson, E.O. Schlemper, D.E. Troutner, L.R. Canning, D.P. Nowotnik, R.D. Neirinckx, *Inorg. Chem.*,1987, **25**, 3576.
[43] D.E. Troutner, W.A. Volkert, T.J. Hoffman, R.A. Holmes, *Int. J. Appl. Radiat. Isot.,* 1984, **35**, 467.
[44] P.K. Sharp, F.W. Smith, H.G. Gemmel, D. Lyall, N.T.S. Evans, D. Gvozdanovic, J. Davidson, D.A. Tyrell, R.D. Pickett, R.D. Neirinckx, *J. Nucl. Med.*, 1986, **27**, 171.

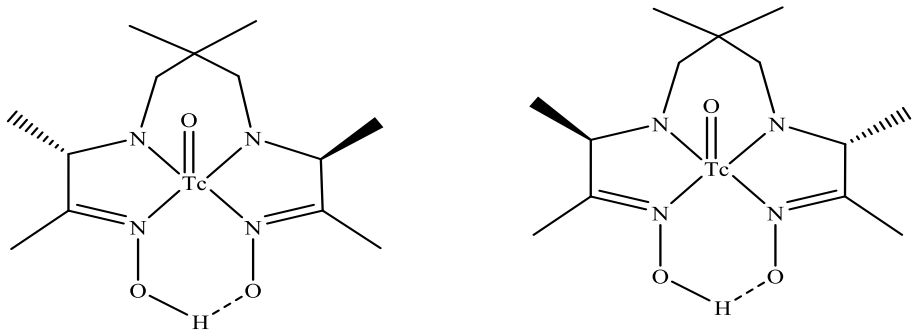

(a) ^{99m}Tc-*d,l*-HMPAO

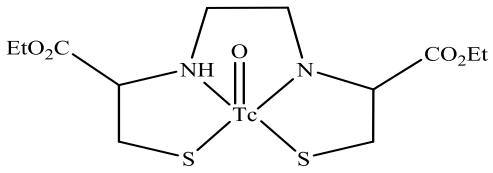

(b) ^{99m}Tc-ECD

Figure 2.6: Structure of (a) ^{99m}Tc-*d,l*-HMPAO and (b) ^{99m}Tc-ECD.[21]

2.8.2 HEART IMAGING

Many ligands like oximes are coordinated to ^{99m}Tc to describe the chemistry of technetium and how it can be utilised in medical applications. The oximes can be converted to dioximes by altering the substituents. The dioxime type ligands are considered as Schiff base bischelates and the first complexes that were described as monocapped [^{99m}Tc(dioxime)$_3$(μ-OH)SnCl$_3$] (dioxime = dimethylglyoxime) complexes consisted of oxime ligands.[45,46,47] The technenium(I) complexes with dioxime ligands are incorporated with the boronic side chain to obtain an efficient heart imaging agent. Different oximes can be used, but major structural modifications of the complex occur at the boronic side chain. The boronic adducts of technetium oxime (BATOs) complexes can be used as both myocardial and cerebral perfusion agents. ^{99m}Tc-teboroxime (Cardiotec®) **(Figure 2.7(a))** is a neutral and seven-coordinate technetium(III) complex that is used as a myocardial perfusion imaging agent. In ^{99m}Tc-teboroxime (Cardiotec®), technetium is coordinated to three N-bonded dioxime molecules and to a Cl or Br atom in the axial position forming seven covalent bonds.[48,49] The

[45] E. Deutsch, R.C. Elder, B.A. Laarge, *Proc. Natl. Acad. Sci.*, 1978, **73**, 653.
[46] G. Bandoli, U. Mazzi, A. Moresco, M. Nicolini, F. Refosco, F. Tisato, *Technetium in Chemistry and Nuclear Medicine*, 2nd Edition, Eds: M. Nicolini, G. Bandoli, U. Mazzi, Cortina International, Verona, Italy,1986, p73.
[47] E.N. Treher, L.C. Francesconi, J.Z. Gougoutas, M. Malley, A. Nunn, *Inorg. Chem.*, 1989, **28**, 3411.
[48] S. Jurrison, *Drugs of the Future*, 1990, **15**, 1085.

formation of $[^{99m}Tc(dmpe)_2Cl_2]^+$, where dmpe = 1,2-bis(dimethylphosphino)ethane is the myocardial perfusion agent, is based on the concept that lipophilic positively charged complexes would accumulate in the heart tissue *via* the Na/K ATPase mechanism as K^+ ion mimics **(Figure 2.7(b))**. When using technetium-essential reagents, technetium is the key component of the targeting vector in order to determine the structure and overall physical and chemical characteristics of a molecule, thus indicating its localization or its biological fate. A classic example of this type of technetium-essential reagent is sestamibi, $[Tc(CNR)_6]^+$ (R = $CH_2C(CH_3)_2OCH_3$). The structural characterization of this Tc(I) complex identifies ^{99m}Tc sestamibi (Cardiolite®) **(Figure 2.7(c))** as a complex with methoxyisobutyl isocyanide (MIBI) ligands which are attached symmetrically to a central Tc(I) atom. The coordination preferences of the Tc^+ cation indicate the octahedral coordination of the 2-methoxy-2-methyl isonitrile ligands to provide a highly lipophilic outer surface of the coordination sphere.[50]

[49] R. Pasqualini, A. Duatti, *J. Chem. Soc.*, 1992, **18**, 1354.
[50] F.J.Th. Wackers, D.S. Berman, J. Maddahi, D.D. Watson, G.A. Beller, H.W. Strauss, C.A. Boucher, M. Pizard, B.L. Holman, R. Fridrich, E. Inglese, B. Delaloye, A. Bischof-Delaloye, L. Camin, K. McKusick, *J. Nucl. Med.*, 1989, **30**, 301.

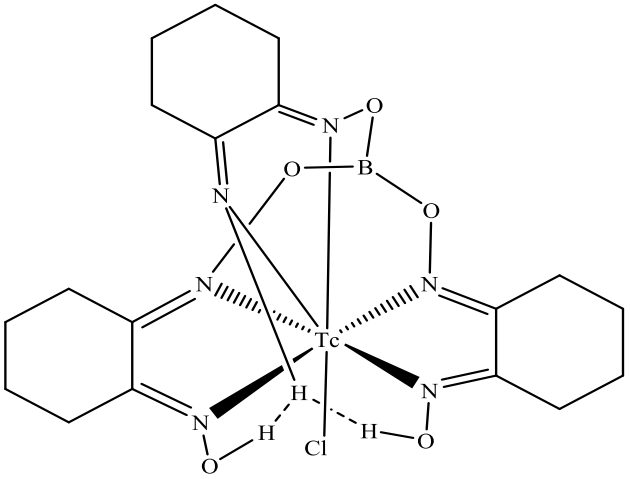

(a) ^{99m}Tc-Teboroxime

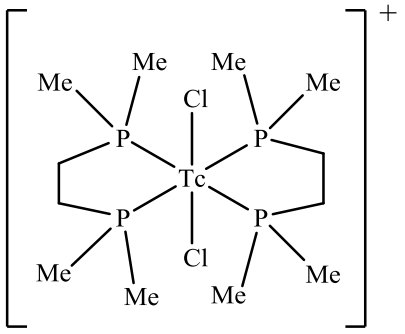

(b) $[^{99m}Tc(dmpe)_2Cl_2]^+$

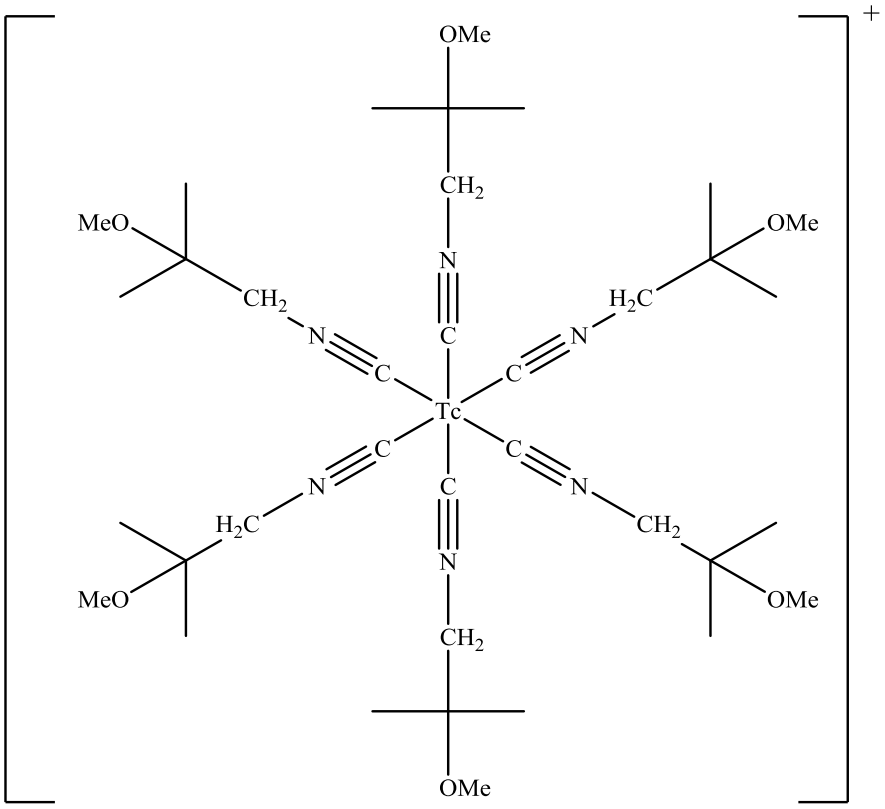

(c) ^{99m}Tc-Sestamibi

Figure 2.7: Structure of (a) ^{99m}Tc-Teboroxime , (b) $[^{99m}Tc(dmpe)_2Cl_2]^+$, (c) ^{99m}Tc-Sestamibi.[21]

2.8.3 BONE IMAGING

A series of ^{99m}Tc complexes coordinated with disphosphonate ligands are used as bone imaging agents.[51,52,53] Generally, the following ligands methylenediphosphonate (MDP), hydroxymethylenediphosphonate (HMDP), 1-hydroxyethylenediphosphonate (HEDP) or 1-hydroxy-4-aminobutylidene-1,1-diphosphonate (ABP) are used in bone imaging.[54] The ^{99m}Tc-MDP **(Figure 2.8)** imaging agent is synthesized from the reaction of the $[^{99m}TcO_4]^-$ generator eluate with MDP in the presence of $SnCl_2.2H_2O$ as reductant.[54,55]

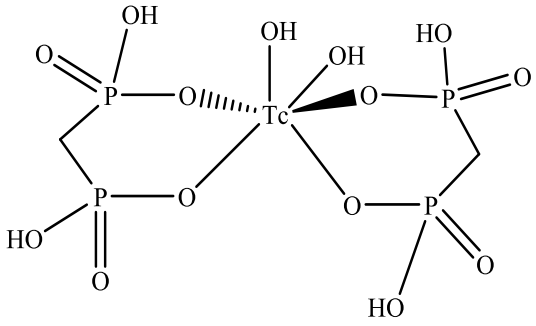

Figure 2.8: Assumed structure of ^{99m}Tc-MDP.[21]

2.9 SECOND GENERATION TECHNETIUM IMAGING AGENTS

The targeting potential lives in a biologically active molecule (BAM) covalently linked to a Tc – complex such as a peptide. The targeting potential of this biologically active molecule can be influenced by the location of the bond with ^{99m}Tc, the size of ^{99m}Tc, lipophilicity, charge and the length of the covalent linker. The second generation Tc imaging agents are classified according to the receptor site or biological function of the targeted molecule.

- *Steroid receptor* – About 60-70% of breast tumors are positive for estrogen receptors and endocrine therapy with the use of drugs such as tamoxifen being effective. Most prostate cancers are androgen and progesterone receptor positive.[56,57]

[51] C.L. De Lingy, W.J. Gelsema, T.G. Tji, Y.M. Huigen, H.A. Vink, *Nucl. Med. Bio.*, 1990, **17**, 161.
[52] W.A. Volkert, E.A. Deutsch, *In Adv. Metals Med.*, Eds: M.J. Abrams, B. Murrer, JAI Press Inc., Connecticut, 1992, **1**.
[53] H.M. Chilton, R.J. Callahan, J.H. Thrall, *In Pharmaceuticals in Medical Imaging*, Eds: D.P. Swanson, H.M. Chilton, J.H. Thrall, Macmillan Publishing Co, New York, 1990, 419.
[54] G. Subramanian, J.G. McAfee, R.G. Blair, F.A. Kallfelz, F.D. Thomas, *J. Nucl. Med.*, 1975, **16**, 744.
[55] K. Libson, E. Deutsch, B.L. Barnett, *J. Am. Chem. Soc.*, 1980, **102**, 2476.
[56] F. Wüst, D. Scheller, H. Spies, B. Johannson, *Eur. J. Inorg. Chem.*, 1998, 789.
[57] J.A. Katzenellenbogen, M.J. Welch, F. Dehdashi, *Anticancer Res.*, 1997, **17**, 1573.

- *Central nervous system (CNS) receptor* – A number of important diseases and psychiatric conditions are associated with the changes in the densities of neurotransmitter receptor site located in the brain such as benzodiazepine (epilepsy), muscarinic and nicotinic (Alzeheimer's disease), dopaminergic (Parkinson's disease, psychiatric conditions).[58]

- *Monoclonal antibodies or antibody fragments* – The monoclonal antibodies, also known as the so-called "magic bullets", are potential ideal vehicles used to target radioisotopes to a specific site and thus provides a radiolabel which is introduced without any interference to the binding of the receptor site such as the PR1A3 monoclonal antibody.[59]

2.10 $^{186/188}$Re CHEMISTRY

Rhenium is a transition metal which was discovered in 1925 and named after the river Rhine.[60] It is the last element in the periodic table discovered to have a stable isotope. After manganese and technetium, rhenium is a third-row transition metal in group 7 with an atomic number of 75 and with an electron configuration of $4f^{14}\ 5d^5\ 6s^2$. Rhenium is chemically similar to manganese and technetium to a certain extent.[60] The key factor in its successful development as a radiopharmaceutical for targeted therapy is the complexation of rhenium with variety of ligands and bifunctional chelating agents. Thus the preparation of rhenium radiopharmaceuticals includes the complexation of rhenium complexes to a bifunctional chelating agent (BFCA) attached to the targeting molecule or include making rhenium an integral part of a molecule which by itself is expected to work as the targeting molecule. Initially, the development of rhenium radiopharmaceuticals were based on the experience gained with ^{99m}Tc radiopharmaceuticals and most methods used were similar to those used in the preparation of these.[61]

[58] H. Spies, T. Fietz, M. Glacer, H.J. Pietsch, B. Johanssen, *Technetium and Rhenium Chemistry and Nuclear Medicine.*, Eds: M. Nicolini, G. Bandoli, U. Mazzi, S.G. Editorali, Padora, 1995, **4**, p243.
[59] D.J. Hnatowich, G. Mardirossan, M. Ruscowski, M. Fargarasi, F. Firzi, P. Winnard, *J. Nucl. Med. Chem.*, 1993, **34**, 172.
[60] A.A. Woolf, *Quart. Rev. Chem. Soc.*, 1961, **15**, 372.
[61] M.R.A. Pillai, J.M. Lo, C.S. John, E.O. Schlemper, D.E. Troutner, *Inorg. Chem.*, 1990, **29**, 1850.

However, the difference between technetium and rhenium chemistry indicated that more fundamental work would be necessary for the development of rhenium chemistry and this could be applied for the manufacturing of radiopharmaceuticals. Comparing both elements (Tc and Re), the rhenium chemistry at the tracer level (nca) is much more complicated than ^{99m}Tc chemistry, and technetium and rhenium complexes with different ligands may have identical structures at the microscopic level, regardless of different synthetic methods.[62] The chemistry between ^{186}Re and ^{188}Re is expected to be similar since they only differ in mass number, but ^{188}Re eluted from the generator usually requires the addition of carrier rhenium to make stable complexes, for example, for Re-HEDP preparation.[63] Two radionuclides of rhenium ($^{186/188}$Re) are of particular interest as they possess favourable physical characteristics shown in **Table 2.5**.[63]

Table 2.5: Some nuclear characteristics of $^{186/188}$Re.[64]

Radionuclide	Characteristics	Assessment
^{186}Re	Energy of β^- Radiation	1.07 MeV
	Energy of γ Radiation	137 keV (12%)
	Half-life, $t_{1/2}$	90 h
^{188}Re	Energy of β^- Radiation	1.95 MeV, 2.11 MeV
	Energy of γ Radiation	155 keV (25%)
	Half-life, $t_{1/2}$	16.9 h

2.11 $^{186/188}$Re RADIOPHARMACEUTICALS

^{186}Re is usually produced in a nuclear reactor by using ^{185}Re(n, γ)^{186}Re reaction and the target being metallic rhenium with 37.07% natural abundance of ^{185}Re or enriched in ^{185}Re up to 96%. ^{186}Re decays to ^{186}Os (stable) **(Table 2.6)** ^{188}Re can be obtained by using the generator ^{188}W/^{188}Re. The advantage of ^{188}Re eluted from the generator is that no carrier added *(nca)* and ^{188}Re is suitable for all applications in nuclear medicine. Hayes and Rafter proposed the use of ^{188}Re as a possible diagnostic agent in 1965 and later in 1966, Lewis and Eldridge were the first to report the preparation of the ^{188}W/^{188}Re generator.[65,66,67]

[62] M.R.A. Pillai, C.L. Barnes, E.O. Schlemper, *Polyhedron*, 1994, **13**, 701.
[63] K. Kothari, M.R.A. Pillai, P.R. Unni, H.H. Shimpi, O.P.D. Noronha, A.M. Samuel, *Appl. Radiat. Isot.*, 1999, **51**, 43.
[64] M.R.A Pillai, A. Dash, F.F. Knapp Jr., *Curr. Radiopharm.*, 2012, **5**, 228.
[65] R.L. Hayes, J.J. Rafter, *ORAU.*, 1965, **101**, 74.
[66] R.E. Lewis, J.S. Eldridge, *J. Nucl. Med.*, 1966, **7**, 804.
[67] R.L. Hayes, J.J. Rafter, *J. Nucl. Med.*, 1966, **7**, 797.

Table 2.6: Decay characteristics and production methods of $^{186/188}$Re.[64]

	Decay Product	Half-life	β^-, E_{max}(MeV)	γ-energy(keV)	Production
^{186}Re	^{186}W (EC, 7.47%) ^{186}Os (β^-, 92.43%)	90 h	1.069 (71.0%) 0.932 (21.54%) 0.581 (5.78%) 0.459 (1.69%)	137 (9.42%)	^{185}Re(n,γ)^{186}Re
^{188}Re	^{188}Os (β^-, 100%)	17h	2.120 (71.1%) 1.965 (25.6%) 1.487 (1.65%)	155 (15.1%)	^{188}W/^{188}Re Generator or ^{187}Re(n,γ)^{188}Re

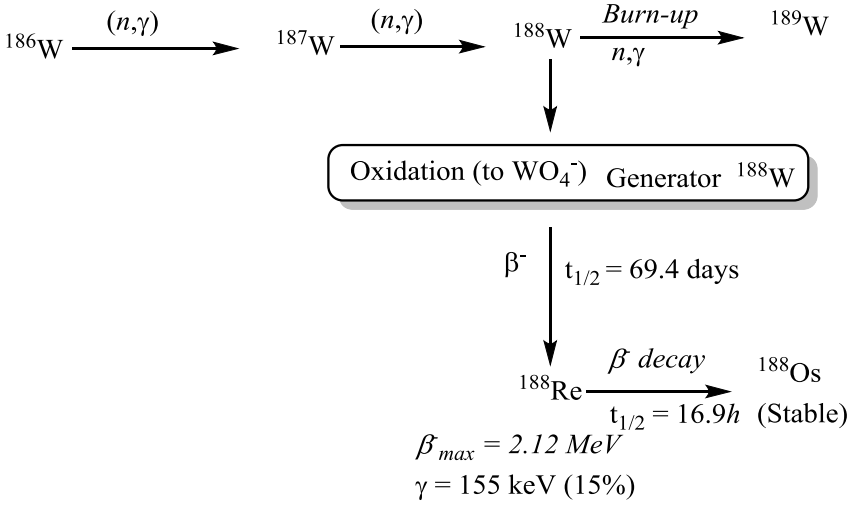

Figure 2.9: Reactor production and decay sequence of ^{188}W.[64]

Many drug molecules with $^{186/188}$Re have been applied as radiopharmaceuticals, for instance, ^{186}Re-HEDP (HEDP = hydroxyethylidene diphosphonate) and ^{188}Re-DMSA (where DMSA is dimercaptosuccinic acid) are often used for bone palliation, the commercially available ^{186}Re-sulphide in the kit is used for synovectomy and ^{188}Re-perrhenate or ^{188}Re-MAG_3 are used for endovascular radiation therapy.[68,69] **Table 2.7** shows some applications of $^{186/188}$Re in radiopharmaceuticals.[70,71]

[68] G. Stőcklin, S.M. Qaim, F. Rősch, *Radiochim. Acta.*, 1995, **70/71**, 249.
[69] J. Weinberger, K.N. Giedd, A.D. Simon, C. Marboe, F.F. Tricher, I. Amots, *Cardiovasc. Radiat. Med.*, 1999, **1**, 252.
[70] J. Kotzerke, H. Hanke, M. Hoher, *Eur. J. Nucl. Med.*, 2000, **27**, 223.
[71] J. Vačina, R. Han, *Med. Pregl.*, 2001, **54**, 245.

Table 2.7: Application of the radiopharmaceuticals labelled with $^{186/188}$Re.[64]

Field of application	Radiopharmaceutical
Bone pair palliation	^{186,188}Re-HEDP, ^{188}Re-DMSA
Synovectomy	^{186}Re-sulphide
Endovascular radiation therapy	^{188}Re-perrhenate, ^{188}Re-MAG_3
Tumor therapy	^{188}Re-peptides
Endoradiotherapy of tumors-catheter administration	^{188}Re-particles
Marrow ablation prior to stem cell rescue	^{188}Re-antigranulocyte antibodies

2.12 CHEMISTRY OF METAL TRICARBONYL COMPLEXES, *fac*-$[M(CO)_3]^+$ OF Tc(I) AND Re(I)

The tricarbonyl core, *fac*-$[M(CO)_3]^+$, consists of three CO ligands which are tightly bonded to the metal centre along with three other ligands to form an octahedral complex and are often smaller than corresponding metals with octahedral or square – pyramidal geometry. Therefore, they are considered to have less likely impact on the important characteristics of the biomolecules they are linked to. The tricarbonyl core, *fac*-$[M(CO)_3]^+$, have low spin d^6 configuration that provide an inert metal centre, thus renders the complexes a high *in vivo* stability which is essential for medical applications.[72] Alberto and Schibli *et al.*[73] reported the first tricarbonyl core of ^{99m}Tc and this allowed for the on-going research on numerous ligand systems and their coordination with *fac*-$[M(CO)_3]^+$. The impact of *fac*-$[M(CO)_3]^+$ in medical applications led to the investigation of biomolecules with *fac*-$[M(CO)_3]^+$, which are linked by bifunctional chelating agents (BFCA). Many *fac*-$[M(CO)_3]^+$ complexes are synthesised in water (Liu *et al.*)[5] with the *fac*-$[M(CO)_3]^+$ core inert. These complexes have been studied in various solvents to explore their different spectroscopic and photochemical results.[73]

2.13 SCHIFF BASE LIGANDS

The condensation of a primary amine and a carbonyl compound leads to a compound containing an azomethine group (-C=N-). This type of compound was described by Hugo Schiff in 1864 as a Schiff base ligand.[74] The classic Schiff base ligands are formed in high yields and their synthesis follows the mechanism of condensation of a carbonyl group with an

[72] T. Mindt, H. Struthers, E. García-Garayoa, D. Debouis, R. Schlibi, *Chimia.*, 2007, **61**, 725.
[73] R. Alberto, R. Schibli, A. Egli, P.A. Schubiger, U. Abram, T.A. Kaden, *J. Am. Chem. Soc.*, 1998, **120**, 7987.
[74] R. Alberto, R. Schibli, A. Egli, P.A. Schubiger, W.A. Herrman, G. Artus, U. Abram, T.A. Kaden, *J. Org. Chem.*, 1995, **493**, 119.

amine **(Figure 2.10)**.[75] Generally, Schiff base ligands are formed via acid or base catalysis or with heat.[76] Schiff bases are readily hydrolyzed by aqueous acids to yield the original amine and carbonyl compound. Schiff bases are one of the most popular ligand groups due to the ease of formation, manipulatible ability and remarkable versatility. Therefore they can be widely used in many fields such as biological, inorganic, analytical and drug synthesis.[75]

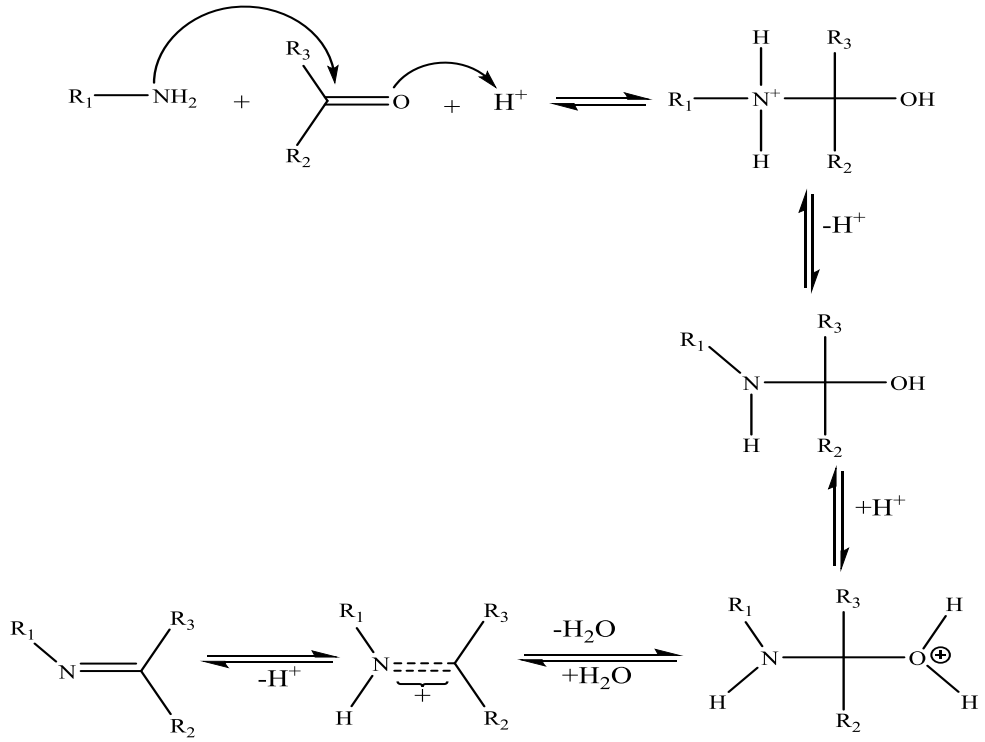

Figure 2.10: Illustration of the mechanism of aldol condensation of carbonyl group with the amines to produce Schiff bases.[76]

Schiff base ligands are an important set of compounds that are utilized in medicinal and pharmaceutical applications. They display biological applications which include antifungal, antibacterial and antitumor activity.[77] Metal Schiff base complexes are studied due to the antitumor and herbicinal use.[77] Schiff bases considered as antibacterial agents are, for example, N-(salicylidene)-2-hydroxyaniline **(Figure 2.11)** which is used to treat mycobacterium tuberculosis. Schiff bases and their complexes have being used as catalysts in various biological systems.[78] They have excellent selectivity, sensitivity and stabilize metal ions such as Ag(II), Co(II), Cu(II), Al(II), Hg(II), Zn(II), Y(II), Pb(II), Gd(II) and Ni(II).[77]

[75] N.E. Borisova, M.D. Reshetova, Y.A. Ultynyuk, *Chem. Rev.*, 2007, **107**, 46.
[76] A. Xavier, N. Srividhya, *J. Appl. Chem.*, 2011, **7**, 2278.
[77] M. Ashraf, A. Wajid, K. Mahmood, M. Maah, I. Yusoff, *Orient. J. Chem.*, 2011, **27**, 363.
[78] M.A. Ashraf, K. Mahmood, A. Wajid, *IPCBEE.*, 2011, **10**, 1.

The Schiff base ligands are characterized by an imine group –N=CH- and this assists in obtaining the mechanism of transamination and racemization reaction that exist in biological system.[77] The cobalt(III) Schiff base complexes are potent antiviral agents that lead to the investigation of Co(III) interactions with proteins and nucleic acids.[79,] Cobalt is not the only metal coordinated to a Schiff base ligand that forms part of medical study. Copper also make a contribution in the medical study as it is known to prevent the activity of purified proteasome.[80]

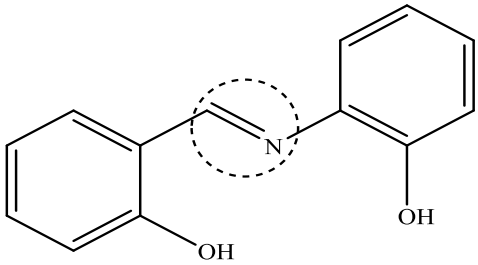

N-(salicylidene)-2-hydroxyaniline

Figure 2.11: *N*-(salicylidene)-2-hydroxyaniline.

Copper complexes have the ability to prevent the cellular proteasome activity and the exact mechanism still has to be determined. The Schiff base ligands coordinated to copper complexes are synthesized from the quinolone scaffold having a formyl/acetyl group, which is adjacent to heterocyclic nitrogen and this quinolone can be attached as pendant with pharmacophores having amino groups.[80,81] However, these copper Schiff base complexes have the unexplored potential of arresting growth of cancer cells. Adsule *et al.*[80] performed a study on copper complexes coordinated with Schiff base ligands of quinolone-2-carboxaldehyde where these have been synthesized and characterized.[80] Another metal used in medical application is zinc (Zn). The metal imine complexes are used to treat diabetes and AIDS.[82] Since they are considered as biological models, they assist in analysing the structure of biomolecules and biological procedures that occurs in the living organisms.

Schiff bases like, Ancistrocladidine **(Figure 2.12)**, are also used to treat cancer drug resistance and as antimalarials.[82,83] There are Schiff base ligands that contains 2,4-dichloro-5-fluoro phenyl compounds obtained from furylglyoxal and *p*-toliudene and these Schiff bases

[79] A. Böttcher, T. Takeuchi, M.I. Simon, T.J. Meade, H.B. Gray, *Inorg. Chem.*, 1995, **59**, 221.
[80] S. Adsule, V. Barve, D. Chen, F. Ahmed, Q.P. Dou, S. Padhye, F.H. Sarkar, *J. Med. Chem.*, 2006, **49**, 7242.
[81] K.G. Daniel, D. Chen, F. Ahmed, Q.P. Dou, *Biochem. Pharmacol.*, 2004, **67**, 1139.
[82] D.M. Boghaei, E. Askarizadeh, A. Bezaatpour, *Spectrochim. Acta Part A.*, 2008, **69**, 624.
[83] Y. Prashanthi, K. Kiranmai, N.J.P. Subhashini, Shivaral, *Spectrochim. Acta Part A.*, 2008, **70**, 30.

also prevents the bacterial growth.[84] Compounds used for designing new antiviral agents are produced from the Schiff bases derived from salicyaldehyde. The isatin Schiff base ligands are considered to be antiviral agents which are used for the treatment of HIV.[85] It also shows antivulsant activity which may provide potential for antiepileptic drugs.[86]

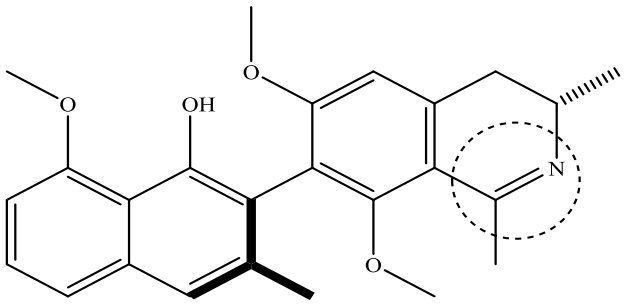

Ancistrocladidine

Figure 2.12: Structure of Ancistrocladidine.

Other Schiff bases consist of high antitumor activity. For instance, N-hydroxy-N'-aminoguanidine contains imine derivatives which inhibit ribonucleotide reductase existing in tumour cells and these can therefore be used to treat leukemia.[87] Schiff bases such as [*N*-(1-phenyl-2-hydroxy-2-phenyl ethylidine)-2',4'-dinitrophenyl hydrazine] (PDH) **(Figure 2.13(a))**, [*N*-(1-phenyl-2-hydroxy-2-phenyl ethylidine)-2'-hydroxy phenyl imine] (PHP) **(Figure 2.13(b))** and [*N*-(2-hydroxy benzylidine)-2'-hydroxy phenyl imine] (HHP) **(Figure 2.13(c))**, are used to reduce the average tumor weight and decrease the growth of the cancer cells.[88] Their ability to successfully coordinate with metal complexes (Re or Tc) has led to an interest in the field of radiopharmacy, since the first rhenium(I) complex coordinated to a Schiff base ligand was reported by Middleton *et al.* in 1979.[89]

[84] C. Silva Da, D. Silva Da, L. Modolo, R. Alves, *J. Ad. Res.*, 2011, **2**, 1.
[85] S.N. Pandeya, D. Sriram, G. Nath, E. De Clercq, *Indian. J. Pharm. Sci.*, 1999, **61**, 358.
[86] S.K. Sridhar, S.N. Pandeya, J.P. Stables, A. Ramesh, *Eur. J. Pharm. Sci.*, 2002, **16**, 129.
[87] M. Jesmin, M.M. Ali, J.A. Khanam, *Thai. J. Pharm. Sci.*, 2010, **34**, 20.
[88] M. Ozaslan, I.D. Karagoz, I.H. Kilic, M.E. Guldur, *Afr. J. Biotechnol.*, 2011, **10**, 2375.
[89] A.R. Middleton, A.F. Masters, G. Wilkinson, *J. Chem. Soc., Dalton Trans.*, 1979, 542.

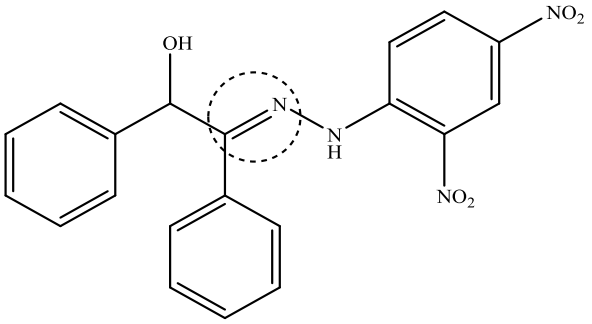

[*N*-(1-phenyl-2-hydroxy-2-phenyl ethylidine)-2',4'-dinitrophenyl hydrazine] (PDH) **(a)**

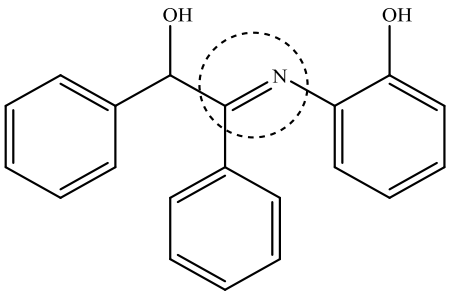

[*N*-(1-phenyl-2-hydroxy-2-phenyl ethylidine)-2'-hydroxy phenyl imine] (PHP) **(b)**

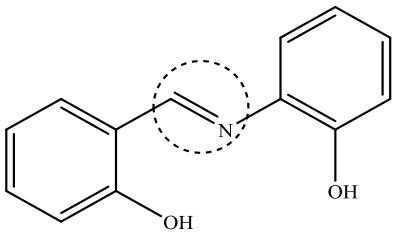

[*N*-(2-hydroxy benzylidine)-2'-hydroxy phenyl imine] (HHP) **(c)**

Figure 2.13: Structure of (a) [*N*-(1-phenyl-2-hydroxy-2-phenyl ethylidine)-2',4'-dinitrophenyl hydrazine] (PDH), (b) [*N*-(1-phenyl-2-hydroxy-2-phenyl ethylidine)-2'-hydroxy phenyl imine] (PHP) and (c) [*N*-(2-hydroxy benzylidine)-2'-hydroxy phenyl imine] (HHP).[88]

The metal(I) tricarbonyl complexes coordinated to Schiff base ligands with potential biological activity is the one aim of this study (see also Chapter 1). Biological derivatives such as bioactive amines are linked to the salicyaldehyde based back-bone for the production of organic molecules which may have the potential to be used for diagnostic and therapeutic applications. Examples of biological amines used for the synthesis of potential biologically active Schiff base ligands are triazoles, tryptamine, carbazole, histamine, etc.[90] Various examples of rhenium(I) tricarbonyl complexes with biological derivatives are synthesized with the formation of the complex, *fac*-$[Re(CO)_3Br(Bid)]$, where Bid = bidentate biologically active ligands. [91]

The good coordination of Schiff base (*N,O*-bid) ligands to the metal(I) complexes of *fac*-$[M(CO)_3]^+$ contributes towards the library of radiopharmaceutical designs. However, tridentate ligands of the type, *N,N',O*-, *N,N',N''*-, *O,N,S*- also form good coordination with metal complexes. Alberto *et al.* conducted a study on dithylenetriamine (dien) (*N,N',N''*-

[90] A. Brink, PhD Thesis, University of the Free State, Bloemfontein, 2011, p100.
[91] R. Alberto, R. Schibli, R. Waibel, U. Abram, A.P. Schibiger, *Coord. Chem. Rev.*, 1999, **190**, 901.

tridentate) coordinated to metal complex[92] and this created a possibility of the study of ethylenediamine (en) (*N,N'*-bid) coordination with the metal complex which forms part of this MSc study.

2.14 KINETIC BEHAVIOUR OF METAL(I) TRICARBONYL COMPLEXES, *fac*-$[M(CO)_3]^+$ (M = Mn(I), Tc(I) AND Re(I))

Elements in group 7 such as Mn(I), Tc(I) and Re(I), have received much attention due to high stability of the metal complex, *fac*-$[M(CO)_3]^+$ and their potential to be utilised in radiopharmaceutical design.[93] Manganese is utilised in medical application as a treatment of human breast cancer (MnSOD)[94] and as mentioned above, technetium and rhenium are investigated for diagnostic and therapeutic imaging as they have a d^6 low-spin configuration and have good coordination properties. The coordination of metal(I) (Tc(I) and Re(I)) tricarbonyl complexes are greatly achieved since Alberto made a significant contribution by reporting the first tricarbonyl complex.[73] The stable tricarbonyl complexes can be obtained from the coordination with mono-, bi- or tridentate chelators.[95] The mixed ligand approach create the possibility for the coordination of mono-, bi- or tridentate ligands with the *fac*-$[M(CO)_3(H_2O)_3]^+$ core to occur, thus replacing the labile aqua ligands.

The development of new methods for the production of radiolabelled complexes in diagnostic or therapeutic applications required kinetic studies to be achieved. The kinetic investigation provides insight into reactivity, stability and the mechanistic behaviour of the formation of tricarbonyl complexes. Several kinetic studies have been performed on the aqua tricarbonyl complexes. The first thermodynamic and kinetic data for water exchange on the *fac*-$[M(CO)_3(H_2O)_3]^+$ (M = Re) synthon was conducted via NMR methods by Salignac[96] and the kinetic analysis for Tc(I) and Mn(I) was performed thereafter.[97] The kinetic behaviour of water exchange and water substitution of *fac*-$[M(CO)_3(H_2O)_3]^+$ have been conducted and

[92] S. Mundwiler, L. Candreia, P. Häfliger, K. Ortner, R. Alberto, *Bioconjucture Chem.*, 2004, **15**, 195.
[93] T.N. Twala, M. Schutte-Smith, A. Roodt, H.G. Visser, *Dalton Trans.*, 2015, **44**, 3278.
[94] C.J. Weydert, T.A. Waugh, J.M. Ritchie, K.S. Iyer, J.L. Smith, L. Li, D.R. Spitz, L.W. Oberley, *Free Radical Biol. Med.*, 2006, **41**, 226.
[95] F. Zobi, O. Blacque, R.K.O. Sigel, R. Alberto, *Inorg. Chem.*, 2007, **46**, 10458.
[96] B. Salignac, P.V. Grundler, S. Cayemittes, U. Frey, R. Scopelliti, A.E. Merbach, *Inorg. Chem.*, 2003, **42**, 3516.
[97] P.V. Grundler, L. Helm, R. Alberto, A.E. Merbach, *Inorg. Chem.*, 2006, **45**, 10378.

reported **(Table 2.8)**.[98] They indicated that the mechanism of the ligand substitution depend on the nature of the entering ligand. The activation parameters of entropy and the similar rates of water exchange and water substitution of entering ligand showed a dissociative activation.

Table 2.8: Kinetic data of water exchange for aqua complexes, *fac*-$[M(CO)_3(H_2O)_3]^+$.[99]

Compound	k_{ex} (at 298 K) (s^{-1})	$\Delta H^{\neq}$ ($kJ.mol^{-1}$)	$\Delta S^{\neq}$ ($J.K^{-1}mol^{-1}$)	Mechanism
fac-$[Mn(CO)_3(H_2O)_3]^+$	23	72.5	+24.4	I_d
fac-$[Tc(CO)_3(H_2O)_3]^+$	0.49	78.3	+11.7	I_d
fac-$[Re(CO)_3(H_2O)_3]^+$	6.3×10^{-4}	90.3	+14.5	I_d

The water exchange experiment was successfully performed by Helm, where the ligand exchange of *fac*-$[Mn(CO)_3(H_2O)_3]^+$ was conducted via ^{17}O NMR. Helm obtained the water exchange rate constant of *fac*-$[Mn(CO)_3(H_2O)_3]^+$ as 23 s^{-1} with the activation parameters, $\Delta H^{\neq}$ = 72.5 kJ. Mol^{-1} and $\Delta S^{\neq}$ = +24.4 $J.K^{-1}$ mol^{-1}. Helm also conducted a study that showed that the rhenium complex reactions are slower than technetium complex reactions. The water exchange rate of *fac*-$[Tc(CO)_3(H_2O)_3]^+$ was obtained as 0.49 s^{-1} with the activation parameters, $\Delta H^{\neq}$ = 78.3 kJ. Mol^{-1} and $\Delta S^{\neq}$ = +11.7 $J.K^{-1}$ mol^{-1}. For *fac*-$[Re(CO)_3(H_2O)_3]^+$, the water exchange rate is 6.3×10^{-4} s^{-1} with the activation parameters, $\Delta H^{\neq}$ = 90.3 kJ. Mol^{-1} and $\Delta S^{\neq}$ = +14.5 $J.K^{-1}$ mol^{-1}. Technetium and rhenium complexes showed an interchange dissociative mechanism.[99]

Not only can positive $\Delta S^{\neq}$ values suggest an I_d mechanism, but the rate of water exchange similar to water substitution rates for a range of entering ligands ranging from neutral N and S donors to halides can also suggest the possible dissociative mechanism.[100] It is reasoned that the mechanism was affected by the fact that the harder N donor ligands made differentiation between water and entering ligands more difficult than for the better nucleophiles (S ligands).[101] Studies have been conducted on metal(I) tricarbonyl complexes with a variety of bidentate ligands (*N,N'*-, *N,O*- or *O,O'*-).[102] The bidentate ligands were specifically chosen to better investigate complexes with varied Bronsted basicities ranging

[98] P.V. Grundler, B. Salignac, S. Cayemittes, U. Frey, R. Scopelliti, A.E. Merbach, *Inorg. Chem.,* 2004, **43**, 3516.
[99] L. Helm, *Coord. Chem. Rev.,* 2008, **252**, 2346.
[100] H.P. Engelbrecht, L. de Drijver, G. Steyl, A. Roodt, *C. R. Chim.,* 2005, **8**, 1660.
[101] A. Roodt, H.G. Visser, A. Brink, *Crystallogr. Rev.,* 2011, **17**, 241.
[102] M. Schutte, G. Kemp, H.G. Visser, A. Roodt, *Inorg. Chem.,* 2011, **50**, 12486.

from a positively charged metal complex (*N,N'*- ligand) to a neutral metal complex (*N,O*- and *O,O'*- ligand).[103,104]

Metal(I) tricarbonyl complexes of the form, *fac*-$[M(CO)_3(X)(L,L'\text{-bid})]^n$ (M = Mn(I), Tc(I) or Re(I), *L,L'*-bid = *N,N'*-, *N,O*- or *O,O'*-bidentate ligands, X = H_2O or MeOH and *n* = 0, +1), can be activated and efficient in radiopharmacy with the aid of [2+1] mixed ligand approach described by Alberto *et al.*[105] Kinetic investigation of M(I) tricarbonyl complexes is based on the study of the effect of bonded mono-, bidentate ligands on the inert metal(I). This will contribute in determining the time required for radiopharmaceutical design, proper ligand labelling procedure and predicting the stability of labelled complexes.

Due to our interest in the kinetics of complex formation of *fac*-$[M(CO)_3(X)(L,L'\text{-bid})]$, previous studies investigating formation kinetics were evaluated. In particular, the protonation and substitution behaviour of dioxotetracyanometalate complexes of Re(V), Tc(V), W(V) and Mo(V) which have been studied in detail and were reviewed.[106] The selected oxygen-containing complexes for systematic studies regarding a ligand, water and proton exchange studies were investigated using ^{17}O and ^{13}C NMR.[107]

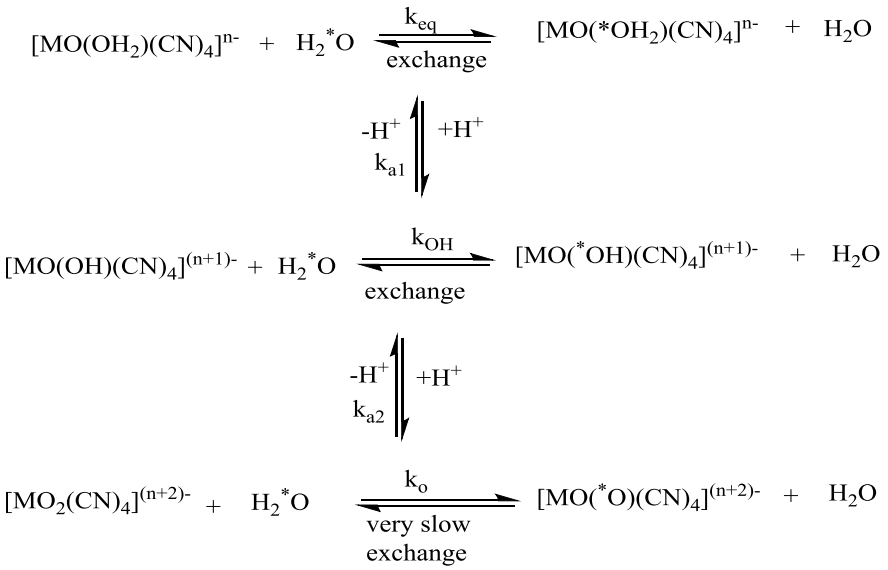

Figure 5.1: A schematic representation of protonation, substitution and ligand exchange in *trans*-$[MO_2(CN)_4]^{n-}$ complexes.[107]

[103] A. Brink, H.G. Visser, A. Roodt, *Inorg. Chem.*, 2014, **53**, 12480.
[104] A. Manicum-Smith, M. Schutte-Smith, G. Kemp, H.G. Visser, *Polyhedron*, 2015, **85**, 190.
[105] R. Alberto, R. Schibli, A. Egli, P.A. Schubiger, W.A. Herrmann, G. Artus, U. Abram, T.A. Kaden, *J. Org. Chem.*, 1995, **493**, 119.
[106] J.G. Leipoldt, S.S. Basson, A. Roodt, *In Advances in Inorganic Chemistry*, Eds: A.G. Sykes, Academic Press, Tallahassec, FL, 1993, **40**, 242.
[107] A. Roodt, H.G. Visser, A. Brink, *Crystallogr Rev.*, 2011, **17**, 241.

It is shown that $[MO_2(CN)_4]^{n-}$ ions of Mo(IV), W(IV), Tc(V) and Re(IV) may undergo successive protonation chemical reactions to yield the corresponding hydroxido oxido and aqua oxido species, and it is shown that the aqua ligand in the $[MO(H_2O)(CN)_4]^{n-}$ ions can be substituted by mono- and bidentate ligands, however this can only occur for Mo(IV) and W(IV) systems. These kinetic analysis lead to predictions that may be used for known dioxo tetracyano complexes of Tc(V) and Os(VI).[107] These predictions determines how fast the reaction is, specifically how fast can a radiopharmaceutical be produced during the application of nuclear medicine.

The formation and synthesis of radiopharmaceuticals is dependent on the mechanism and kinetics of the formation. A consistent dissociative mechanism may simplify matters as the formation rate will be independent on the type of entering ligand. An associative, interchange, equilibrium or combinations thereof would complicate the understanding of the drug-complex formation considerably. Substitution studies on the sixth position of the *fac*-$[M(CO)_3(X)(L,L'\text{-bid})]^n$ (M = Mn(I), Tc(I) or Re(I), *L,L'*-bid = *N,N'*-, *N,O*- or *O,O'*-bidentate ligands, X = H_2O or MeOH and n = 0, +1) complexes have been intensively studied by our research group.[93,103,104,108] However, the mechanism of bidentate ligand coordination to *fac*-$[M(CO)_3]^+$ has received little attention to date.[109] Therefore during this study, the formation reaction of *fac*-$[M(CO)_3]^+$ with bidentate ligands, such as salicylaldehyde derivatives and ethylenediamine (en), is analysed to obtain the reactivity, rate constants as well as activation parameters of formation reaction between *fac*-$[NEt_4]_2[Re(CO)_3(Br)_3]$ and ethylenediamine (en) in methanol.

2.15 CONCLUSION

The impact of the metals, rhenium (^{188}Re and ^{186}Re) for therapy and technetium (^{99m}Tc) for diagnostic, applications are quite recognizable and important. It is used for the imaging of organs such as the liver, kidney, heart, etc. This chapter gives information regarding the potential of tricarbonyl metal complexes from the isotopes ^{99m}Tc, $^{186/188}$Re in the study of nuclear medicine. From the above literature, it is concluded that the coordination of *N,O*-bidentate Schiff base ligands with metal tricarbonyl complexes, in particular with rhenium and technetium, offers a good prospective in developing new models of radiopharmaceuticals and forms part of the study in nuclear medicine.

[108] A. Brink, H.G. Visser, A. Roodt, *Inorg. Chem.*, 2013, **52**, 8950.
[109] T.D. Marake, MSc Dissertation, University of the Free State, Bloemfontein, 2014.

This study will investigate the potential and kinetic mechanistic behaviour of these proposed complexes. The following chapters consist of a detailed description of the ligand systems and complexes synthesized, followed by the solid state investigation as elucidated by single crystal X-ray diffraction (SC-XRD). Finally the formation kinetic behaviour of the rhenium complexes will be discussed which should give further insight into how such rhenium tricarbonyl complexes are formed and the factors affecting the mechanism.

3 SYNTHESIS OF SCHIFF BASE LIGANDS AND *fac*-[M(CO)$_3$X(*N,O*-*Bid*) COMPLEXES

3.1 INTRODUCTION

The study of radiopharmacy has been increasing over the years, due to the developing interest on the chemistry of the metal complexes, *fac*-[M(CO)$_3$X(*N,O*-bid)] with M = Tc(I) and Re(I). Their chemistry consists of the radionuclides, ^{99m}Tc and $^{186/188}$Re, which form part of the diagnostic and therapeutic nuclear medicine applications, respectively.[1,2] The preparation of non-radioactive rhenium complexes to evaluate the chemistry thereof as models is relatively straightforward but the synthesis of technetium complexes is challenging due to radiation safety requirements. It is therefore advantageous to synthesize the rhenium complexes (to obtain the general experimental procedure for synthesizing technetium complexes) since rhenium is not naturally radioactive and it is safer to work with compared to technetium. Technetium is a radioactive element that has no stable isotopes and requires safety measures when used.[1,3,4]

The metal complexes, *fac*-[M(CO)$_3$(X)$_3$]$^+$ (with M = Tc(I) or Re(I) and X = H_2O, Cl^-, Br^-, or MeOH) are synthesized by the gentle reduction of M(VII) to M(I) in the presence of CO. This compound consist of three coordination sites that are occupied by CO groups in the stable *fac*-configuration and the remaining three coordination sites occupied by X. Two of these three X positions may be occupied by bidentate (*O,O'*- or *N,O*-) ligands and the third position can be substituted by a variety of ligands such as imidazole, pyrazole and pyridine.[5,6,7,8] Alternatively, all three X positions may be occupied by a tridentate ligand or three equivalents of monodentate ligands.[9] As mentioned in Chapter 2, the aldol condensation

[1] J. Bernard, K. Ortner, B. Spingler, H.-J. Pietzsch, R. Alberto, *Inorg. Chem.*, 2003, **42**, 1014.
[2] A.E. Miroslavov, Y.S. Polotskii, V.V. Gurzhiy, A.Y. Ivanov, A.A. Lumpov, M.Y. Tyupina, G.V. Sidorenko, P.M. Tolstoy, D.A. Maltsev, D.N. Suglobov, *Inorg. Chem.*, 2014, **53**, 7861.
[3] N. Dharmaraj, P. Viswanathamurthi, K. Natarajan, *Trans. Met. Chem.*, 2001, **26**, 105.
[4] U. Abram, R. Alberto, *J. Braz. Chem. Soc.*, 2006, **17**, 1486.
[5] M. Sagnou, C. Tsoukalas, C. Triantis, C.P. Raptopoulou, A. Terzis, I. Pirmettis, M. Pelecanou, M. Papadopoulos, *Inorg. Chim. Acta.*, 2010, **363**, 1649.
[6] M. Schutte, G. Kemp, H.G. Visser, A. Roodt, *Inorg. Chem.*, 2011, **50**, 12486.
[7] M. Schutte, H.G. Visser, A. Roodt, *Acta Cryst.*, 2010, **E66**, m859.
[8] AL. Manicum, H.G. Visser, I. Engelbrecht, A. Roodt, *Z. Kristallogr NCS*, 2015, **230**, 150.
[9] A. Brink, H.G. Visser, A. Roodt, *Inorg. Chem.*, 2013, **52**, 8950.

between an aldehyde and an amine yields a Schiff base ligand and this ligand has the ability to coordinate with a large number of metal centres through the nitrogen (imine) and oxygen (aldehyde).

In this study, the *N,O*-bidentate ligand synthesised is 5-methyl-(2-(cyclohexyliminomethyl)phenol, **5Me-Sal-Cyhex (Figure 3.1)** ligand and the ligand consist of an aliphatic and aromatic amino functionalities. Rhenium and technetium complexes coordinated by Schiff base ligands which are produced from salicylaldehyde mono- and diamines have been given much attention over the past few years due to their ability to form good coordination.[9,10] Compounds like SalH-*m*Tol[11], SalH-3meBu and SalH-tBu are produced from salicylaldehyde and may be coordinated to rhenium complexes.

However, the aldehyde used in this work is 2-hydroxy-4methylbenzaldehyde and the ligand produced is 5Me-Sal-Cyhex. The ligand, 5Me-Sal-Cyhex, is coordinated to the rhenium complex, **ReAA**, $[Re(CO)_3(Br)_3]^{2-}$. The coordination of a Schiff base ligand to rhenium complex follows a schematic representation which shows that MeOH can be used as an alternative solvent and may be substituted by monodentate ligands such as pyridine, imidazole and pyrazole.[12]

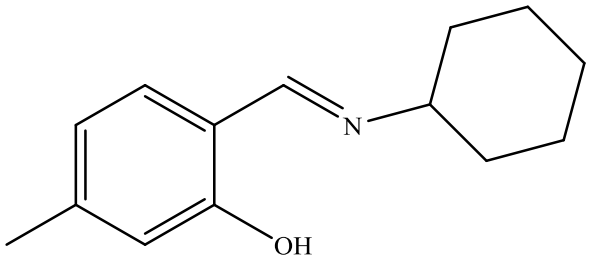

5-methyl-(2-cyclohexyliminomethyl)phenol - **5Me-Sal-Cyhex**

Figure 3.1: Structure of the ligand used.

[10] A. Brink, H.G. Visser, A. Roodt, *Inorg. Chem.*, 2014, **53**, 12480.
[11] A. Brink, A. Roodt, H.G. Visser, *Acta Cryst.*, 2009, **E65**, o3175.
[12] A. Brink, H.G. Visser, A. Roodt, *J. Coord. Chem.*, 2011, **64**, 122.

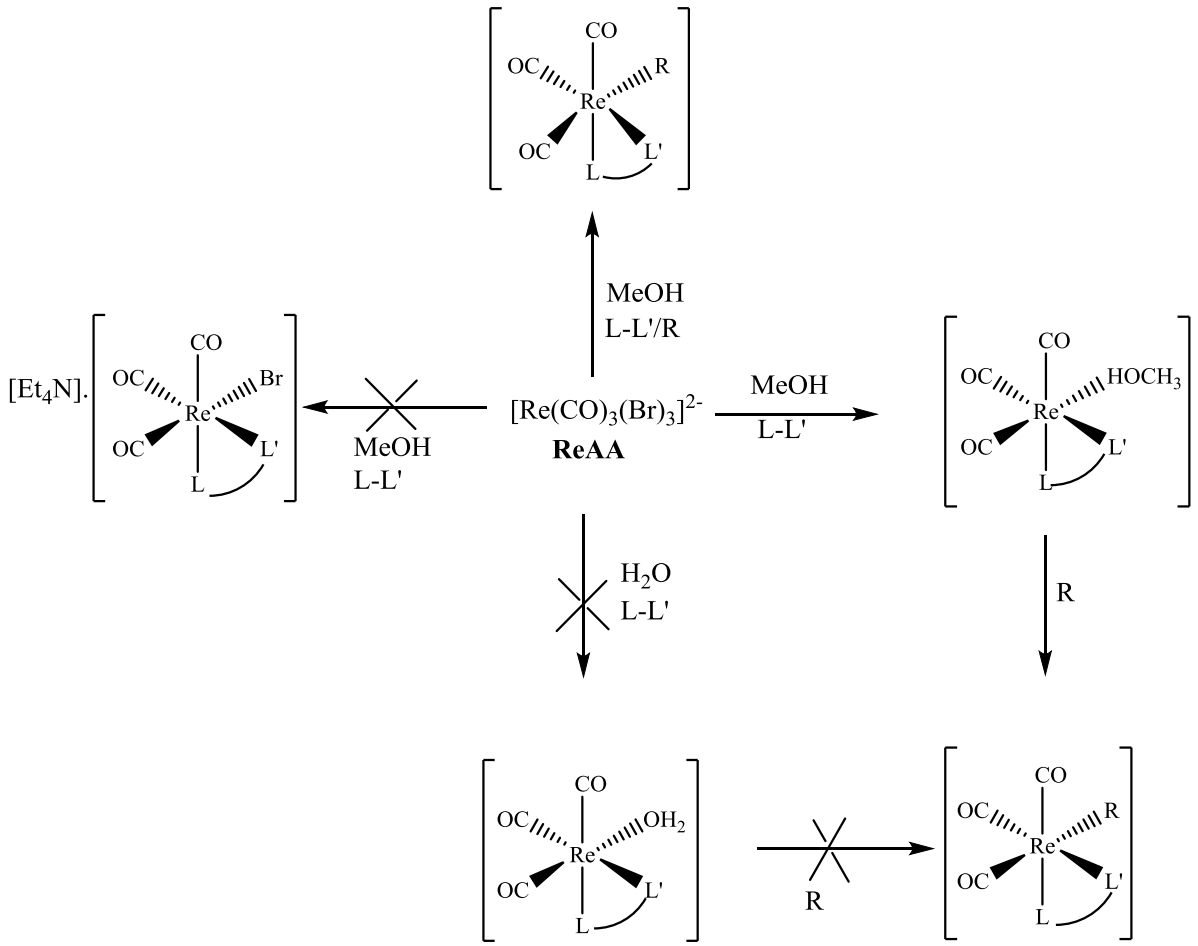

Figure 3.2: Representation of a general reaction schematic for the synthesis of [Re(L-L')(CO)$_3$(S)] (L-L'= bidentate ligand, R = Pyridine, Imidazole, MeOH and pyrazole, S = coordinating ligand).[12]

3.2 REAGENTS AND EQUIPMENT

All reagents used for the synthesis and characterization of Schiff base ligands and metal complexes, *fac*-[M(CO)$_3$X(*N*,*O*-bid)], were of analytical grade and were purchased from Sigma Aldrich or Merck, South Africa, unless otherwise stated. The reagents of analytical grade were not purified and were used as received. The solvents were purified and dried according to the literature procedure.[13] *fac*-[NEt$_4$]$_2$[Re(CO)$_3$(Br)$_3$] – **[ReAA]** was synthesised with the procedure described by Alberto *et al.* (1996)[14] and it was used for synthesising all rhenium complexes. Similarly *fac*-[NEt$_4$]$_2$[^{99}Tc(CO)$_3$(Cl)$_3$] – **[^{99}TcAA]** was synthesized at the University of Zurich, Switzerland by the procedure described by R. Alberto *et al.* (1995).[15] ^{99}TcAA was used to synthesise all the technetium complexes, which was conducted at the

[13] D.D. Perrin, W.L.F. Armarego, *Purification of Laboratory Chemicals*, 3rd Ed, Pergamon Press, 1988.
[14] R. Alberto, R. Schibli, P.A. Schubiger, U. Abram, T.A. Kaden, *Polyhedron*, 1996, **15**, 1079.
[15] R. Alberto, R. Schibli, A. Egli, P.A. Schubiger, W.A. Herrmann, G. Artus, U. Abram, T.A. Kaden, *J. Organomet. Chem.*, 1995, **493**, 119-127.

University of Zurich, Switzerland. Methods used for characterization were Elemental Analysis, Infrared Spectroscopy (IR), Nuclear Magnetic Resonance (NMR) and Ultraviolet-Visible Spectroscopy (UV-Vis). Infrared spectra of the ligand and metal complexes were recorded at room temperature, on a Bruker Tensor 27 Standard System Spectrophotometer with a laser range of 4000-370 cm^{-1} and the solid samples were analysed as KBr pellets. The ^{1}H and ^{13}C FT-NMR spectra of the ligands and metal complexes were obtained at 600 MHz and 151 MHz respectively, from the analysis performed on a Bruker AXS 600 MHz instrument or spectra were obtained at 300 MHz and 75 MHz on Bruker AXS 300 MHz spectrometer at 25^{o}C in C_3H_6O (2.05 ppm) and $CDCl_3$ (7.26 ppm); all chemical shifts are recorded in ppm and coupling constants in Hz. The ^{99}Tc NMR spectrum of the complexes were obtained at 400 MHz at 25^{o}C. The UV-Vis spectra were collected on a Varian Cary 50 Conc UV-Visible Spectrophotometer, equipped with a Julabo F12-mV temperature cell regulator (accurate within 0.1^{o}C) in a 1.000 ± 0.001 cm quartz cuvette cell.[16] The HPLC analysis of the technetium complexes was performed on a Merk-Hitachi L-700 apparatus with a Macherey-Nagel C-18ec reversed-phase column with 5 μm particle size, 100 Å pore size and 250 x 3 mm. The solvents used were the 0.1% trifluoroacetic acid solution in water (Solvent A) and HPLC-grade methanol or acetonitrile (Solvent B). The flow rate was 0.5 ml/min at 250 nm and the TFA gradient was used unless otherwise stated.

3.3 WORKING WITH RADIOACTIVE COMPOUNDS

As mentioned in Chapter 2, for diagnostic and therapeutic nuclear medicine applications, technetium and rhenium are utilized respectively. Rhenium has radioactive isotopes such as ^{186}Re with half-life of 90 hours and ^{188}Re with half-life of 16.9 hours and all radioisotopes are treated with the required safety precautions.[17] In this work, ^{99}Tc was used and since this radionuclide is a long-lived isotope with half-life of 2.12 x 10^5 years, all reactions are performed in the sealed atmosphere controlled glove box. All the ^{99}Tc reactions were conducted in a certified radiation laboratory at the Institute of Inorganic Chemistry at the University of Zurich in Switzerland. ^{99}Tc chemicals used were stored in the protected glove box and protective clothing (lab coat, gloves, safety goggles, feet caps over the shoes) and

[16] D. L. Pavia, G. M. Lampman, G. S. Kriz, *Introduction to Spectroscopy*, 3rd Ed., USA, Thomson Learning, Inc., 2001.
[17] M.R.A. Pillai, A. Dash, F.F. Knapp Jr, *Curr. Radiopharm.*, 2012, **5**, 228.

radiation detector were worn at all times in the radiation laboratory. The ^{99}Tc chemical waste materials were disposed in the radioactive equipped containers.

3.4 SYNTHETIC EXPERIMENTAL PROCEDURE

3.4.1. SYNTHESIS OF 5-Methyl-(2-cyclohexyliminomethyl)phenol ligand

3.4.1.1. General Synthesis of 5Me-Sal – "M" ligand Synthesis

The general synthesis of the **5Me-Sal – "M" ("M" = aliphatic or aromatic substituent)** ligand was conducted as follows unless stated otherwise. The respective amine was dissolved in methanol and added dropwise to the chosen aldehyde (1:1 mol equivalents) dissolved in methanol. The reaction mixture was refluxed at 80°C for 3 hours. The solvent was carefully removed under vacuum at 25°C.

3.4.1.2. 5-Methyl-(2-cyclohexyliminomethyl)phenol – 5Me-Sal-Cyhex[18]

The title compound, 5Me-Sal-Cyhex, was synthesised according to the experimental procedure mentioned above in §3.3.1.1, using 2-hydroxy-4-methylbenzaldehyde (0.252 g, 1.850 x 10^{-3} mol) and cyclohexylamine (0.2020 g, 2.036 x 10^{-3} mol) which were dissolved in methanol. The reaction mixture was refluxed at 80°C for 3 hours and the solvent was carefully removed under vacuum at 25°C. Crystals suitable for X-ray diffraction were obtained from acetone at 25°C. (Yield of yellow crystalline product: 0.371 g, 83.74%) IR(KBr, cm^{-1}), υ = 2926, 2855, 1625, 1572, 1394, 1279, 1207, 1151, 1126, 1080, 640-890. ^{1}H NMR (300 MHz, acetone-d_6) : δ(ppm) 1.29-1.81 (m, 11H), 2.29 (s, 3H), 6.70 (s, 2H), 7.24 (s, 1H), 8.48 (s, 1H, -CH=N), 13.50 (s, 1H, -OH). ^{13}C NMR (151 MHz, acetone-d_6) : δ(ppm) 21.5, 24.8, 27.6, 35.4, 78.1, 117.2, 119.9, 132.0, 144.7, 162.1, 163.2, 164.8.

3.4.2. SYNTHESIS OF RHENIUM(I) TRICARBONYL COMPLEXES

3.4.2.1. *fac*-$[Et_4N]_2[Re(CO)_3Br_3]$ – ReAA

$[Et_4N]Br$ (4.89g, 0.0233 mol) was ground to a fine powder in a mortar and pestle. This compound was dried under vacuum overnight. 2,5,8-trioxanone diglyme (150 ml) was added to the $[Et_4N]Br$ under a dry nitrogen atmosphere and slurred on an oil-bath, preheated to

[18] M. Tsosane, A. Brink, *Z. Kristallogr, NCS*, 2014, **229**, 281.

80°C, for 30 min. The system was evacuated and purged with N_2 gas several times. $[Re(CO)_5Br]$ (4.70 g, 0.0116 mol) was added and the reaction was stirred at 115 °C for 15 h. Good stirring and ventilation is essential because of the continuous evolution of CO. The reaction mixture was cooled to room temperature and the precipitate was filtered, washed twice with cold ethanol and cold DCM and then the product was dried. The white powdered product was dried under vacuum overnight.[7] (Yield of white powder: 8.466 g, 95.05%). IR (KBr, cm^{-1}), $\upsilon_{(CO)}$ 1995, 1883.

3.4.2.2. *fac*-[Re(CO)$_3$(HOCH$_3$)(5Me-Sal-Cyhex)]

fac-$[NEt_4]_2[ReBr_3(CO)_3]$ (**ReAA**) (52.5 mg, 0.0681 mmol) was dissolved in (10 ml) MeOH. 5Me-Sal-Cyhex (14.10 mg, 0.0649 mmol) dissolved in (10 ml) MeOH was mixed with ReAA solution. The reaction mixture was refluxed at 80℃ for 8 hours and the solvent was carefully removed under vacuum at 25℃. The product was recrystallized from methanol to obtain crystals for XRD. (Yield of yellow crystalline product: 0.0189 g, 56.44%) UV-Vis (nm, $L.mol^{-1}.cm^{-1}$) : λ_{max} = 266.4 , ε = 3.170 x 10^3. IR (KBr, cm^{-1}), $\upsilon_{(CO)}$ = 2002, 1886, 1862. ^{1}H NMR (300 MHz, acetone-d_6) : δ(ppm) 1.30 (s, 6H), 1.41 (s, 4H), 2.31 (s, 3H), 3.51 (s, 1H), 3.56 (s, 3H), 6.37 (s, 1H), 6.73 (s, 1H), 7.24 (s, 1H), 8.50 (s, 1H). ^{13}C NMR (151 MHz, acetone-d_6) : δ(ppm) 21.87 (CH_3), 22.66 (2 x CH), 24.19, 27.56, 31.12, 35.41 (2 x CH), 118.32 (Ar), 127.75, 128.37, 134.13, 140.45, 155.94, 162.58 (C=N).

3.4.2.3. *fac*-[Re(CO)$_3$(Imid)(5Me-Sal-Cyhex)]

fac-$[NEt_4]_2[ReBr_3(CO)_3]$ (**ReAA**) (50.0 mg, 0.0649 mmol) was dissolved in (10 ml) MeOH. 5Me-Sal-Cyhex (13.90 mg, 0.0640 mmol) dissolved in (10 ml) MeOH and imidazole (4.49 mg, 0.0660 mmol) were mixed with ReAA solution. The reaction mixture was refluxed at 80℃ for 8 hours and the solvent was carefully removed under vacuum at 25℃. The product was recrystallized from methanol to obtain crystals. (Yield pf yellow crystalline product: 0.0053 g, 15.74%) UV-Vis (nm, $L.mol^{-1}.cm^{-1}$) : λ_{max} = 267.2 , ε = 8.176 x 10^3. IR (KBr, cm^{-1}), $\upsilon_{(CO)}$ = 2017, 1897. ^{1}H NMR (300 MHz, acetone-d_6) : δ(ppm) 1.39 (d, *J* = 8.8 Hz, 6H), 1.82 (d, *J* = 3.9 Hz, 4H), 2.31 (s, 3H), 3.53 (d, *J* = 7.2 Hz, 1H), 6.70 (s, 2H), 7.06 (s, 2H), 7.24 (s, 1H), 7.67 (s, 1H), 8.51 (s, 1H). ^{13}C NMR (151 MHz, acetone-d_6) : δ(ppm) 21.42 (CH_3), 22.88 (2 x CH_2), 27.98, 30.63, 31.98 (2 x CH_2), 106.80, 116.37 (Ar), 121.56 (Ar),

121.92 (Ar), 130.01(Ar), 133.48 (C-N), 133.78 (C=N), 139.96 (Ar), 158.54 (Ar), 160.33 (C=N).

3.4.2.4. *fac*-[Re(CO)$_3$(Pyrazole)(5Me-Sal-Cyhex)]

fac-[NEt$_4$]$_2$[ReBr$_3$(CO)$_3$] (**ReAA**) (53.5 mg, 0.0694 mmol) was dissolved in (10 ml) MeOH. 5Me-Sal-Cyhex (14.60 mg, 0.0672 mmol) dissolved in (10 ml) MeOH and pyrazole (4.0 mg, 0.0588 mmol) were mixed with ReAA solution. The reaction mixture was refluxed at 80℃ for 8 hours and the solvent was carefully removed under vacuum at 25℃. The product was recrystallized from methanol to obtain crystals. (Yield a yellow crystalline product : 0.0103 mg, 29.10%) UV-Vis (nm, L.mol^{-1}.cm^{-1}) : λ_{max} = 264.2 , ε = 5.778 x 10^3. IR (KBr, cm^{-1}), $\upsilon_{(CO)}$ = 2013, 1897, 1872. ^{1}H NMR (300 MHz, acetone-d$_6$) : δ(ppm) 1.42 (s, 6H), 1.84 (s, 4H), 2.31 (s, 3H), 3.52 (s, 1H), 6.56 (d, *J* = 8.2 Hz, 1H), 6.70 (s, 1H), 7.13 (s, 1H), 7.24 (s, 1H), 7.90 (s, 1H), 8.27 (s, 1H), 8.50 (s, 1H). ^{13}C NMR (151 MHz, acetone-d$_6$) : δ(ppm) 21.51 (CH$_3$), 23.14 (2 x CH$_2$), 28.15, 30.97, 32.68 (2 x CH$_2$), 117.63 (Ar), 121.63 (Ar), 121.95 (Ar), 123.03, 123.61(C-N), 130.51 (Ar), 130.95 (N-C=N), 140.56 (Ar), 159.45 (Ar), 160.60 (C=N).

3.4.2.5. *fac*-[Re(CO)$_3$(Py)(5Me-Sal-Cyhex)]

fac-[NEt$_4$]$_2$[ReBr$_3$(CO)$_3$] (**ReAA**) (50.0 mg, 0.0649 mmol) was dissolved in (10 ml) MeOH. 5Me-Sal-Cyhex (14.10 mg, 0.0649 mmol) dissolved in (10 ml) MeOH and pyridine (5.13 mg, 0.0649 mmol) were mixed with ReAA solution. The reaction mixture was refluxed at 80℃ for 8 hrs and the solvent was carefully removed under vacuum at 25℃. The product was recrystallized from methanol to obtain crystals. (Yield a yellow crystalline product : 0.0053 g, 15.74%) UV-Vis (nm, L.mol^{-1}.cm^{-1}) : λ_{max} = 243.3 , ε = 1.333 x 10^3. IR (KBr, cm^{-1}), $\upsilon_{(CO)}$ = 2010, 1888. ^{1}H NMR (300 MHz, acetone-d$_6$) : δ(ppm) 1.50 (m, 10H), 2.33 (s, 3H), 3.30 (s, 1H), 6.60 (m, 2H), 7.31 (m, 2H), 8.50 (s, 1H). ^{13}C NMR (151 MHz, acetone-d$_6$) : δ(ppm) 21.69 (CH$_3$), 22.14 (2 x CH$_2$), 27.86, 30.49, 34.98 (2 x CH$_2$), 102.96 (Ar), 108.52, 120.68, 122.03, 125.06 (2 x CH$_2$), 130.86, 139.76, 144.04, 146.77 (2 x CH$_2$), 151.26, 167.86 (C=N).

3.4.2.6 *fac*-[Re(CO)$_3$(HOCH$_3$)(5Hydr-Sal-R)] (Synthesis unsuccessful)

In an attempt to explore the synthesis of novel rhenium complexes with a variety of ligand systems, numerous options were considered. However, the synthesis are at present not completely successful. The continuation of the work will proceed in future, for example, rhenium complexes with furyl ligands **(5Hydr-Sal)** were not successful **(Figure 3.3)**. Two assumptions were made in terms of a possible coordination; either (a) coordination through the oxygen of the hydroxyl group or (b) possible coordination would occur at the oxygen in the 5-membered ring.

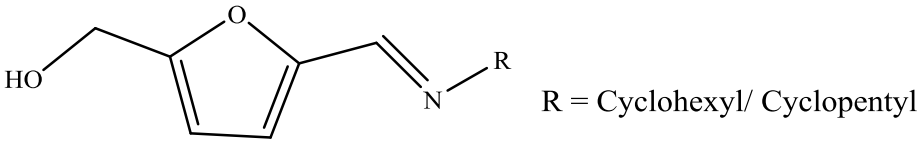

Figure 3.3: Structure of the furyl ligand.

The product that would have formed was assumed as *fac*-[Re(CO)$_3$(HOCH$_3$)(5Hydr-Sal-R)], all products obtained were oily-brown and no crystals were obtained. From the NMR analysis, the ^{1}H-NMR of *fac*-[Re(CO)$_3$(HOCH$_3$)(5Hydr-Sal-R)] show the peaks of the substituents (R), the methyl group between the hydroxyl oxygen and the 5-membered ring. The peaks of the protons on the 5-membered ring are not observed on the spectrum. The NMR of all rhenium complexes with furyl ligands, *fac*-[Re(CO)$_3$(HOCH$_3$)(5Hydr-Sal-R)], were impure. Purification of the complexes have not yet been fully successful, but will be continued at a future date.

fac-[Re(CO)$_3$(HOCH$_3$)(5Hydr-Sal-Cyhex)] ^{1}H-NMR (300 MHz, acetone-d$_6$) : δ(ppm) 1.44 (s, 2H), 1.87 (s, 1H), 1.97 (s, 3H), 2.28 (s, 1H), 3.54 (s, 2H).

fac-[Re(CO)$_3$(HOCH$_3$)(5Hydr-Sal-Cypent)] ^{1}H-NMR (300 MHz, acetone-d$_6$) : δ(ppm) 0.89 (s, 1H), 1.30 (s, 1H), 1.41 (ddd, *J* = 7.2, 5.4, 1.7 Hz, 4H), 3.53 (q, *J* = 7.3 Hz, 2H).

3.4.3 SYNTHESIS OF TECHNETIUM(I) TRICARBONYL COMPLEXES

3.4.3.1 *fac*-[NEt$_4$]$_2$[^{99}Tc(CO)$_3$(Cl)$_3$] – ^{99}TcAA

NH$_4$[^{99}TcO$_4$] (0.665 g, 3.675 x 10^{-3} mol) was dissolved in 4 ml of sodium hypochloride (however the oxidation was slow, so 4 ml of hydrogen peroxide was added and heat was

applied to increase the oxidation). The solution of $NH_4[^{99}TcO_4]$ was left to stir for 30 min. TBACl (1 g, 3.48 x 10^{-3} mol) (TBA^+ = tetra(*n*-butyl)ammonium cation) was dissolved in 2 ml of H_2O. The TBACl solution was added in $NH_4[^{99}TcO_4]$ solution and the reaction mixture was stirred for 10 min. The solution was filtered using the vacuum and the colourless (white) precipitate was left to dry. Thereafter, 1 ml of conc. HCl was added to the colourless precipitate $TBA[^{99}TcO_4]$ to form a green precipitate of $TBA[^{99}TcOCl_4]$. $TBA[^{99}TcOCl_4]$ (493.5 mg) was dissolved in 2 ml of THF (tetrahydrofuran) and was added to BH_3.THF under an atmosphere of CO gas. The resulting solution was dissolved in 2 ml of ethanol, NEt_4Cl and HCl were added to remove the excess BH_3.THF. The solution was stirred for 2 hrs and then filtered.[14,15] (Yielded colourless powder product: 0.485 g, 35.13%) IR (ATR, cm^{-1}), υ(CO) = 2026, 1917, 1890. ^{99}Tc NMR : -749.04 ppm (broad peak)

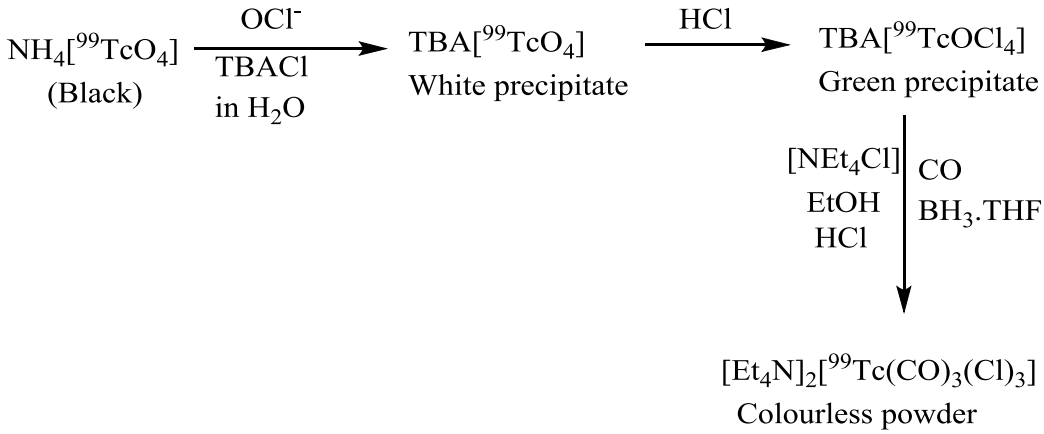

Figure 3.4: Schematic illustration of the formation of $[Et_4N]_2[^{99}Tc(CO)_3(Cl)_3]$.

3.4.3.2 *fac*-$[^{99}Tc(CO)_3(HOCH_3)$(5Me-Sal-Cyhex)]

In MeOH:

^{99}TcAA ($[NEt_4]_2[^{99}Tc(CO)_3(Cl)_3]$) (0.0226 g, 5.240 x 10^{-5} mol) was dissolved in 5 ml MeOH and 5Me-Sal-Cyhex (0.0135 g, 6.212 x 10^{-5} mol) was added to 1.5 ml of ^{99}TcAA solution. The reaction mixture was refluxed in 10 ml MeOH at 80°C for 8 hours. The solvent was removed under vacuum and two equivalents of $[Et_4N]$ were removed with THF and recrystallized with MeOH. **HPLC :** R_t = 24.87 min.

In MeCN:

^{99}TcAA (0.0087 g, 1.670 x 10^{-5} mol), 5Me-Sal-Cyhex (0.00354 g, 1.629 x 10^{-5} mol) were flushed by N_2 gas in a round bottom flask. 0.1 ml of dry Triethylamine was added to reaction mixture. The solution was refluxed in a dry acetonitrile (MeCN) at 60°C for 8 hours. The solvent was removed under vacuum and two equivalents of [Et_4N] were removed with THF and the solution was recrystallized with MeOH. **HPLC :** R_t = 24.95 min.

3.4.3.3 SYNTHESIS OF TECHNETIUM(I) TRICARBONYL COMPLEXES

In addition to the synthesis of rhenium(I) tricarbonyl complexes, *fac*-[$Re(CO)_3(X)$(*N*,*O*-Bid)], technetium(I) complexes, *fac*-[$^{99}Tc(CO)_3(HOCH_3)$(*N*,*O*-Bid)] were synthesized by refluxing the solution at ~60°C for 8 hours in a specific solvent with the ligand 5Me-Sal-Cyhex. HPLC was used for identification of the formation and completion of the product.

The first reaction was performed at 65°C in MeOH in **Figure 3.5**.

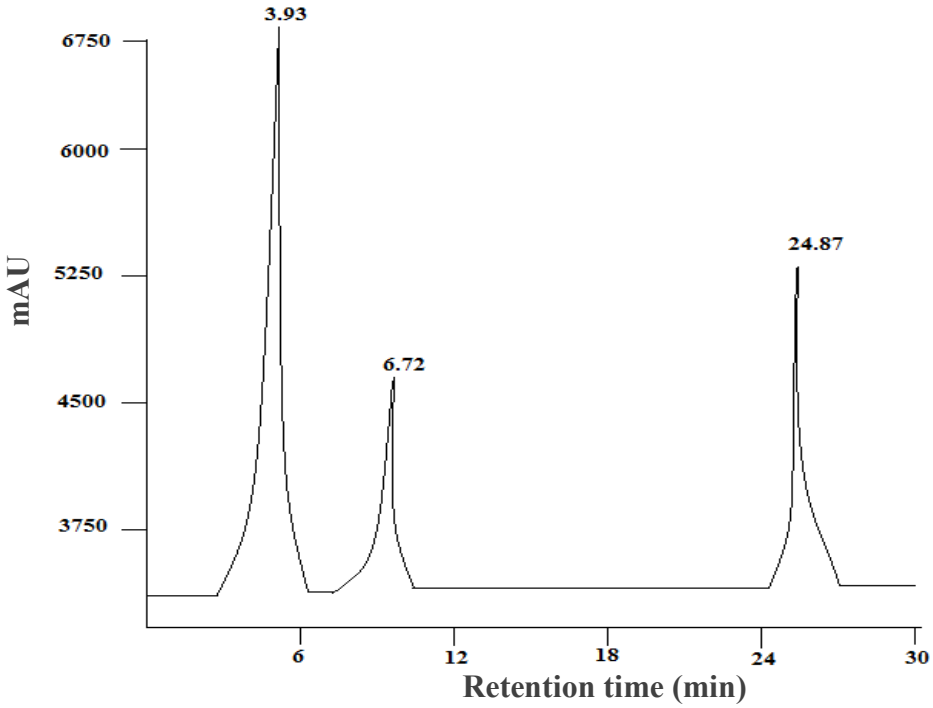

Figure 3.5: HPLC graph of the synthesis of *fac*-[$^{99}Tc(CO)_3$(MeOH)(5Me-Sal-Cyhex)] complex refluxed at 65°C in MeOH for two hours.

The peak observed at R_t = 3.93 min represent the pertechnetate, [$^{99}TcO_4]^-$ (the existence of [$^{99}TcO_4]^-$ comes from *fac*-[$^{99}Tc(CO)_3(Cl)_3]^+$ which contains [$^{99}TcO_4]^-$, as *fac*-

$[^{99}Tc(CO)_3(Cl)_3]^+$ can be synthesized from $[^{99}TcO_4]^-$ under 1 atm of CO)[19], and the peak at R_t = 6.72 min represent $[NEt_4]_2[^{99}Tc(CO)_3(Cl)_3]$. The desired HPLC graph should only display the starting material and the product, *fac*-$[^{99}Tc(CO)_3$(MeOH)(5Me-Sal-Cyhex)] at R_t = 24.87 min, thus the pertechnetate was not wanted. More base (triethylamine) was added for 100% completion of the reaction and formation of the product, *fac*-$[^{99}Tc(CO)_3$(MeOH)(5Me-Sal-Cyhex)].

To remove the pertechnetate, $[^{99}TcO_4]^-$, the synthesis of technetium(I) complex was performed at 60°C under Schlenk conditions and the solvent was changed to dry acetonitrile. It was observed that the pertechnetate disappeared and the HPLC graph showed the product, *fac*-$[^{99}Tc(CO)_3$(MeOH)(5Me-Sal-Cyhex)] and starting material **(Figure 3.6)**. The peak at R_t = 7.02 min represent the starting material, $[NEt_4]_2[^{99}Tc(CO)_3(Cl)_3]$ and the peak at R_t = 24.95 min represent the product, *fac*-

$[^{99}Tc(CO)_3$(MeCN)(5Me-Sal-Cyhex)]. For 100% completion of the reaction and the complete formation of the product, *fac*-$[^{99}Tc(CO)_3$(MeCN)(5Me-Sal-Cyhex)], more base (triethylamine) could be added to reaction.

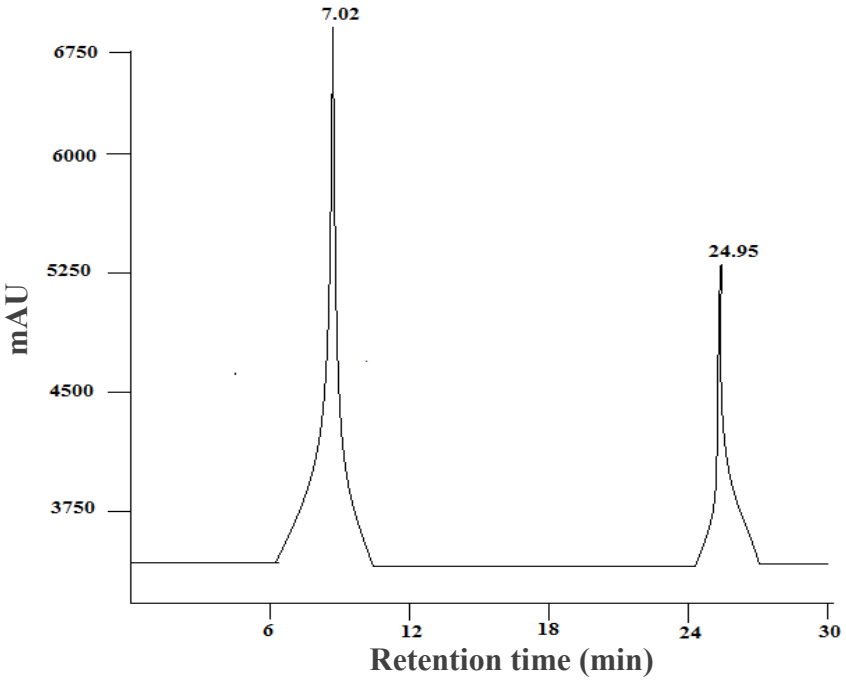

Figure 3.6: HPLC graph of the synthesis of Technetium-99(I) tricarbonyl complex refluxed at 60°C in dry MeCN under N_2 gas, after 1 hour.

[19] R. Alberto, R. Schibli, A. Egli, A.P. Schubiger, U. Abram, T.A. Kaden, *J. Am. Chem. Soc.*, 1998, **120**, 7987-7988.

3.5 DISCUSSION

Rhenium(I) tricarbonyl complexes, *fac*-[Re(CO)$_3$(X)(*N*,*O*-Bid)], should ideally, for pharmaceutical purposes, be synthesized in aqueous medium. However, in this work, the synthesis of rhenium(I) complexes are performed in methanol to form *fac*-[Re(CO)$_3$(MeOH)(*N*,*O*-Bid)] complex in order to improve purity and solubility. The synthesized rhenium(I) complexes have bidentate ligands that activates the metal centre and the bromide (Br^-) is substituted by methanol, imidazole, pyrazole and pyridine to form purified crystalline products. All the synthesized products were characterized with methods such as UV-Vis, IR, elemental analysis and NMR (^{1}H and ^{13}C). Characterization performed on the obtained ligand and rhenium complexes were as follows: UV-Vis was utilized to obtain the maximum wavelength (λ_{max}) and extinction coefficient (ε), IR was used to obtain the IR stretching frequencies of the tricarbonyl ligands of the rhenium complexes and were observed at ~1800-2100 cm^{-1} range.[20]

It is established that compounds with good electron density on the rhenium metal core, *fac*-[Re(CO)$_3$]$^+$ and backbonding occurring from the carbonyl ligands have lower stretching frequencies. IR spectra of the metal complexes indicated the stretching frequency of the carbonyl group to characterize the metal complexes. From the results, it is observed that the complex, *fac*-[Re(CO)$_3$(Imid)(5Me-Sal-Cyhex)], has a higher stretching frequency than the rest of the complexes synthesised. Since the complex, *fac*-[Re(CO)$_3$(Imid)(5Me-Sal-Cyhex)], has a higher stretching frequency, $\upsilon_{(CO)}$, this compound has lower electron density existing on the rhenium(I) metal centre **(Table 3.1)**.[21,22]

Table 3.1: The carbonyl stretching frequencies of various complexes with *N*,*O*-bidentate ligands.

Metal complex	Stretching frequency (Carbonyl) $\upsilon_{(CO)}$, cm^{-1}		
[Re(CO)$_3$(HOCH$_3$)(5Me-Sal-Cyhex)]	2002	1886	1862
[Re(CO)$_3$(Py)(5Me-Sal-Cyhex)]	2010		1888
[Re(CO)$_3$(Pyrazole)(5Me-Sal-Cyhex)]	2012	1897	1872
[Re(CO)$_3$(Imid)(5Me-Sal-Cyhex)]	2017		1897

Imid = Imidazole, Py = Pyridine

[20] B. Stuart, *Infrared Spectroscopy: Fundamentals and Apllications*, John Wiley and Sons, Ltd, 2004, 106.
[21] S. Otto, A. Roodt, *Inorg. Chim. Acta*, 2004, 1.
[22] A. Brink, H.G. Visser, A. Roodt, G. Steyl, *Dalton Trans.*, 2010, 1246.

The monodentate ligands substituted on the rhenium(I) tricarbonyl complexes in the sixth position have different pKα values and their pKα values are as follows, imidazole: pyrazole: pyridine: 6.9: 19.8: 5.2.[23] NMR was also used for characterization of all compounds acquired in this work. Particularly, ^{13}C-FT-NMR spectra showed no peaks for the tricarbonyl carbon atoms for all rhenium complexes synthesized and this is assumed to be due to the fact that the carbon atoms of the tricarbonyl group have large relaxation time. The time required to measure the carbons of tricarbonyl group was considered an unwise use of optimal NMR time as the presence of the carbonyl atoms may be established with other analytical methods, i.e. IR and X-ray diffraction.

In the chemical reaction of a rhenium(I) complex with the Schiff base ligand (5Me-Sal-Cyhex), the bidentate ligand activates the Re metal centre enough to replace the monodentate ligand (Br^-) by R = methanol, imidazole, pyrazole or pyridine to form pure crystalline *fac*-[$Re(CO)_3$(R)(5Me-Sal-Cyhex)] product. The synthesis of rhenium(I) tricarbonyl complexes was performed without the use of $AgNO_3$, the bromide ions were removed and replaced with a mono- and bidentate ligand (Schiff base ligand) in the solution. The ligand was recrystallized with acetone and all complexes were recrystallized in MeOH, EtOH and acetone. The majority of crystals were obtained from MeOH. The rhenium(I) tricarbonyl complexes, *fac*-[$Re(CO)_3$(Imid)(5Me-Sal-Cyhex)], *fac*-[$Re(CO)_3$(Pyrazole)(5Me-Sal-Cyhex)] and *fac*-[$Re(CO)_3$(Pyridine)(5Me-Sal-Cyhex)] were obtained in low yields due to the recrystallization process. Using $AgNO_3$ to remove the bromide atoms would increase the yields considerably.

As mentioned above, rhenium(I) tricarbonyl complexes such as *fac*-[$Re(CO)_3(HOCH_3)$(5Me-Sal-Cyhex)], *fac*-[$Re(CO)_3$(Imid)(5Me-Sal-Cyhex)], *fac*-[$Re(CO)_3$(Pyrazole)(5Me-Sal-Cyhex)], *fac*-[$Re(CO)_3$(Py)(5Me-Sal-Cyhex)] and the ligand, 5Me-Sal-Cyhex, are successfully synthesized in methanol at 80^{o}C. The single crystals of the following compounds are obtained: 5-methyl (2-cyclohexyliminomethyl)phenol (5Me-Sal-Cyhex), *fac*-[$Re(CO)_3(HOCH_3)$(5Me-Sal-Cyhex)], *fac*-[$Re(CO)_3$(Imid)(5Me-Sal-Cyhex)]. The X-ray crystallographic data which elucidates the absolute configuration will be discussed in the following section **(Chapter 4)**.

[23] B. Richter, *Heterocyclic Chem.*, www.scripps.edu/baran/heterocycles/Essentials1-2009.pdf Accessed at 4.49 pm on 27-11-2015.

Chapter 3

4 X-RAY CRYSTALLOGRAPHIC STUDY OF *N,O-Bid* LIGAND AND *fac*-[Re(CO)$_3$(X)(*N,O-Bid*)] COMPLEXES

4.1 INTRODUCTION

The coordination of Schiff base ligands to rhenium(I) tricarbonyl complexes are developing and contributes towards the study of radiopharmacy as described in Chapter 2 during the literature review of rhenium and technetium tricarbonyl complexes.[1] Few Schiff base ligands, however, have been produced from salicylaldehyde[2,3] and then coordinated with Re(I) tricarbonyl complexes.[5] During the course of this study the Schiff base ligand synthesized from 2-hydroxy-4-methylbenzaldehyde was coordinated to *fac*-[Re(CO)$_3$]$^+$ core and single crystals suitable for X-ray diffraction were obtained. The Schiff bases act as bidentate ligands and their purpose is to activate the inert M(I) (M = Tc(I) and Re(I)) tricarbonyl center according to [2+1] mixed ligand[4] approach as described by Brink.[5] The ideal is to investigate whether this may influence the medical applications of such complexes, *fac*-[M(CO)$_3$(X)(*L,L'-Bid*)] (*L,L'-Bid* =bidentate ligand), which are used in radiopharmacy.

This chapter primarily describes the structure of *N,O-Bid* ligand with the respective Re(I) tricarbonyl complexes and the configuration as studied by X-ray diffraction. The use of the Schiff base bidentate ligand allows substitution on the third position by effectively blocking two reactive sites and leaving one site open for substitution. Substituents in the third position as synthesized during the course of this study are as follows; methanol, imidazole, pyrazole and pyridine. Hence the coordinating 5-methyl-(2-cyclohexyliminomethyl)phenol ligand **(5Me-Sal-Cyhex)** bonded to **ReAA**, allowed the following Re(I) tricarbonyl complexes to be crystallized and the absolute configuration to be reported **(Figure 4.1)**:

a) *fac*-[Re(CO)$_3$(HOCH$_3$)(5Me-Sal-Cyhex)]
b) *fac*-[Re(CO)$_3$(Imid)(5Me-Sal-Cyhex)]

[1] Z. Li, Y. Li, L. Lei, C. Che, X. Zhou, *Inorg. Chem.*, 2005, **8**, 307.
[2] H. Xu, X. Gong, H. Wang, *Acta Cryst.*, 2008, **E64**, o638.
[3] A. Brink, A. Roodt, H.G. Visser, *Acta Cryst.*, 2009, **E68**, o1071.
[4] S. Mundwiler, M. Kündig, K. Ortner, R. Alberto, *Dalton Trans.*, 2004, 1320.
[5] A. Brink, H.G. Visser, A. Roodt, *Inorg. Chem.*, 2013, **52**, 8950.

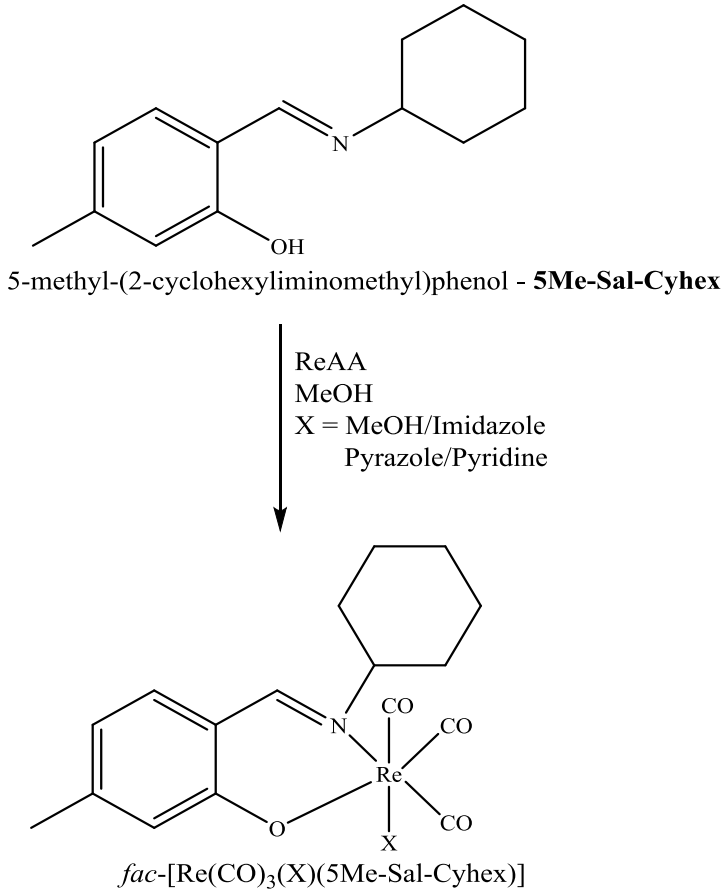

Figure 4.1: Chemical formation of *fac*-[Re(CO)$_3$(X)(5Me-Sal-Cyhex)].

All crystal structures obtained in this work were characterized with X-ray diffraction (XRD), where hydrogen bonding and interactions (π-π, C-H…Cg, C-O…Cg O…O and O…C) are utilized to describe all structures in detail. The centroid (Cg) of a plane figure or a ring is the arithmetic mean (average) position of all points in a ring or shape.[6] Hydrogen bonding and π-π interactions are considered to be important aspects in crystallography that are associated with structural chemistry and the bonding mode of a molecule. Both hydrogen bonding and π-π interactions of the compounds described here are used to discuss in detail the existence intra- and intermolecular interactions.

[6] I.N. Herstein, *Non Commutative Rings*, The Mathematical assosciation of America, USA, 1994, 46.

4.2 EXPERIMENTAL

The reflection data used to determine the crystal structures were collected on a Bruker X8 ApexII[7] 4K CCD diffractometer, which was equipped with a graphite monochromated Mo Kα radiation source with wavelength (0.71073 Å) with ω and φ – scans at 100 K. The cell refinement and frame interaction were performed using Bruker SAINT-PLUS,[8] and data reduction was performed using the XPREP.[8] Data corrections for absorption effects were conducted using a multi-scan technique and SADABS.[9] The crystal structures in this chapter were solved using the SIR-97[10] direct method package, and were refined using the packages of WinGX[11] and SHELXL.[12,13] The molecular graphical representation of the crystal structures were conducted with the use of DIAMOND.[14] All structures are shown with thermal ellipsoids drawn at 50% probability level, unless stated otherwise. All non-hydrogen atoms were refined with anisotropic displacement parameters, while the methyl, methane and aromatic hydrogen atoms were placed in a geometrically idealized positions and have constrained to ride on their parent atoms, with (C – H = 0.98-0.95 Å) and $U_{iso}(H)$ = $1.5U_{eq}(C)$ and $1.2U_{eq}(C)$, respectively. A summary of crystallographic data of the free ligand and complexes, 5Me-Sal-Cyhex **(1)**, *fac*-[$Re(CO)_3(HOCH_3)$(5Me-Sal-Cyhex)] **(2)**, *fac*-[$Re(CO)_3$(Imid)(5Me-Sal-Cyhex)] **(3)** are shown in **Table 4.1**.

[7] Bruker APEX2 (Version 1.0-27), Bruker AXS Inc, Madison, Wisconsin, USA, 2005.
[8] Bruker SAINT-PLUS (including XPREP) (Version 7.12), Bruker AXS Inc, Madison, Wisconsin, USA, 2004.
[9] Bruker SADABS (Version 2004/1), Bruker AXS Inc, Madison, Wisconsin, USA, 1998.
[10] A.Altomare, M.C. Burla, M. Camalli, G.L. Cascarano, C. Giacovazzo, A. Guagliardi, A.G.G. Moleterni, G. Polidori, R. Spagna, *J. Appl. Cryst.*, 1999, **32**, 115.
[11] L.J. Farrugia, *J. Appl. Cryst.*, 1999, **32**, 837.
[12] G.M. Sheldrick, SHELX 97, *Program for refinement of crystal structures*, University of Göttigen, Germany, 1997.
[13] G.M. Sheldrick, *Acta. Crystallogr.*, 2008, **A64**, 112.
[14] K. Brandenburg, H. Putz, *Visual Crystal Structure Information System*, Release 3.0c, Crystal Impact CnbR, Bonn, Germany, 2004.

Table 4.1: Summary of the crystallographic data and refinement parameters of 5Me-Sal-Cyhex = 5Methyl(2-cyclohexyliminomethyl)phenol (1), *fac*-[Re(CO)$_3$(HOCH$_3$)(5Me-Sal-Cyhex)] (2) and *fac*-[Re(CO)$_3$(Imid)(5Me-Sal-Cyhex)] (Imid = imidazole) (3).

Crystallographic data	**(1)**	**(2)**	**(3)**
Compounds	**5Me-Sal-Cyhex**	***fac*-[Re(CO)$_3$(HOCH$_3$)(5Me-Sal-Cyhex)]**	***fac*-[Re(CO)$_3$(Imid)(5Me-Sal-Cyhex)]**
Empirical formula	$C_{14}H_{19}NO$	$C_{18}H_{22}NO_5Re$	$C_{20}H_{21}N_3O_4Re$
Formula weight (g.mol^{-1})	217.30	519.11	554.11
Crystal system	Orthorhombic	Monoclinic	Monoclinic
Space group	$P2_12_12_1$	$C2/c$	$P2_1/n$
Unit cell dimensions			
a (Å)	6.9081(9)	19.789(5)	16.326(5)
b (Å)	7.9422(10)	14.446(5)	7.984(5)
c (Å)	22.936(3)	13.998(5)	16.483(5)
α (^{o})	90	90	90
β (^{o})	90	109.206(5)	102.983(5)
γ (^{o})	90	90	90
Volume (Å^3)	1253.4(3)	3779(2)	2093.6(2)
Z	4	8	4
Temperature (K)	100(2)	100(2)	100(2)
Wavelength (Å)	0.71073	0.71073	0.71073
Density$_{calc.}$ (g.cm^{-1})	1.147	1.823	1.760
Crystal colour	Colourless	Colourless	Yellow
Crystal morphology	Cuboid	Cuboid	Cuboid
Crystal size (mm)	0.31x0.27x0.20	0.37x0.14x0.09	0.70x0.22x0.20
μ (mm^{-1})	0.072	6.457	5.834
F (000)	472	2016	1080
Theta range (^{o})	3.1, 21.2	1.782, 25.465	1.586, 27.999
Completeness (%)	99.8	93.1	99.9
Index ranges	h = -9 → 8	h = -23 → 23	h = -21 → 21
	k = -10 → 10	k = -17 → 17	k = -10 → 10
	l = -30 → 30	l = -16 → 16	l = -21 → 21
Reflections collected	25156	42811	40082
Unique reflections	3028	3191	5052
R_{int}	0.106	0.058	0.070
Refinement method	Full-matrix least-squares on F^2	Full-matrix least-squares on F^2	Full-matrix least-squares on F^2
Data / restraints / parameters	3028/0/148	3191/0/231	5052/0/258
GooF	1.020	1.065	1.168
Reflections with I>2σ(I)	1901	2732	4420
Final R indices	R1 = 0.0500	R1 = 0.0211	R1 = 0.0318
	wR2 = 0.1300	wR2 = 0.0375	wR2 = 0.0883
R indices (all data)	R1 = 0.0496	R1 = 0.0300	R1 = 0.0402
	wR2 = 0.1300	wR2 = 0.1061	wR2 = 01079
ρ_{max} and ρ_{min} (e.Å^{-3})	0.24 and -0.18	0.973 and -0.867	1.929 (0.86 Å from Re1) and -1.432
Flack parameter	-1.2(9)	-	-

4.3 CRYSTAL STRUCTURE OF 5Me-Sal-Cyhex

The cuboid colourless 5Me-Sal-Cyhex **(1)** crystallized in an orthorhombic crystal system in the $P2_12_12_1$ space group with four molecules per unit cell (Z = 4). The 5Me-Sal-Cyhex compound is asymmetric and crystallizes as the *trans* phenol-imine tautomer with strong intramolecular O1-H2···N1 hydrogen bond, which is unequivocally obtained by the indicated hydroxyl hydrogen atom geometry. It falls under the aromatic Schiff-base group, 2-(phenyliminomethyl)phenol.[15] The aromatic Schiff-base group are a typical class of photochromic materials[15] that can undergo both excited state intramolecular proton transfer and *cis-trans* isomerization. The 5Me-Sal-Cyhex compound rotates around - C = N- double bond with a rotation that suggest that it can influence the thermo- and photochromic capabilities for this type of the ligand system. This compound is essentially non-planar with a torsion angle (C1-N1-C21-C22) of 116.0(2)^o between the aromatic and cyclohexyl ring. The molecular structure of 5Me-Sal-Cyhex is represented in **Figure 4.2**, illustrating the numbering scheme. The bond lengths and bond angles are represented in **Table 4.2**.

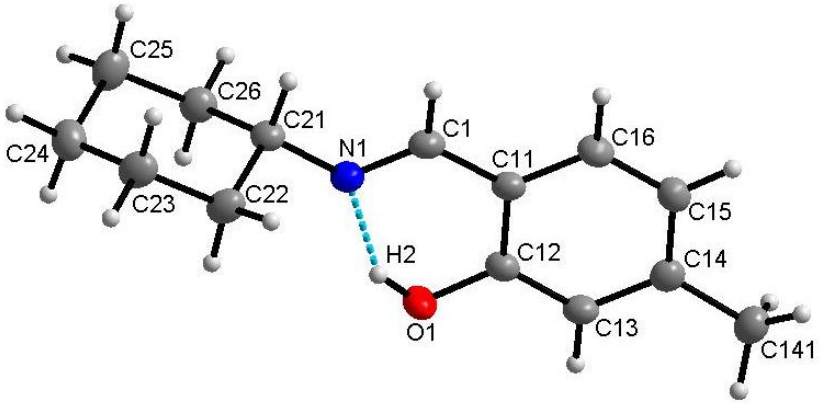

Figure 4.2: Molecular structure of 5Me-Sal-Cyhex showing the numbering scheme of the atoms. Displacement ellipsoids are drawn at 30% probability level for more clarity of the structure.

[15] M. Tsosane, A. Brink, *Z. Kristallogr. NCS*, 2014, **229**, 281.

Table 4.2: Selected bond distances and angles of the compound, 5Me-Sal-Cyhex.

Bond distances (Å)		Bond angles (°)	
C1-N1	1.272(2)	N1-C1-C11	122.44(2)
N1-C21	1.457(2)	C1-N1-C21	120.16(2)
C1-C11	1.447(3)	N1-C21-C22	108.78(2)
C11-C12	1.413(3)	C12-O1-H2	109.5
C12-O1	1.354(2)	C11-C12-O1	120.79(19)
C21-C22	1.526(3)	C22-C23-C24	111.54(2)
C23-C24	1.512(3)	C26-C21-C22	110.99(2)
N1-H2	1.824	C24-C25-C26	111.8(2)

The distance of N1···O1 (2.572 Å) is considered to be shorter than the Van Der Waals radii for N and O atom with the distance of 3.07 Å. [5,16,17,18] The C1-N1 bond distance is only 1.272(2) Å and is indicative of a double bond. It is established that all other bond lengths and angles reported are in the normal ranges. [19] To further characterize this crystal structure, planes are drawn to obtain dihedral angles, rotation of the structure and possible distortion.

Plane 1 is formed by the aromatic backbone (C11, C12, C13, C14, C15, C16), plane 2 is formed by the *pseudo* ring (O1, C12, C11, C1, N1), and plane 3 is formed by the cyclohexyl ring (C21, C22, C23, C24, C25, C26). Plane 1 and 2 exhibit a dihedral angle of 2.975(4)°, plane 1 and 3 shows a dihedral angle of 89.739(2)° and plane 2 and 3 shows a dihedral angle of 88.368(3)°, represented in **Figure 4.3**. The following three planes are obtained to analyse the orientation of the ligand:

a) Plane 1: formed with atoms, C11, C12, C13, C14, C15, C16. (Aromatic backbone of 5Me-Salen ligand)

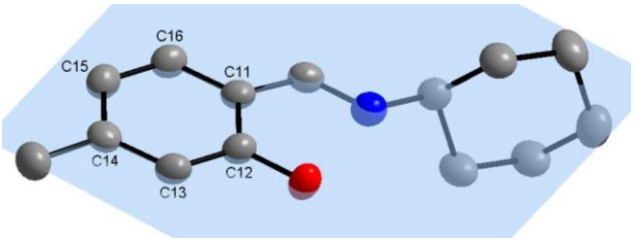

[16] A. Bondi, *J. Phys. Chem.*, 1964, **68**, 441.
[17] H-J. Xu, X-X. Gong, H. Wang, *Acta Cryst.*, 2008, **E64**, o638.
[18] A. Brink, A. Roodt, H.G. Visser, *Acta Cryst.*, 2009, **E65**, o3175.
[19] F.H. Allen, O. Kennard, D.G. Watson, L. Brammer, A.G. Orpen, R. Taylor, *J. Chem. Soc., Perkin Trans* II., 1987, S1.

b) Plane 2: formed through atoms, O1, C12, C11, C1, N1. (*Pseudo* ring)

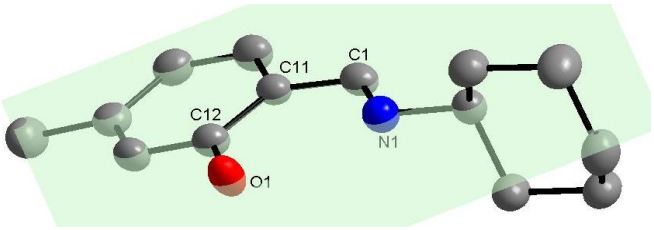

c) Plane 3: formed through atoms, C21, C22, C23, C24, C25, C26. (Cyclohexl ring).

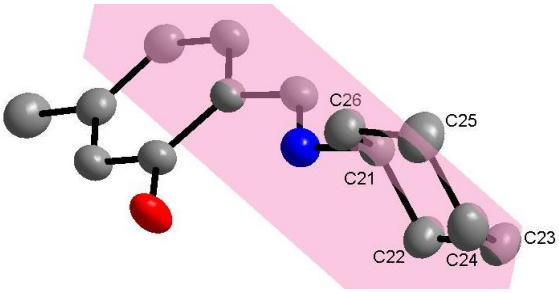

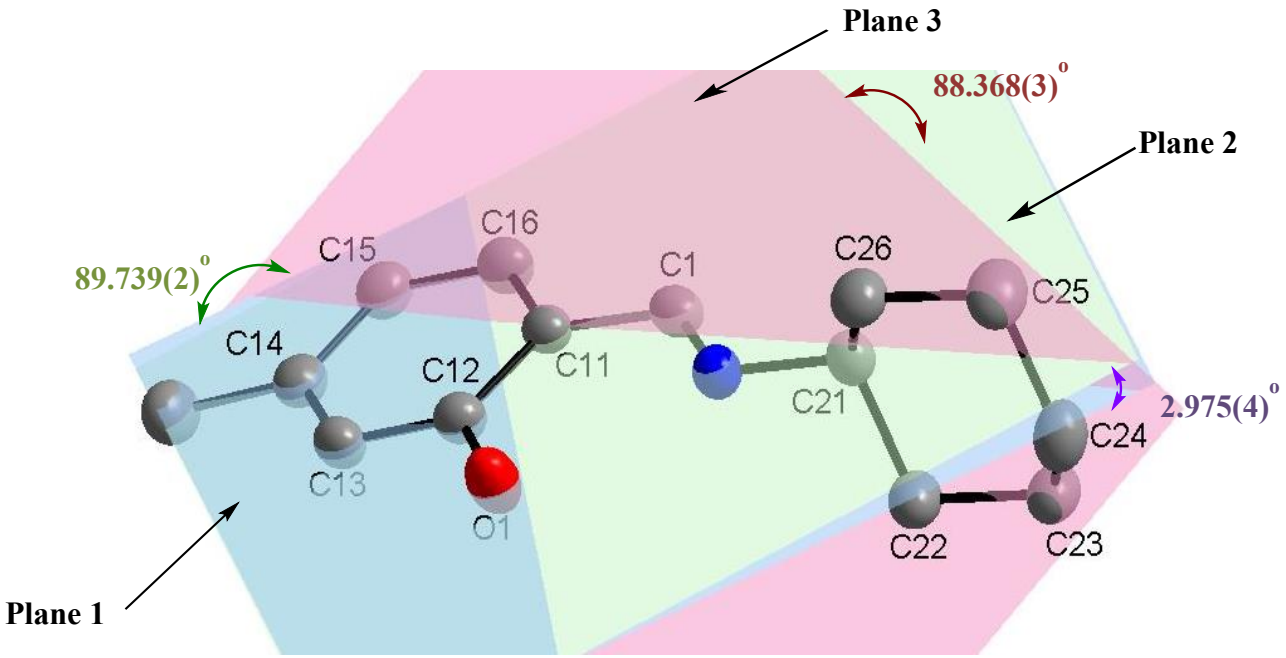

Figure 4.3: Illustration of plane 1, 2 and 3 and dihedral angles obtained between planes of 5Me-Sal-Cyhex.

Table 4.3: Hydrogen bond geometry (Å, º).

D*−H···*A	**D−H (Å)**	**H···*A* (Å)**	***D*···*A* (Å)**	***D*−H···*A* (º)**
O1−H2···N1	0.84	1.82	2.572(2)	147

Symmetry codes and transformation used to generate equivalent atoms:
#1 x, y, z.

Intermolecular C-H…π interactions occur between the methylene moiety and centroid ring (Cg) with atoms C1-H1…Cg1$^{\#1}$ and C13-H13…Cg1$^{\#2}$ indicated in **Figure 4.4**, **4.5** and **Table 4.4**. (Symmetry operation: $^{\#1}$ 2-x, 1/2+y, 1/2-z and $^{\#2}$ 1-x, -1/2+y, 1/2-z)

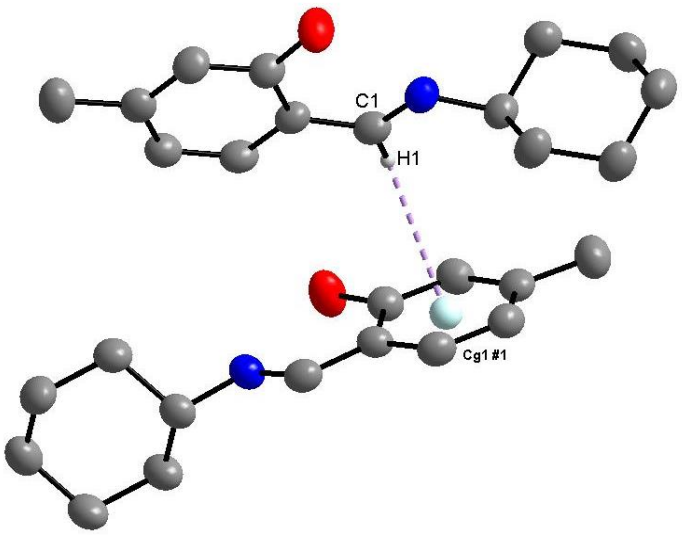

Figure 4.4: A schematic illustration of C-H...*π* interaction (purple line) with centroid atom (Cg) in the aromatic ring, forming C1-H1…Cg1 interaction.

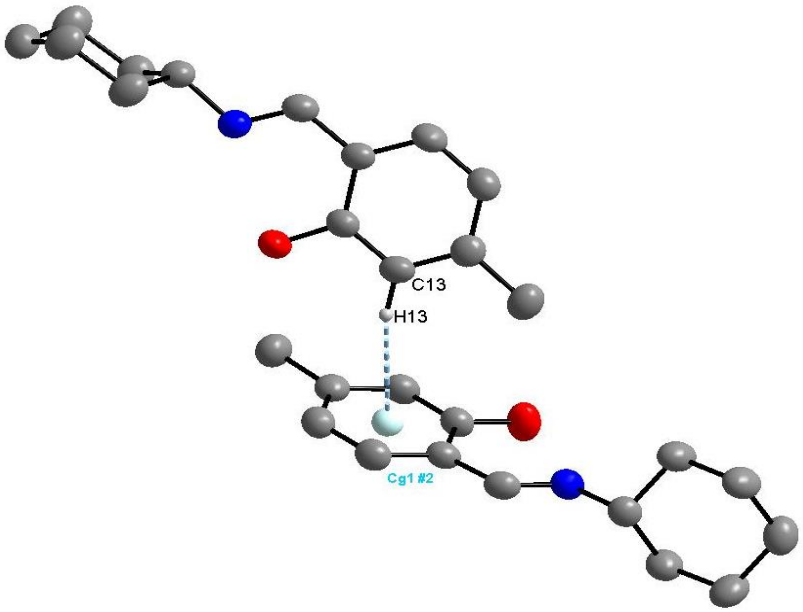

Figure 4.5: A schematic illustration of C-H...π interaction (blue line) with centroid atom (Cg) in the aromatic ring, forming C13-H13…Cg1 interaction.

Table 4.4: Hydrogen bonds distances and angles of C-H…π interaction (Å, º).

C-H…Cg1	d(C-H) (Å)	d(H…Cg1) (Å)	d(C…Cg1) (Å)	<(C-H…Cg1) (º)
C1-H1…Cg1 #1	0.95	2.98	3.806	147
C13-H13…Cg1 #2	0.95	2.92	3.721	143

Symmetry codes and transformation used to generate equivalent atoms:
#1 2-x, 1/2+y, 1/2-z, #2 1-x, -1/2+y, 1/2-z.

The molecular packing is stabilized by C-H…π interactions between C1-H1…Cg1[#1] **(Figure 4.4)** and C13-H13…Cg1[#2] **(Figure 4.5)**. This compound packs with parallel overlapping plates along *a, b* axis. The molecular packing along both axes is illustrated in **Figure 4.6**.

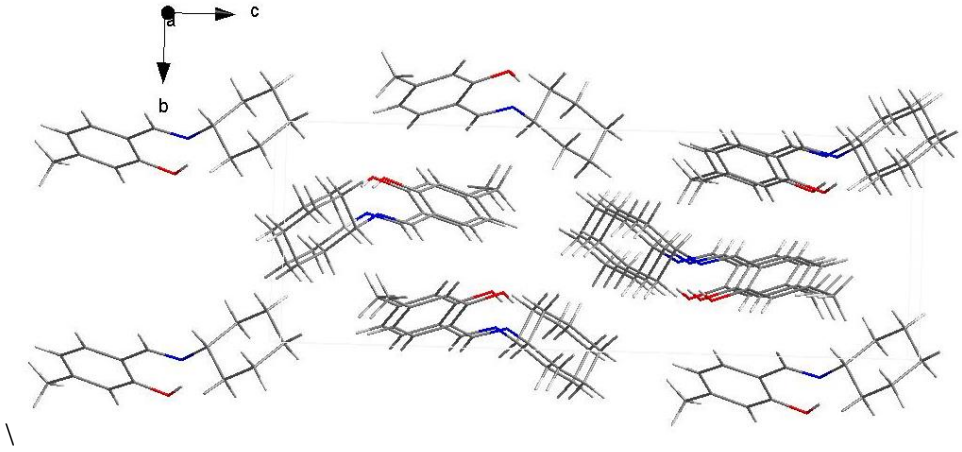

(a)

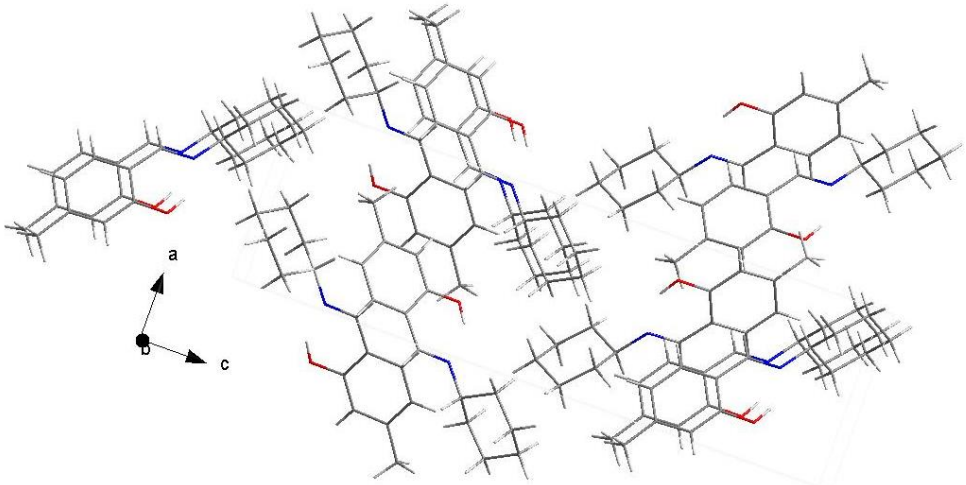

(b)

Figure 4.6: Molecular packing along (a) *a*-axis and (b) *b*-axis.

4.4 CRYSTAL STRUCTURE OF *fac*-[Re(CO)$_3$(HOCH$_3$)(5Me-Sal-Cyhex)]

The cuboid colourless crystal of *fac*-[Re(CO)$_3$(HOCH$_3$)(5Me-Sal-Cyhex)] **(2)** crystallised in the monoclinic crystal system in the *C*2/*c* space group with eight formula units per unit cell (Z = 8). The molecular structure of *fac*-[Re(CO)$_3$(HOCH$_3$)(5Me-Sal-Cyhex)] is represented in **Figure 4.7**, illustrating the numbering scheme. The most important bond lengths and bond angles are shown in **Table 4.5**. The completeness of the data, collected at 100 K indicates a value of 91% at theta$_{max}$ = 25^o, this was due to an assumed higher symmetry during data collection strategy. However the absolute configuration of the complex can still be clearly identified with well-defined thermal ellipsoids.

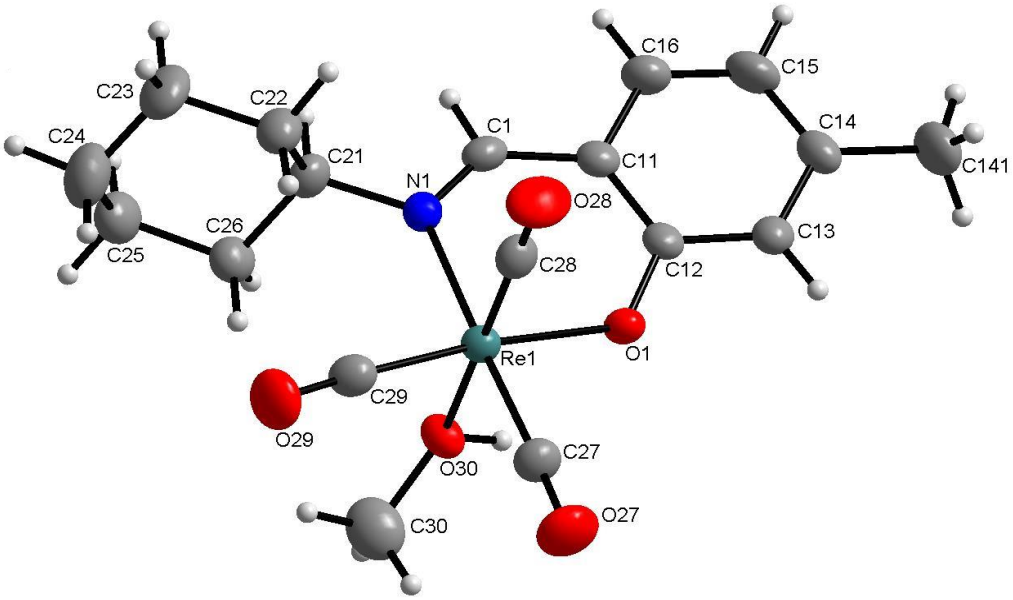

Figure 4.7: Molecular structure of *fac*-[Re(CO)$_3$(HOCH$_3$)(5Me-Sal-Cyhex)] showing the numbering scheme of the atoms. Displacement ellipsoids are drawn at 50% probability level.

Table 4.5: Selected bond distances and angles of *fac*-[Re(CO)$_3$(HOCH$_3$)(5Me-Sal-Cyhex)].

Bond distances (Å)		Bond angles (°)	
Re1-N1	2.198(5)	N1-Re1-O1	85.38(2)
Re1-O1	2.112(4)	O30-Re1-C28	175.8(2)
Re1-C29	1.886(7)	N1-Re1-C29	98.1(2)
Re1-C28	1.883(8)	O1-Re1-C27	91.6(2)
Re1-C27	1.905(7)	O1-Re1-C29	173.5(2)
Re1-O30	2.183(5)	N1-Re1-O30	84.43(2)
C1-N1	1.284(8)	Re1-C24-O29	176.4(6)
C1-C11	1.438(9)	C1-N1-C21	114.4(5)
N1-C21	1.495(8)		
O1-C12	1.335(7)		

The six membered ring formed by Re1, O1, C12, C11, C1 and N1 through the central rhenium metal centre is formed by coordination through the nitrogen atom of the imine and oxygen atom of the phenol group from 5Me-Sal group. The three tricarbonyl groups are facially coordinated to the rhenium metal centre with methanol bonded in the 6th position. The bond distance of Re1-O1 is 2.112(4) Å and lies in the bond distance range of 2.063-2.156 Å as indicated in the literature.[1,19,20,21] The bond distance of Re1-N1 is 2.198(5) Å and falls in the bond distance range of 2.152-2.199 Å of the salicylidene structures reported in the literature.[3,18,22,23] The O30-Re1-C28 bond angle (85.38(2)^o) as well as the 175.8(2)^o, 173.5(2)^o and 176.4(6)^o for O30-Re1-C28, O1-Re1-C29 and Re1-C29-O29, respectively, gives some indication of the distorted octahedral geometry of the molecule.

Plane 1 (as indicated in **Figure 4.8**) is formed by the aromatic backbone of 5Me-Sal ligand system through C11, C12, C13, C14, C15, C16, C141 and plane 2 through N1, O1, Re1, C29, O29, C27, O27, the two planes exhibits a dihedral angle of 15.585^o displaying the twist which occurs in the 5Me-Sal-Cyhex backbone. The dihedral angle of these two planes differ by ~5^o from the planes of the complexes presented by A. Brink.[27]

[20] É. Tozzo, S. Romera, M.P. dos Santos, M. Muraro, R.H. de A. Santos, L.M. Lião, L. Vizotto, E.R. Dockal, *J. Mol. Struct.*, 2008, **876**, 110.
[21] A. Bourkoula, M. Paravatou-Petsons, A. Papadopoulos, I. Santos, H.J. Pietzsch, E. Livaniou, M. Pelecanou, M. Papadopoulos, I. Pirmettis, *Eur. J. Med. Chem.*, 2009, **44**, 4021.
[22] S. Burstone, *Enzyme Histochemistry*, Academic Press, New York, 1962.
[23] J. Burgees, F. Fawcett, D.R. Russell, S.R. Gilani, V. Palma, *Acta Cryst.*, 1999, **C55**, 1707.

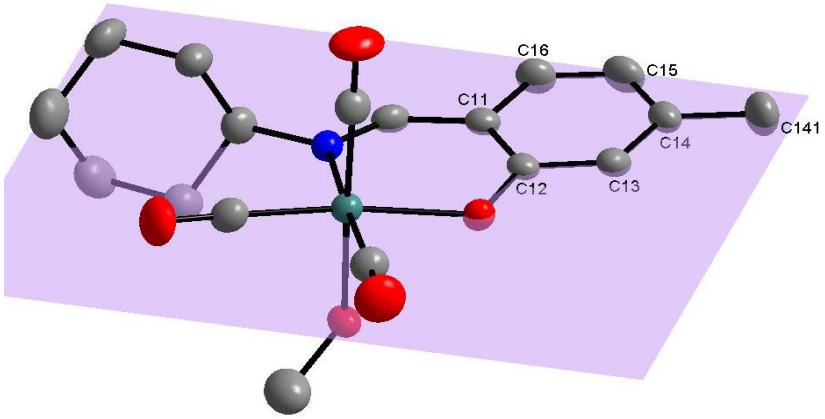

(a)

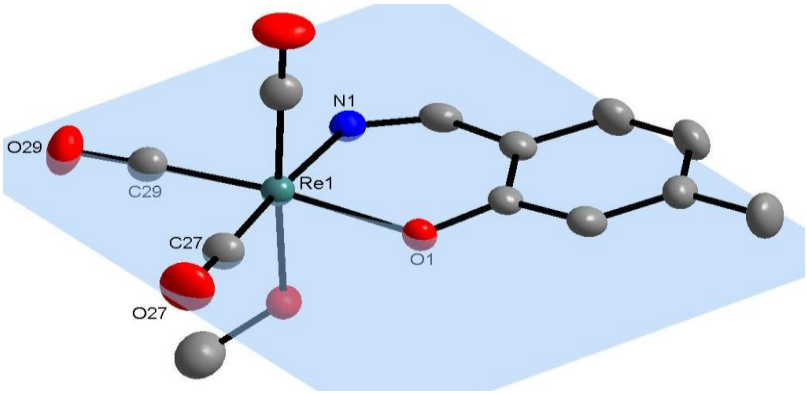

(b)

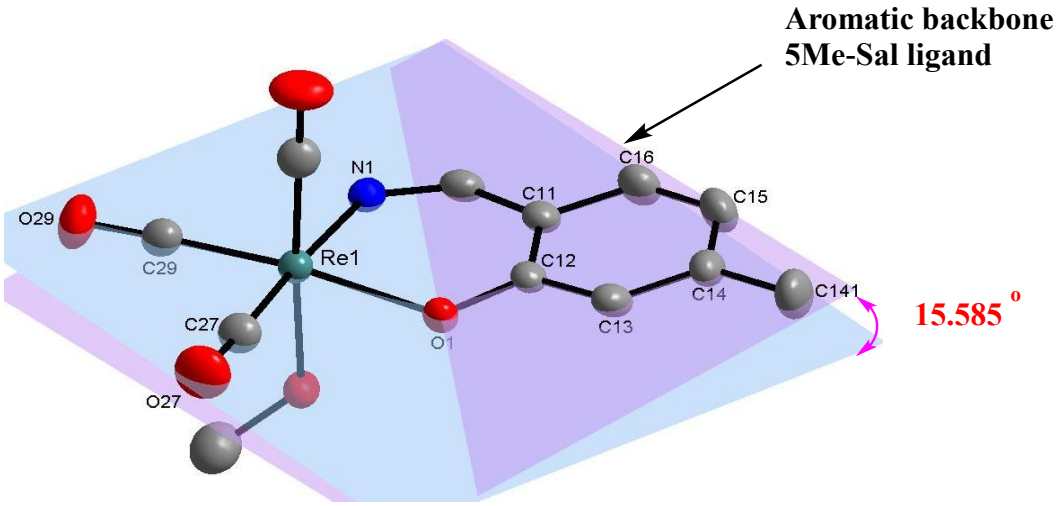

(c)

Figure 4.8: Illustration of (a) plane 1, (b) plane 2 and (c) dihedral angle between plane 1 and 2. H atoms omitted for clarity.

A strong π-π interaction occurs between two centroid rings, Cg2 and Cg2$^{\#1}$, in a unit cell, as indicated in **Table 4.6** and **Figure 4.9**.

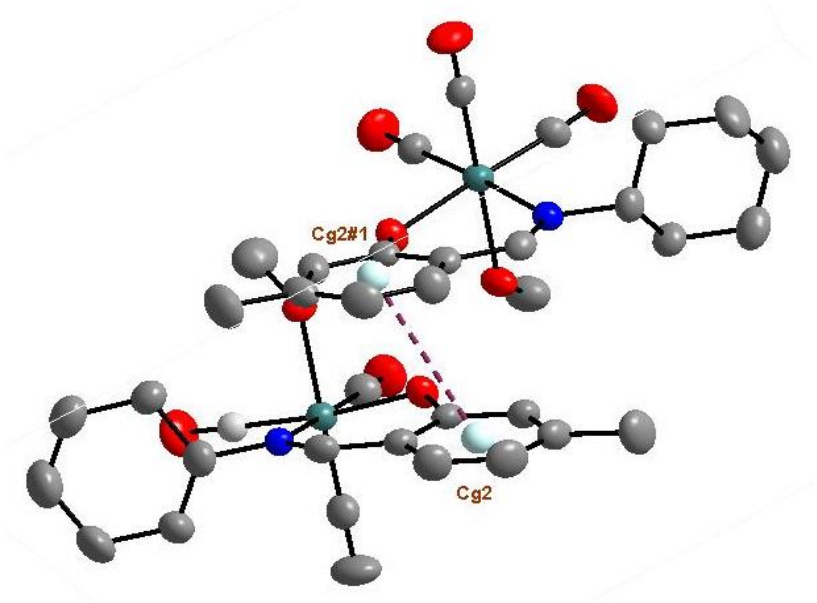

Figure 4.9: A schematic illustration of π-π interaction (purple line) with centroid atom (Cg2). H atoms are omitted for clarity.

Table 4.6: The π-π interactions of aromatic rings of the *fac*-[Re(CO)$_3$(HOCH$_3$)(5Me-Sal-Cyhex)] (2).

Centroid atom	Centroid atom	Distance between centroid atoms (Å)
Cg2	Cg2 $^{\#1}$	3.809(4)

Symmetry codes and transformations used to generate equivalent atoms:
#1 1-x, y, 1/2-z
Cg2 = centroid atom of C11, C12, C13, C14, C15, C16.

The molecule has classic hydrogen bonds **(Figure 4.10 and Table 4.7)**. The intermolecular O…O contact occurs between O1…O30$^{\#1}$, O1…O1$^{\#1}$, with bond distances of 2.606(7) and 3.194(6) Å **(Figure 4.11)**, respectively and O30…C13$^{\#1}$ with a distance of 3.323(7) Å **(Figure 4.12)**, respectively. The intermolecular O…C contact occurs between O1…C30$^{\#1}$ with distance of 3.368(11) Å **(Figure 4.11)** (Symmetry operation: #1 1-x, y, 1/2-z). The π-π interaction occurs in the aromatic (5Me-Sal ligand) ring (C11, C12, C13, C14, C15, C16).

Table 4.7: Classical hydrogen bond of the *fac*-[Re(CO)$_3$(HOCH$_3$)(5Me-Sal-Cyex)] (2).

O-H…O	d(O-H) (Å)	d(H…O) (Å)	d(O…O) (Å)	<(O-H…O) (°)
O30-H30…O1$^{\#1}$	0.99(5)	1.63(6)	2.606(7)	165

Symmetry codes and transformation used to generate equivalent atoms:
#1 1-x, y, ½-z

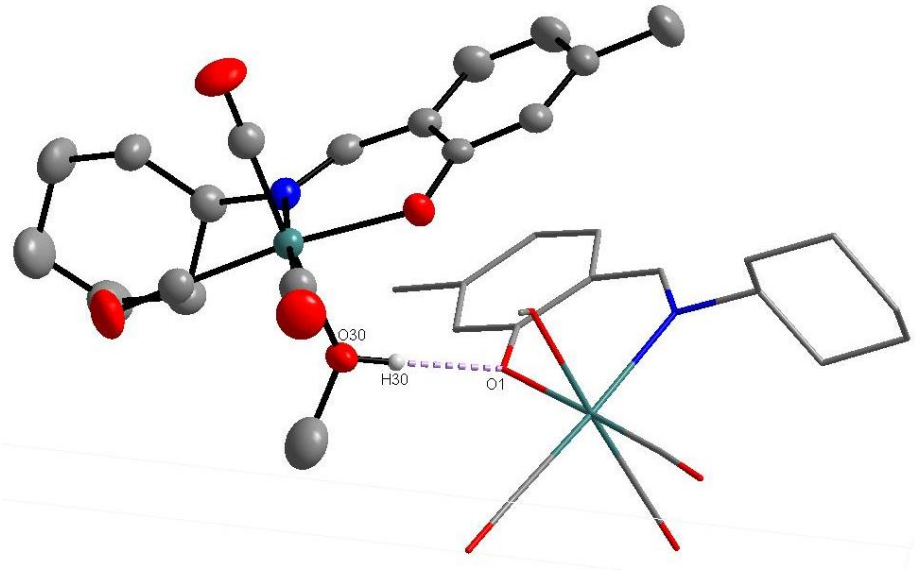

Figure 4.10: Classic intermolecular hydrogen bond of *fac*-[Re(CO)$_3$(HOCH$_3$)(5Me-Sal-Cyhex)] (2).

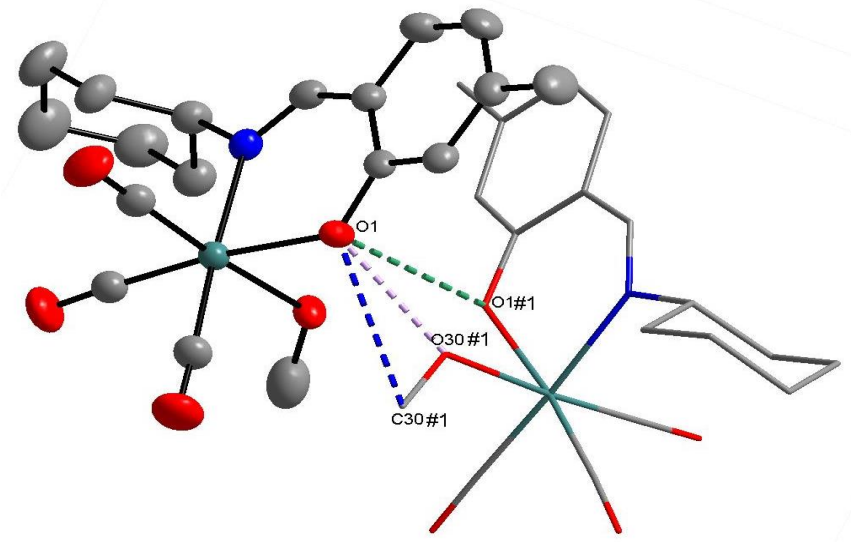

Figure 4.11: Intermolecular contact of O1…O1$^{\#1}$ (green line), O1…O30$^{\#1}$ (purple line) and O1…C30$^{\#1}$ (blue line). H atoms are omitted for clarity of the structure.

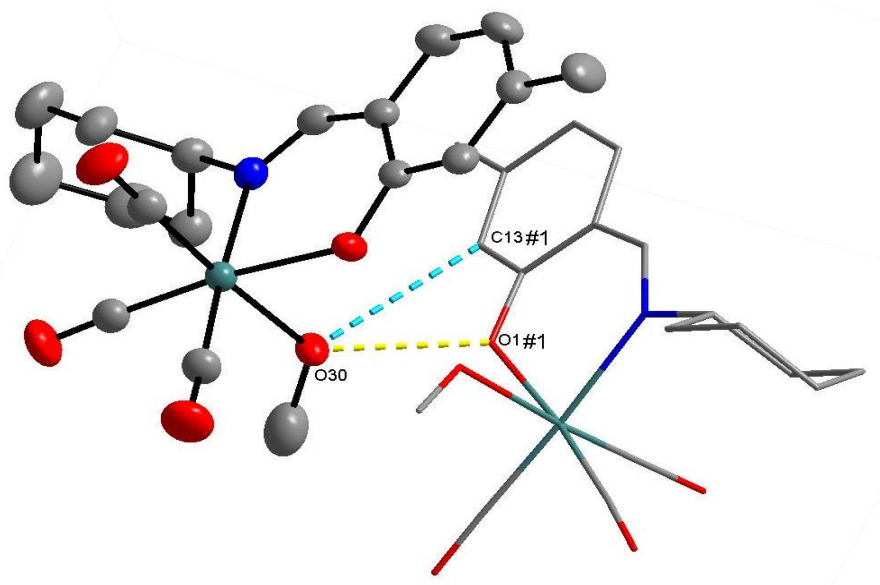

Figure 4.12: Intermolecular contact of O30…O1$^{\#1}$ (yellow line) and O30…C05$^{\#1}$ (light blue line). H atoms are omitted for clarity of the structure.

The molecular packing along *c*-axis shows π-π interaction on the aromatic group of adjacent molecules and there occurs parallel packing of the cyclohexyl ring system **(Figure 4.13)**.

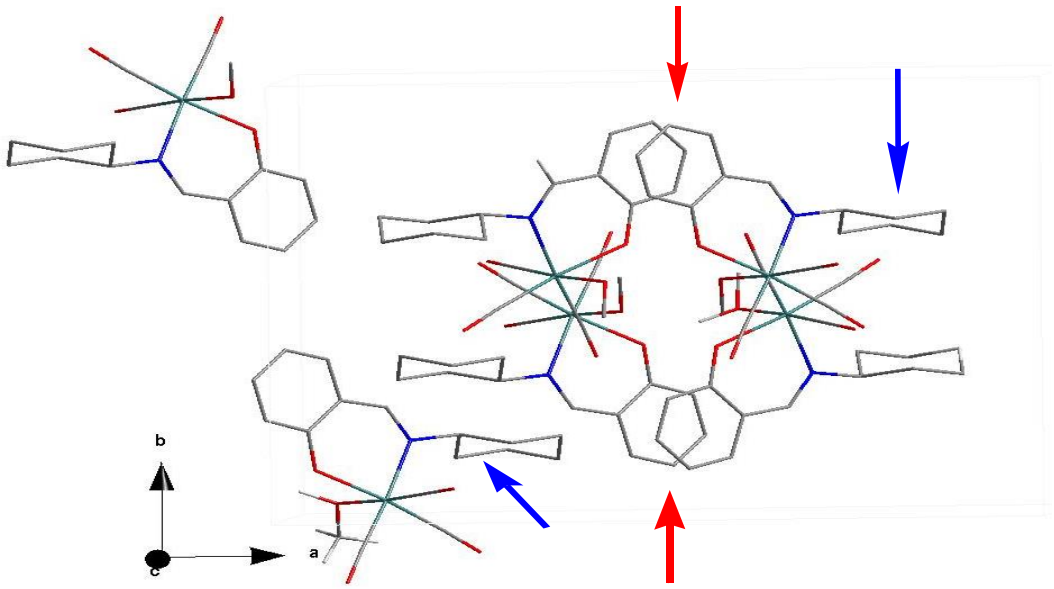

Figure 4.13: Molecular packing along *c*-axis showing π-π interactions (red arrow) and parallel packing of the cyclohexyl ring (blue arrow). All H atoms are omitted for clarity.

4.5 CRYSTAL STRUCTURE OF *fac*-[Re(CO)$_3$(Imid)(5Me-Sal-Cyhex)]

The cuboid colourless *fac*-[Re(CO)$_3$(Imid)(5Me-Sal-Cyhex)] **(3)** crystallize in the monoclinic crystal system in the non-standard space group, $P2_1/n$ with a combined figure of merit (CFOM) of 2.7. The refinement of the structure is unstable in the standard space group setting, i.e. $P2_1/c$ and is therefore retained in $P2_1/n$ space group. Four rhenium molecules crystallize in the unit cell (Z = 4). This crystal contains a large electron density peak (1.929 e.A^{-3}), which lies 0.86 Å from the Re1 metal centre. The molecular structure of *fac*-[Re(CO)$_3$(Imid)(5Me-Sal-Cyhex)] is represented in **Figure 4.14**, illustrating the numbering scheme. The bond lengths and bond angles are packed in **Table 4.8**.

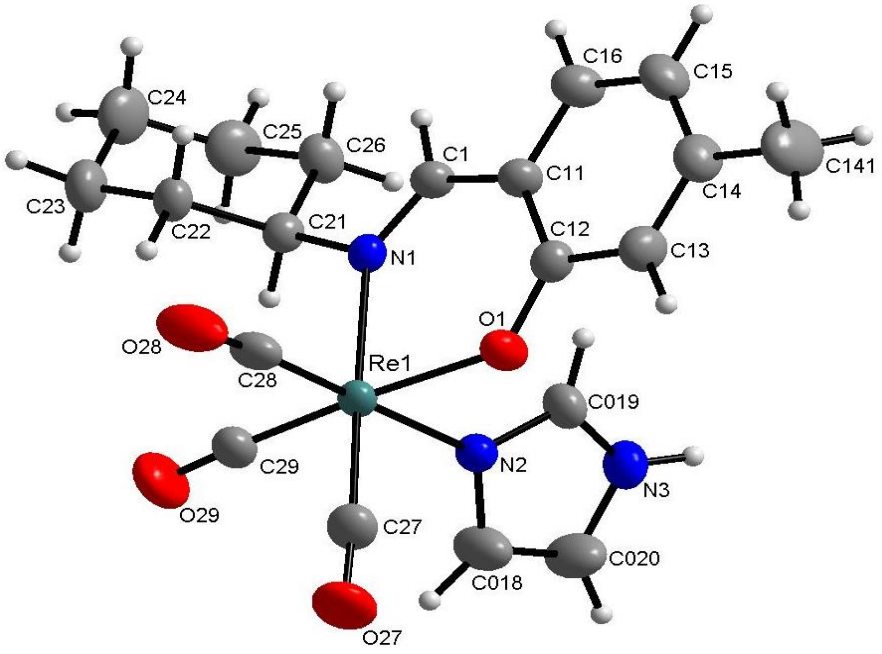

Figure 4.14: Molecular structure of *fac*-[Re(CO)$_3$(Imid)(5Me-Sal-Cyhex)] showing the numbering scheme of the atoms. Displacement ellipsoids are drawn at 50% probability level.

Table 4.8: Selected bond distances and angles of *fac*-[Re(CO)$_3$(Imid)(5Me-Sal-Cyhex)] (3).

Bond distances (Å)		Bond angles (°)	
Re1-N1	2.181(4)	N1-Re1-O1	84.75(1)
Re1-O1	2.123(4)	N2-Re1-C28	178.6(2)
Re1-C29	1.881(6)	N1-Re1-C29	96.1(2)
Re1-C28	1.911(6)	O1-Re1-C27	94.5(2)
Re1-C27	1.912(6)	O1-Re1-C29	175.6(2)
Re1-N2	2.185(4)	N1-Re1-N2	86.49(2)
C1-N1	1.293(6)	Re1-C24-O29	177.3(5)
C1-C11	1.447(7)	C1-N1-C21	116.2(4)
N1-C21	1.509(6)		
O1-C16	1.318(6)		

The central rhenium metal atom is coordinated with nitrogen atom of the imine and oxygen atom of the hydroxyl group attached to phenol group to form a six membered ring. The three tricarbonyl atoms coordinate facially to the rhenium metal centre and imidazole is coordinated in the final 6th position. The Re1-O1, Re1-N1 and Re1-N2 bond distances of 2.123(4) Å, 2.181(4) Å and 2.185(4) Å, are compared to other N,O ligand-to-metal bond distances and lies in the range of 2.099-2.1844 Å for Re-O bond and 2.162-2.186 Å for Re-N bond.[1,4,24,25,26] This compound **(3)** has a distorted octahedral geometry as indicated by N1-Re1-O1 bond angle of 84.75(1)^o and N2-Re1-C28 bond angle of 178.6(2)^o which deviates from the ideal 90 ^{o} and 180 ^{o} angle.

The dihedral angle between the aromatic backbone of 5Me-Sal ligand (plane 1: C11, C12, C13, C14, C15, C16) and plane 2: N1, O1, Re1, C29, C27. The 5-membered ring of imidazole is rotated perpendicular to Re1 equatorial plane (plane 2). The following three planes have been defined for compound **(3)** in order to investigate the orientations of the ligands:

[24] R. Czerwieniec, A. Kapturkiewicz, R. Anulemicz-Ostrowska, J. Nowacki, *J. Chem. Soc.*, 2002, 3434.
[25] M. Schutte, H.G. Visser, *Acta Cryst.*, 2008, **E64**, m1226.
[26] M. Schutte, H.G. Visser, A. Roodt, *Acta Cryst.*, 2008, **E64**, 1610.

a) Plane 1: formed with atoms, C11, C12, C13, C14, C15, C16. (Aromatic backbone of 5Me-Sal ligand)

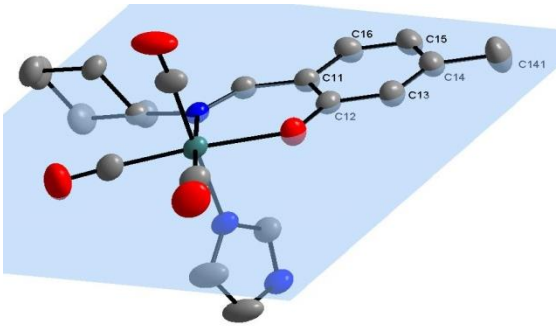

b) Plane 2: formed with atoms, N1, O1, Re1, C29, C27.

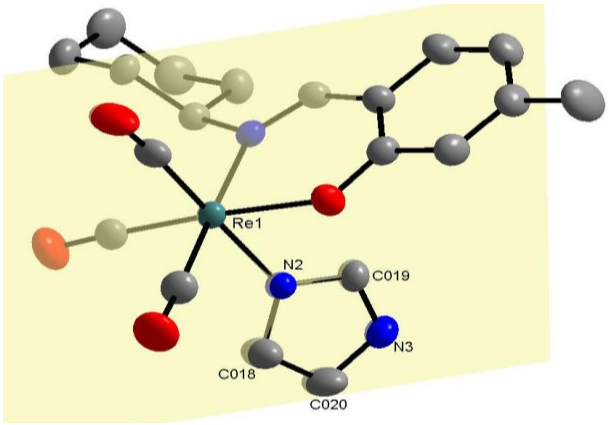

c) Plane 3: formed with atoms, Re1, N2, C018, C020, N3, C019.

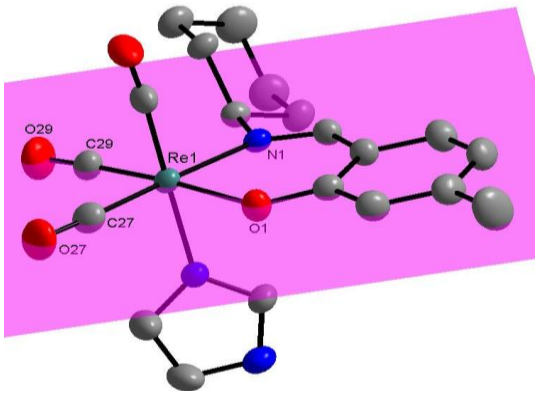

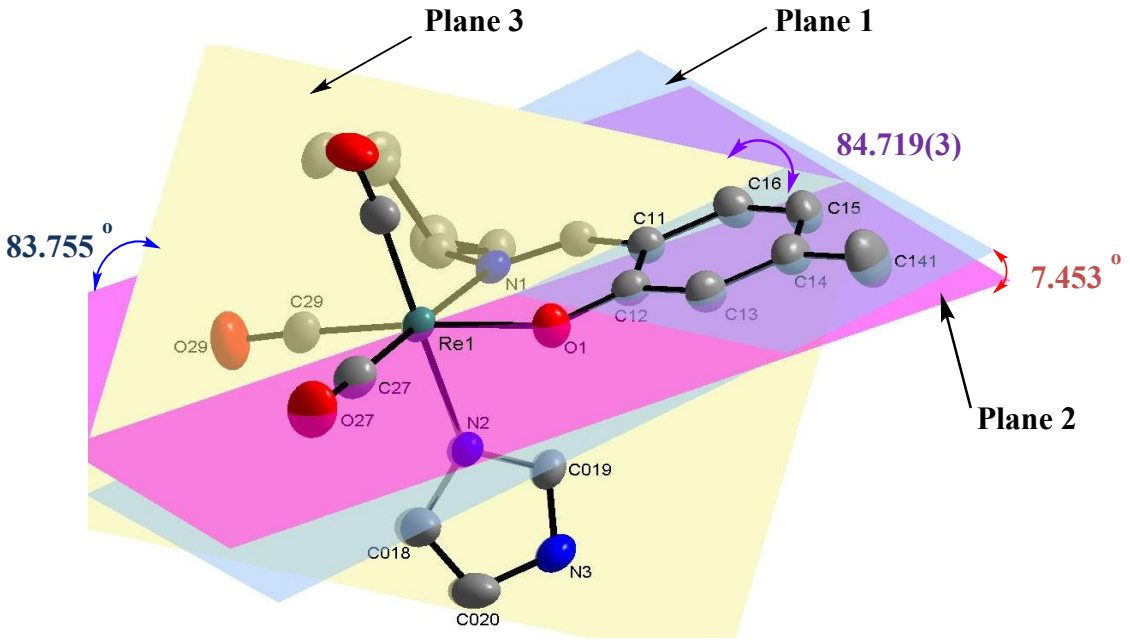

Figure 4.15: Illustration of the dihedral angle between plane 1 and 2 (blue arrow), plane 2 and 3 (purple arrow) and plane 1 and 3 (red arrow).

The π-π interaction occur between two centroid rings, Cg1 (N2, C019, C018, C020, N3) and Cg2 (Re1, O1, C16, C1, C11, N1). This interaction is indicated in **Figure 4.16** and the bond distance is shown in **Table 4.9**. (Symmetry operation: x, y, z)

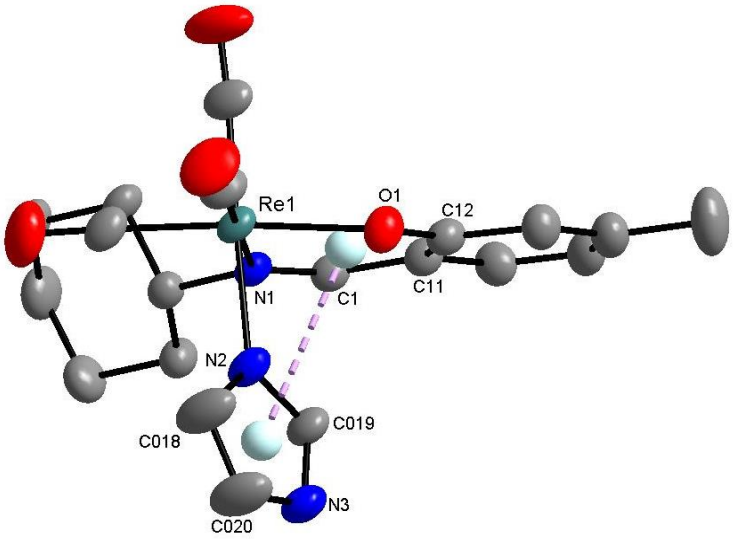

Figure 4.16: A schematic illustration of a π-π interaction with a centroid atoms (Cg1 and Cg2). All H atoms are omitted for clarity.

Table 4.9: The π-π interaction of the compound (3).

Centroid atom	Centroid atom	Distance between centroid atoms (Å)
Cg2	$Cg1^{\#1}$	3.815(4)

Symmetry codes and transformations used to generate equivalent atoms:
#1 x, y, z

Intermolecular hydrogen bond occurs as C019-O019…$Cg2^{\#1}$ (Cg2 = Re1, O1, C16, C11, C1, N1) and C13-H13E…$Cg3^{\#2}$ (Cg3 = C11, C12, C13, C14, C15, C16) with six membered ring represented by the centroid atoms as indicated in **Figure 4.17** and **4.18**, and all bond distances are indicated in **Table 4.10**. (Symmetry codes $^{\#1}$ x, y, z and $^{\#2}$ 1-x, -y, 1-z)

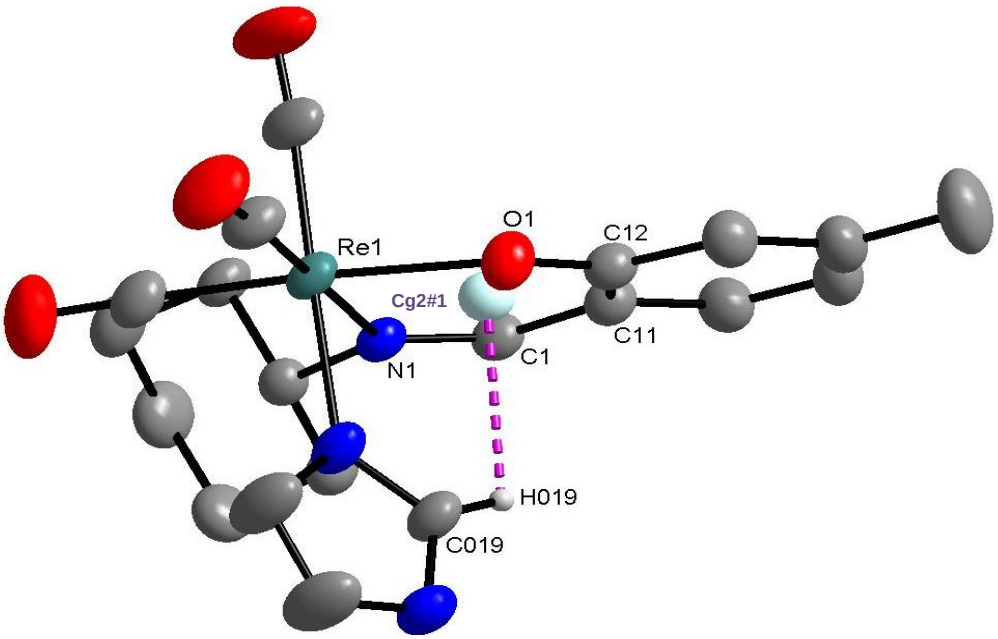

Figure 4.17: A schematic illustration of C-H…π interaction (purple dotted line). All H atoms are omitted for clarity.

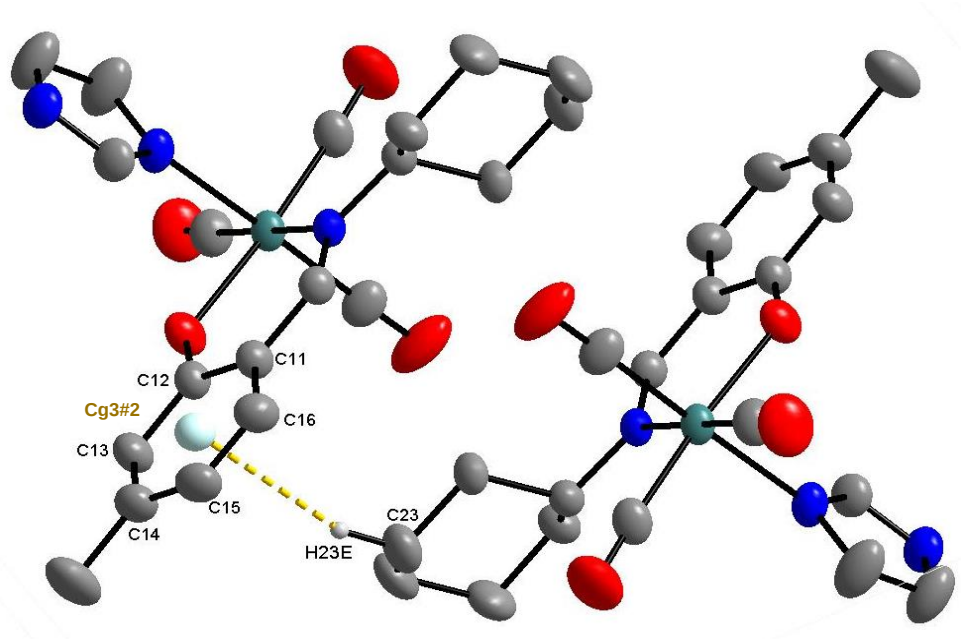

Figure 4.18: A schematic illustration of C-H…π interaction showing C23-H23E…Cg3$^{\#2}$ (purple dotted line). All H atoms are omitted clarity.

Table 4.10: The C-H…π interaction of the compound (3).

C-H…Cg	d(C-H)	d(H…Cg)	d(D…Cg)	<(C-H…Cg)
C019-H019…Cg2$^{\#1}$	1.09	2.55	3.020(7)	111
C23-H23E…Cg3$^{\#2}$	0.97	2.85	3.796(8)	161

Symmetry code and transformations used to generate equivalent atoms:
#1 x, y, z.
#2 1-x, -y, 1-z.
Cg2 = Re1, O1, C16, C11, C1, N1 and Cg3 = C11, C12, C13, C14, C15, C16.

The C-O…Cg interaction occur between O and the centroid ring, Cg1 (N3, C020, C018, N2, C019) as indicated in **Figure 4.19** and **Table 4.11**. This interaction occurs similarly compared to interaction presented by A. Brink[27] with the O…π distance of 3.42-3.81 Å and the C-O…π angle of <93^{o}.

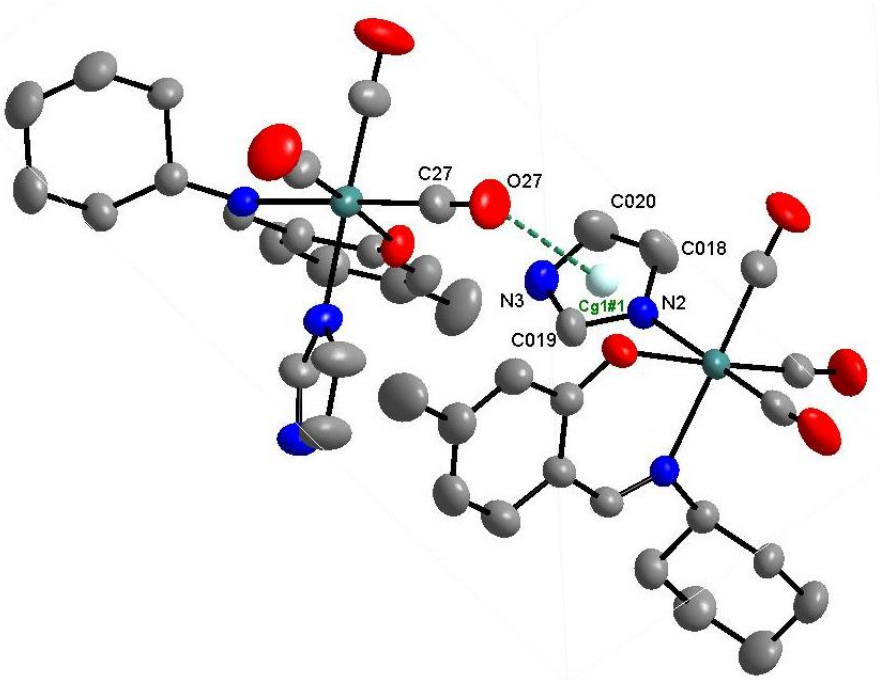

Figure 4.19: Illustration of C-O…Cg interaction (green dotted line). All H atoms are omitted for clarity.

Table 4.11: The C-O…Cg interaction of the compound (3).

C-O…Cg	d(C-O)	d(O…Cg)	d(C…Cg)	<(C-O…Cg)
C27-O27…Cg1$^{\#1}$	1.154	3.436(6)	3.673(7)	93

Symmetry code and transformations used to generate equivalent atoms:
#1 x, y, z.

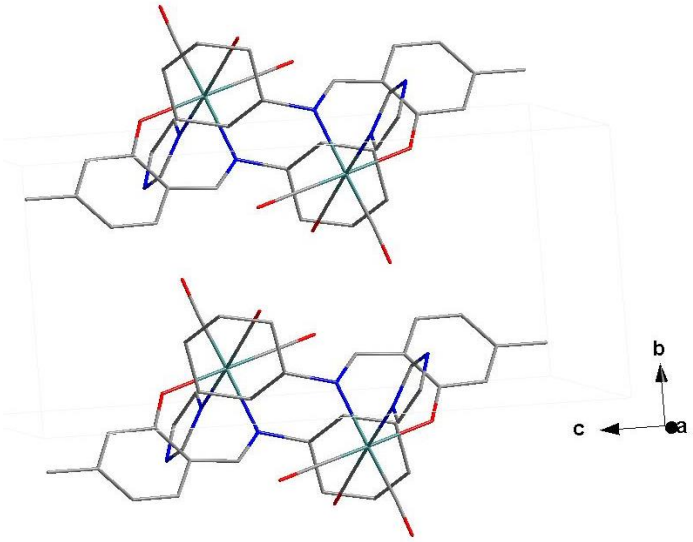

Figure 4.20: Molecular packing along *a*-axis.

The π-π interaction stabilizes the molecular packing of the compound in the unit cell. The π-π interaction and parallel overlapping plates occur along *b*-axis.

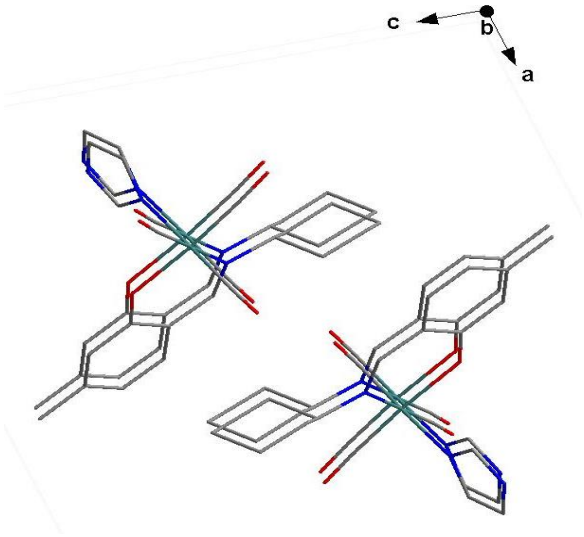

Figure 4.21: Molecular packing along *b*-axis.

The molecular packing along *c*-axis shows π-π interaction between the aromatic rings of the 5Me-Sal backbone.

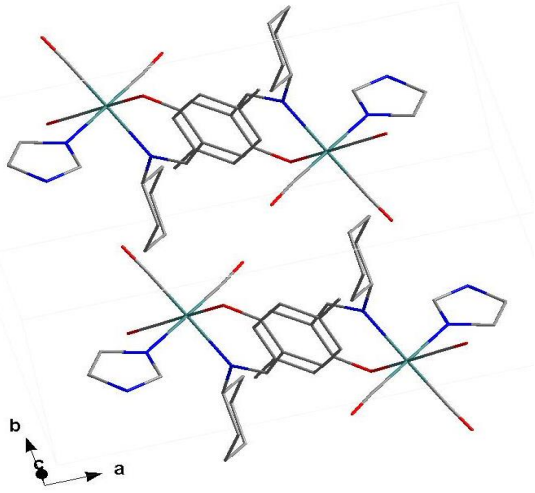

Figure 4.22: Molecular packing along *c*-axis.

4.6 CONCLUSION

The *N*,O-bidentate (Schiff base) ligand, 5-methyl-(2-cyclohexyliminomethyl)phenol, produced in this study is used as a coordinating ligand for *fac*-$[M(CO)_3]^+$ moieties (M = Re,Tc). In this chapter, the crystal structures of 5Me-Sal-Cyhex **(1)**, *fac*-$[Re(CO)_3(HOCH_3)$(5Me-Sal-Cyhex)] **(2)** and *fac*-[Re(CO)$_3$(Imid)(5Me-Sal-Cyhex)] **(3)** are fully discussed. The Schiff base ligand crystallizes in $P2_12_12_1$ and this similar to other reported salicylidene compounds.[27] It falls under the salicylidene ligand group with methyl substituent on the aromatic ring and is a non-planar with the dihedral angles of 2.975(4)^o between plane 1 and 2 (plane1 = C11, C12, C13, C14, C15, C16 and plane 2 = O1, C12, C11, C1, N1), 89.739(2)^o between plane 1 and 3 (plane 3 = C21, C22, C23, C24, C25, C26) and 88.368(3)^o resulting the rotation around the –C=N- bond. This compound is comparable to SalH-mTol[3] which is non-planar. The 5Me-Sal-Cyhex compound has bond distance of C1-N1 atoms as 1.272(2) Å indicating the double bond and this is comparable to C1-N1 bond distance (1.287(3) Å) of the compound (5Me-Sal-mTol) in Brink *et al.*[3] The 5Me-Sal-Cyhex compound has intermolecular interactions, C-H…Cg with centroid ring, Cg and this compound has no π-π interactions occurring.

The crystal structures of all rhenium tricarbonyl complexes crystallizes in a space group of *C*2/*c* for *fac*-[Re(CO)$_3$(HOCH$_3$)(5Me-Sal-Cyhex)] **(2)** and $P2_1/n$ for *fac*-[Re(CO)$_3$(Imid)(5Me-Sal-Cyhex)] **(3)**. Compound **(2)** has a dihedral angle of 15.585^o between plane 1 and plane 2 (plane 1: C11, C12, C13, C14, C15, C16 and plane 2: N1, O1, Re1, C29, C27) which is nearly twice as the dihedral angle of compound **(3)** (7.5343^o between plane 1 and 2). The octahedron geometry around Re(I) centre of compound **(2)** is distorted as indicated by N1-Re1-O1 bond angle of 85.38(2)^o and the distortion of compound **(3)** is indicated by N1-Re1-O1 bond angle of 84.75(1)^o. Both of these compounds have π-π interactions and are discussed above. Compound **(2)** has intermolecular O…O contacts with different bond distances. Compound **(3)** has the intermolecular hydrogen bond C-H…π interactions and C-O…π interactions. The interactions of all three crystal structures are discussed in full detail and are clearly shown in figures. All hydrogen bonds of the crystal structures are also discussed and tabulated, and all the planes are drawn with facial atoms to obtain dihedral angles of crystal structures obtained. The crystallographic study gathered in

[27] A. Brink, PhD Thesis, University of the Free State, Bloemfontein, South Africa, 2011.

this chapter is an addition to data available in the Crystallographic Structural Database[28], where none of the rhenium(I) tricarbonyl complexes coordinated with ligand containing 5-methyl-(2-cyclohexyliminomethyl)phenol (5Me-Sal-Cyhex) ligand system have been reported previously.

[28] Cambridge Structural Database (CSD), Version 5.37, Nov 2015 update. F.H. Allen, *Acta Cryst.*, 2002, **B58**, 380. Accessed on 06-04-2016 at 02h37 pm.

5 KINETIC STUDY OF Re(I) TRICARBONYL COMPLEXES WITH BIDENTATE LIGANDS

5.1 INTRODUCTION

Chemical kinetics is the study of the time dependence of a chemical reaction. It focuses on the manner in which a system alternates from one state to another and the time it takes for the transition. Chemical kinetics monitor reaction rates and focuses on all factors that may affect the reaction rate, such as concentration, temperature, homogeneity of the system, etc. Kinetics also considers how the rate can be described by utilizing the complete reaction mechanism. It provides a statistical average state of the molecules of a compound that participated in the chemical reaction.[1,2]

This chapter focuses on the chemical kinetic analysis of the formation of the complexes, *fac*-$[M(CO)_3(X)(L,L'\text{-bid})]^n$ (M = Re(I), *L,L'*-bid = *N,O*-, *N,N'*-bidentate ligands such as Schiff bases or ethylenediamine and X = MeOH), that may be utilized as models in the study of radiopharmaceuticals. As mentioned in Chapter 1, the aim of this study is to develop new complexes that can be utilized as models in radiopharmaceutical design and Chapter 2 provides the known labelling techniques of radiopharmaceuticals described in literature. The labelling method of radiopharmaceuticals used is the [2+1] mixed ligand approach,[3] this approach provides the possibility of the coordination of mono-, bi- or tridentate ligands with a metal complex, *fac*-$[M(CO)_3]^+$. The labelling of a radiopharmaceutical is critically dependent on the kinetic behaviour of the complexes.[4]

The purpose of conducting the kinetic analysis is to gain information on reactivity, stability and the mechanistic behaviour of the formation reaction of metal complex, *fac*-$[M(CO)_3(X)(L,L'\text{-bid})]^n$ (M = Re(I), *L,L'*-bid = *N,O*- and *N,N'*-bidentate ligands such as Schiff bases or ethylenediamine and X = MeOH). This will assist towards determining the

[1] K.A. Connors, *Chemical Kinetics: The Study of Reaction Rates in Solution*, VCH Publisher, New York, 1990.
[2] J.W. Moore, R.G. Pearson, *Kinetics and Mechanism*, 3rd Ed, New York, John Wiley and Sons Ltd, 1981.
[3] S. Mundwiler, M. Kündig, K. Ortner, R. Alberto, *Dalton Trans.*, 2004, 1320.
[4] R. Alberto, R. Schibli, A. Egli, P.A. Schubiger, W.A. Herrmann, G. Artus, U. Abram, T.A. Kaden, *J. Org. Chem.*, 1995, **493**, 119.

time required for radiopharmaceutical design, proper labelling systems involving many variables which may affect the formation and predicting the stability of labelled complexes.

^{99m}Tc and $^{186/188}$Re radionuclides are used in diagnostic and therapeutic nuclear medicine applications and their chemical behaviour should be kinetically understood. The chemical kinetics and reaction mechanism are studied to characterize the metal complexes that are created for the development of radiopharmaceuticals, understand the factors that may affect biodistribution, influence the formation and kinetic stability of the complex of interest.[5,6]

5.2 EXPERIMENTAL

5.2.1 GENERAL PROCEDURE

All chemicals and reagents used were of analytical grade, except the dry methanol which was prepared according to literature[7] and *fac*-$[NEt_4]_2[Re(CO)_3(Br)_3]$ – **[ReAA]** was synthesized as described in Chapter 3. Preliminary UV/Vis measurements were performed on a Varian Cary 50 Conc UV-Vis spectrophotometer, equipped with a Julabo F12-mV temperature cell regulator (accurate within 0.1^{o}C) in a 1.000±0.001 cm quartz cuvette cell. The stability tests for all chemical reactions were performed on the UV-Vis spectrophotometer. The metal complex and the ligands were observed to be stable in methanol over at least a 48 hour period. For the kinetic analysis, the ligand concentrations were used in excess in all chemical reactions. The *in situ* analysis of the reactants and products was performed on a ^{1}H FT-NMR Bruker AXS 600 MHz and 300 MHz spectrometers at 25^{o}C, with ethylenediamine [en] = 0.002 M and [ReAA] = 0.001 M in dry CD_3OD (3.31 ppm and 4.78 ppm). All chemical shifts are reported in ppm. The dry CD_3OD was prepared (or stored) on molecular sieves under dry conditions.[7]

[5] A. Roodt, A. Abou-Hamdan, H.P. Englebrecht, A.E. Merbach, *Advances in Inorganic Chemistry*, 2000, **49**, 59.
[6] E.A. Deutsch, K. Libson, J.L. Van der Heyden, *In Technetium and Rhenium in Chemistry and Nuclear Medicine*, Eds: M. Nicolini, G. Bandoli, U. Mazzi, Raven Press, New York, 1990, 13.
[7] D.D. Perrin, W.L.F. Armarego, *Purification of Laboratory Chemicals*, 3rd Ed, London, Bitterworth-Heinemann Ltd, 1998.

5.2.2 CHEMICAL KINETICS

5.2.2.1 Equipment and Procedure

The kinetic analysis of the reaction between ReAA with ethylenediamine was performed on a Varian Cary 50 Conc UV-Vis spectrophotometer. *Pseudo* first-order reaction conditions were used for all kinetic measurements. The formation reaction between ethylenediamine and ReAA was conducted with [ReAA] = $1x10^{-4}$ M and [en] = 0.03, 0.05, 0.07, 0.10 and 0.15 M. This reaction was monitored at λ = 280 nm, at 14.8^{o}C, 25.2^{o}C, 35.0^{o}C and 45.0^{o}C in dry methanol.

The preliminary ^{1}H NMR kinetic analysis was performed on Bruker AXS 600 MHz and 300 MHz spectrometers at 25^{o}C. The formation reaction between ReAA and ethylenediamine was conducted with [ReAA] = 0.001 M and [en] = 0.002 M in dry CD_3OD.

The programs utilized to fit the data to appropriate equations were Scientist Micromath,[8] Version 2.011 and Microsoft Office Excel 2010.[9] The solid lines on the figures represent the least-squares fit of the data while individual data points represent the actual experimental values, illustrated by selected symbols.

5.2.2.2 Treatment of Data

The experimental kinetic data obtained were fitted to the equations, as given below, in order to evaluate the results obtained during the chemical kinetics studies. From Appendix A, the Beer-Lambert's law is denoted by

$$A = \varepsilon bc \qquad \text{Eq 5.1}$$

The Beer's law equation is integrated and incorporated into the first-order exponential, as given below in Eq 5.4.

For a simple first-order reaction as in Eq 5.2 (L = entering ligand), the rate law is given in Eq 5.3

$$M \xrightarrow{k + [L]} N \qquad \text{Eq 5.2}$$

[8] MicroMath Scientist for Windows, Version 2.01, Copyright © 1986-1995, MicroMath
[9] Microsoft Office Excel, Version 14.0.7166.5000, Copyright © 2010, Microsoft Corporation.

$$\frac{-d(M)}{dt} = k[M][L], \text{ where } k_{obs} = k_1[L] \text{ when } [L] >> [M] \qquad \text{Eq 5.3}$$

Upon integration and utilizing time resolved UV/Vis absorbance data, or NMR signal integration data, the first-order rate constant is obtained from Eq 5.4 via non-linear least-squares fitting

$$A_{obs} = A_\infty - (A_\infty - A_o)e^{k_{obs}t} \qquad \text{Eq 5.4}$$

Eq 5.4 is written in terms of Beer's law, where

A_{obs} = observed absorbance at a specific wavelength/NMR signal integrates at a fixed chemical shift, A_∞ = final absorbance and A_o = initial absorbance

The *pseudo* first-order constant, k_{obs} was calculated from the least-squares fit of absorbance versus time data to Eq 5.4. The rate constants obtained are reported in Appendix C, with the rate data given further below.

The Eyring equation was used to calculate the activation parameters, standard enthalpy change of activation ($\Delta H^{\neq}$) and standard entropy change of activation ($\Delta S^{\neq}$). The logarithmic form of the Eyring equation is expressed by:

$$\ln\frac{k}{T} = \ln\frac{k_B}{h} - \frac{\Delta H^{\neq}}{RT} + \frac{\Delta S^{\neq}}{R} \qquad \text{Eq 5.5}$$

where the graph of $\ln\frac{k}{T}$ vs. $\frac{1}{T}$ gives a slope of $-\frac{\Delta H^{\neq}}{T}$ and an intercept of $\ln\frac{k_B}{h} + \frac{\Delta S^{\neq}}{R}$; k_B is the Boltzmann constant and h is Planck's constant.

5.2.2.3 Formation of *fac*-[Re(CO)$_3$(X)(*L,L'*-bid)] Complexes

The reaction of the coordination of the *N,O*- or *N,N'*- bidentate ligands to the Re(I) tricarbonyl complex was studied kinetically. The reaction utilizes the *fac*-$[M(CO)_3]^+$ core from *fac*-$[NEt_4]_2[Re(CO)_3(Br)_3]$ **(ReAA)** coordinated by a general *L,L'*-bidentate ligand as entering moiety. This chemical reaction is expressed by

$$\underset{\textbf{ReAA}}{fac\text{-}[NEt_4]_2[Re(CO)_3(Br)_3]} + L,L'\text{-}bid \underset{k_{-1}}{\overset{k_1,\, K_1}{\rightleftharpoons}} fac\text{-}[Re(CO)_3(X)(L,L'\text{-bid})], \text{ where X = MeOH/Br}^- \qquad \text{Eq 5.6}$$

The rate of this reaction is denoted by

$$\text{Rate} = k_1[\text{ReAA}][L,L'\text{-bid}] - k_{-1}[fac\text{-}[\text{Re(CO)}_3\text{(X)}(L,L'\text{-bid})]] \quad \text{Eq 5.7}$$

In Eq 5.7, k_1 represents the forward reaction and k_{-1} the reverse reaction. ReAA is the reactant complex whilst *L,L'*-bid is an entering ligand and *fac*-[Re(CO)$_3$(R)(*L,L'*-bid)] is the final product complex. By using *pseudo* first-order conditions with [*L,L'*-bid] >> [ReAA], eq 5.7 gives:

$$k_{obs} = k_1[L,L'\text{-bid}] + k_{-1} \quad \text{Eq 5.8}$$

where k_{obs} is the observed rate constant. For an equilibrium reaction, the equilibrium constant, K_1, is given by;

$$K_1 = \frac{k_1}{k_{-1}} \quad \text{Eq 5.9}$$

5.3 RESULTS

5.3.1 PRELIMINARY EVALUATION OF FORMATION OF *fac*-[Re(CO)$_3$(MeOH)(5Me-Sal-Cyhex)]

The aim of the kinetic investigation is based on analysing the reaction between *fac*-[NEt$_4$]$_2$[Re(CO)$_3$(Br)$_3$] **(ReAA)** and *N,O*-bidentate ligands, specifically using examples of Schiff base ligands. This analysis attempts to monitor if there is one, two or multi-coordination of the Schiff base ligands coordinated to the metal core, *fac*-[M(CO)$_3$]$^+$. The ligand may coordinate to *fac*-[M(CO)$_3$]$^+$ by two ways namely, by binding in a bidentate fashion to the *fac*-[M(CO)$_3$]$^+$ core and/or by binding to the sixth position in a monodentate fashion as illustrated by **Figure 5.1**.[10]

[9] T.D. Marake, MSc Dissertation, University of the Free State, Bloemfontein, 2014.

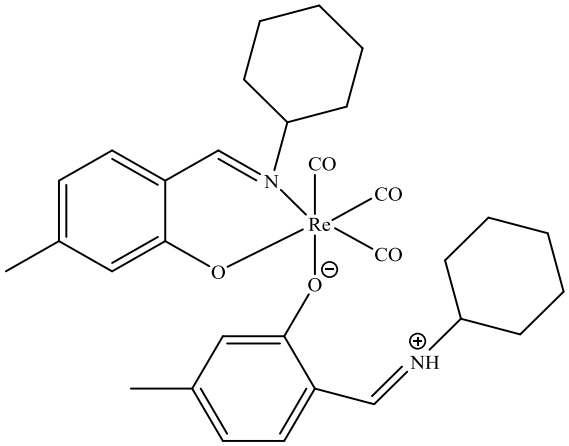

Figure 5.1: Illustration of the possible bidentate coordination and sixth position substitution of the Schiff base ligand to *fac*-$[M(CO)_3]^+$ core, assuming an excess in the ligand concentration.

The kinetic analysis of the reaction between *fac*-$[NEt_4]_2[Re(CO)_3(Br)_3]$ **(ReAA)** and the Schiff base ligand (5-methyl(2-cyclohexyliminomethyl)phenol – 5Me-Sal-Cyhex was firstly evaluated under *pseudo* first-order conditions, where the smallest ligand concentration is at least 10 times more than the concentration of the metal complex, *fac*-$[NEt_4]_2[Re(CO)_3(Br)_3]$.

Figure 5.2 illustrates a stacked UV/Vis plot of absorbance *vs* wavelength of the formation reaction between ReAA and 5Me-Sal-Cyhex in dry methanol at 25.0^{o}C. The reaction could not be studied on the UV-Vis spectrophotometer because the absorbance change was quite small, see below in **Figure 5.2(c)**.

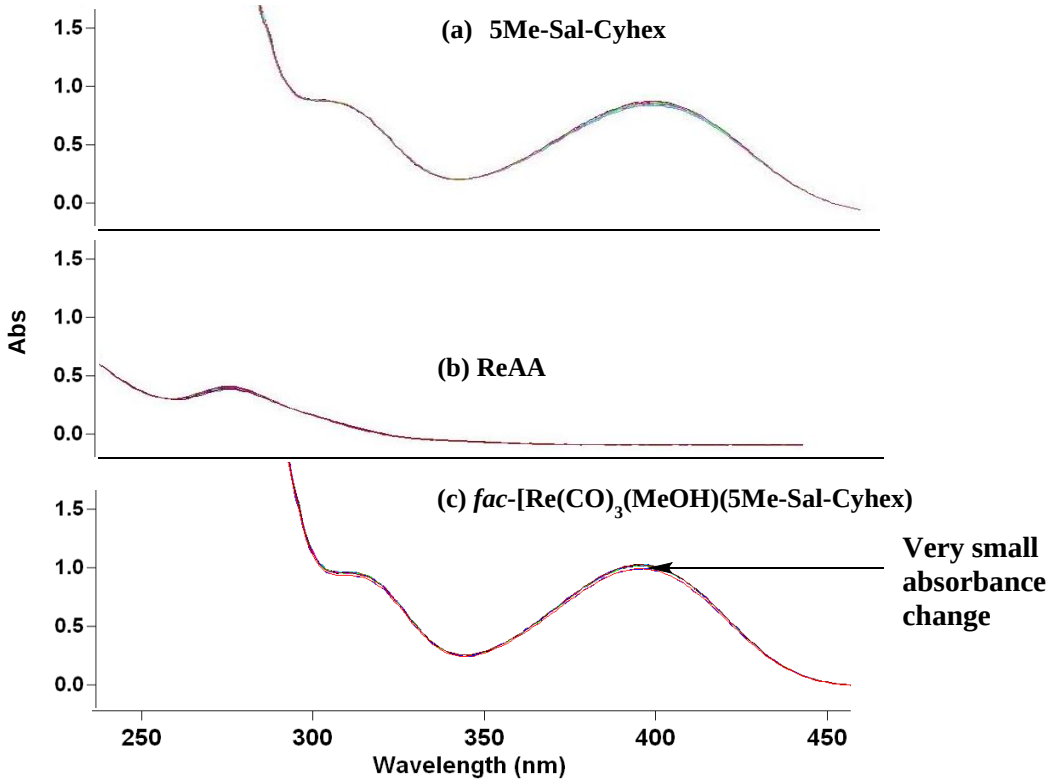

Figure 5.2: Characteristic UV-Vis spectra for the formation reaction of *fac*-[Re(CO)$_3$(MeOH)(5Me-Sal-Cyhex)] between 5Me-Sal-Cyhex and ReAA showing (a) spectrum of [5Me-Sal-Cyhex] = 0.001 M, (b) spectrum of [ReAA] = 1x10^{-4} M, (c) spectrum of the reaction mixture of (a) and (b) for ~24 hours, Δt = 3 min, λ = 307 nm in dry methanol at 25.0^{o}C.

As indicated above, the formation reaction of *fac*-[Re(CO)$_3$(MeOH)(5Me-Sal-Cyhex)] was attempted with the ratio, [ReAA] : [5Me-Sal-Cyhex] = 1 : 10 at 25.2^{o}C in dry methanol. It is clear from the stacked plot of the absorbance versus wavelength that the absorbance of the free ligand (5Me-Sal-Cyhex) is quite high and also shows a complex reaction between 5Me-Sal-Cyhex and ReAA. Moreover, this reaction occurred slowly and showed multiple absorbance, but very small changes, at various wavelengths for the ligand and reaction. This very small change in absorbance made it impossible to study the kinetics via UV/Vis absorbance measurements and the individual reaction rates could therefore not be studied in detail.

Due to the complexity of these kinetic results of the formation reaction of ReAA with the Schiff base ligand, a symmetrical ligand such as ethylenediamine was therefore used to study its coordination to the rhenium complex via kinetic analysis.

5.3.2 EVALUATION OF THE FORMATION OF *fac*-[Re(CO)$_3$(X)(en)], (X = Br, MeOH)

5.3.2.1 Characterization of Reactants and Products

The formation kinetics between ethylenediamine bidentate ligand and ReAA was performed to better understand the mechanistic parameters that may occur or affect the labelling of a radiopharmaceutical. To enable a complete kinetic investigation, the reactants and product of the specific reaction must be properly characterized. The reaction of ReAA with ethylenediamine, to isolate the solid state product, was performed according to the literature.[4] ReAA (20 mg, 0.026 mmol) was added to 2 eq. of ethylenediamine in dry methanol and was stirred at 25^{o}C for 8 hrs. The product was dried and yielded ca 12.1 mg (60.5% yield), it was then extracted with THF to remove excess Et$_4$NBr. Below is a given stepwise ^{1}H NMR and UV/Vis characterization study **(Figure 5.3)**.

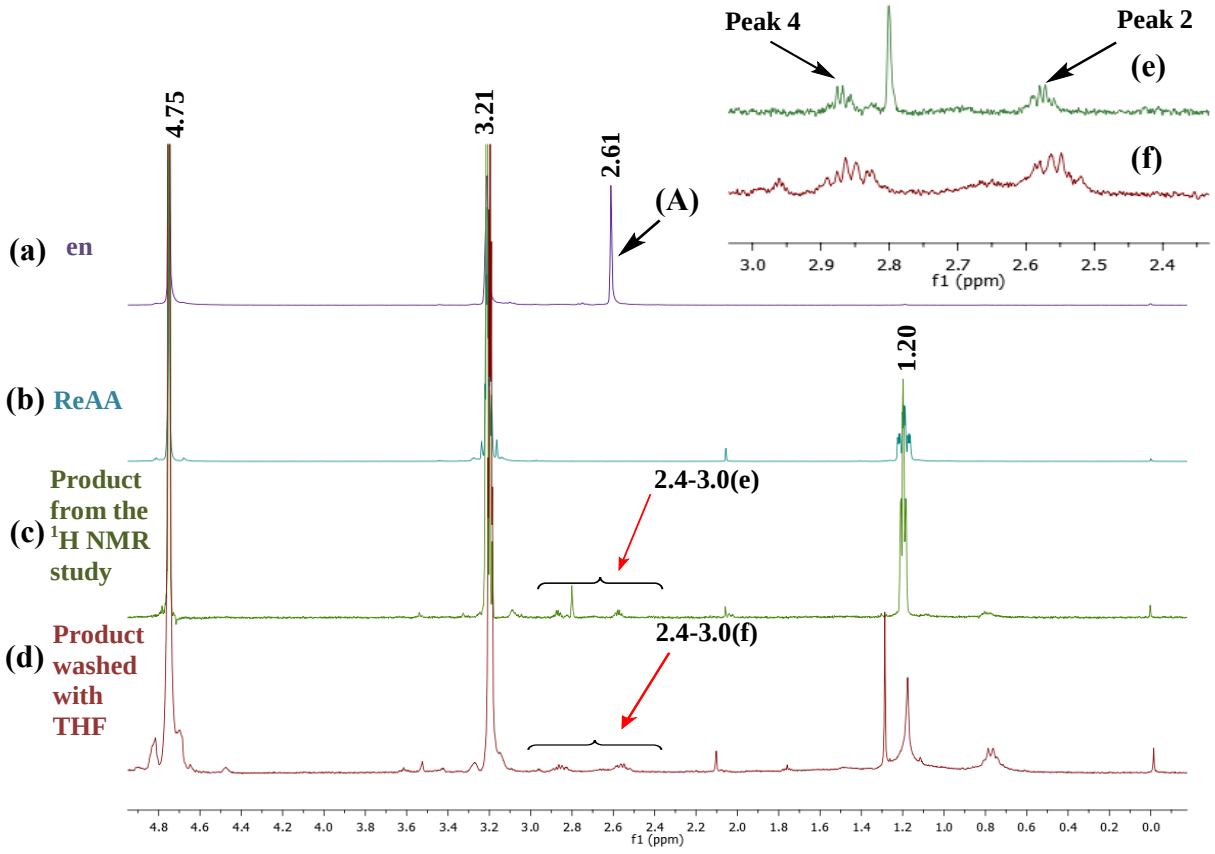

Figure 5.3: ^{1}H NMR spectrum of (a) pure ethylenediamine [en] = 0.001 M (A) in solution, (b) [ReAA] = 0.002 M, (c) reaction product with ReAA (20 mg) and 2 equivalents of ethylenediamine (en) in dry CD_3OD at 25^{o}C obtained from the ^{1}H NMR study in Figure 5.4, (d) reaction product synthesized as (c) and extracted with THF at 25^{o}C *in situ*, (e) and (f) represent the product's aliphatic –CH_2- groups used to monitor the reaction by ^{1}H NMR, see also Figure 5.4 for peak allocation.

It is clear from the above spectra that a reaction between ethylenediamine and ReAA is observed, with the final product **(red arrows, δ = 2.4-3.0 ppm)** showing quite complex signals, indicating that virtually all the protons in the coordinated ethylenediamine (en) are non-equivalent. The fact that the signals are also broadened, suggest an additional fast dynamics, attributed to potential 'shifting' of the ethylene backbone.

5.3.2.2 Preliminary ^{1}H NMR Evaluation of the Formation Reaction

The reaction progress of the formation reaction between ethylenediamine and ReAA, as monitored by ^{1}H NMR is presented in **Figure 5.4**.

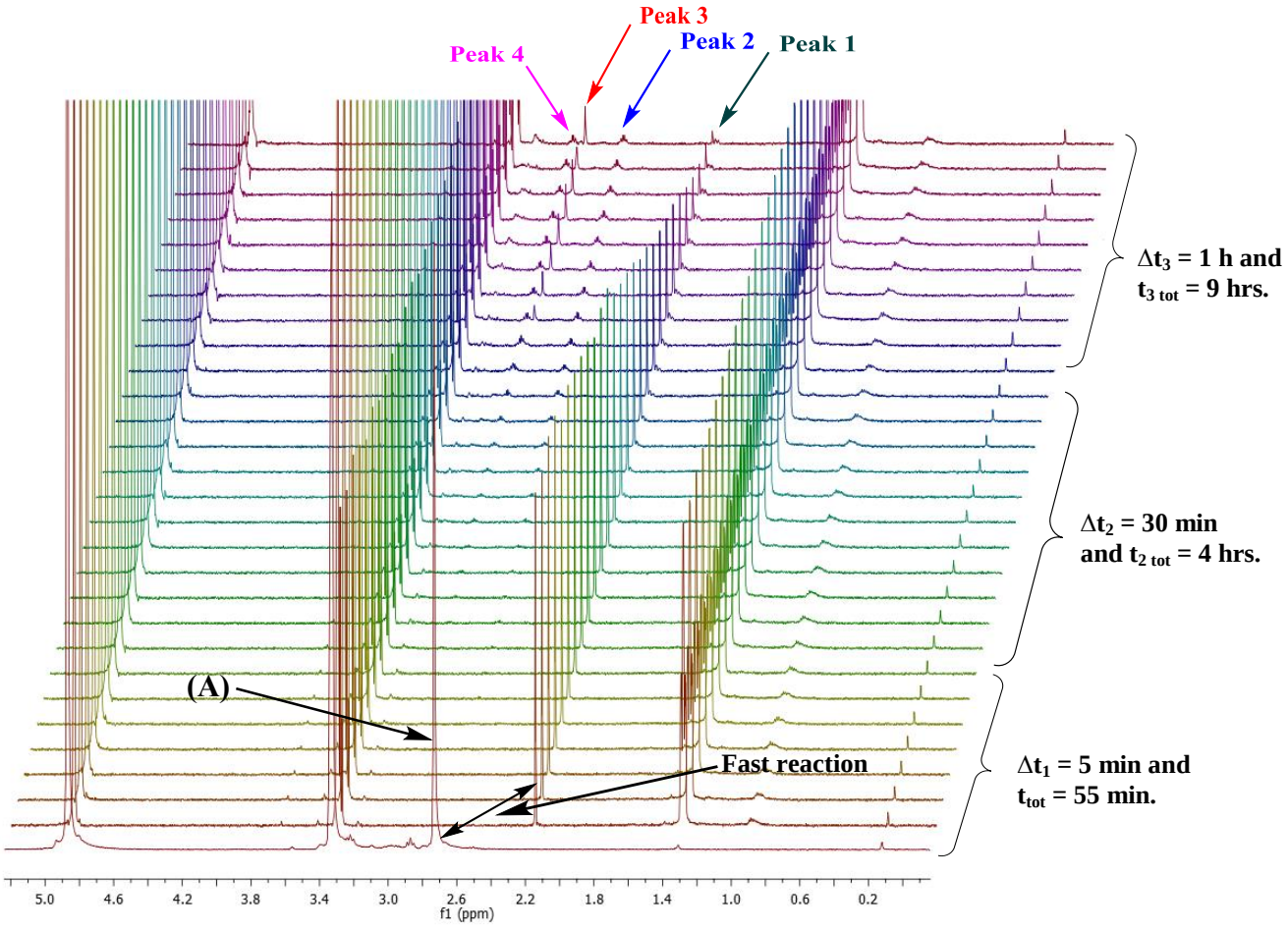

Figure 5.4: Observed formation reaction between ethylenediamine, [en] = 0.002 M and ReAA, [Re] = 0.001 M in dry CD_3OD with the aid of ^{1}H NMR at 25°C. Peak 1 = 2.18 ppm, peak 2 = 2.70 ppm, peak 3 = 2.92 ppm and peak 4 = 3.00 ppm with (A) as pure ethylenediamine and showing fast reaction.

Three general observations are made from **Figure 5.3** and **5.4** (i) the peak at δ = 2.61 ppm **(Figure 5.3(a))**, denoted by **(A)**, shifts very rapidly to 2.2 ppm after mixing ethylenediamine with ReAA (shown in **Figure 5.4**), which indicates a fast reaction; NOTE: The fast shift in the ethylenediamine (en) signal at 2.6 to 2.2 ppm is not due to pH effects, this has been checked by lowering the pH to ~2 by addition of a drop of 2 M of H_2SO_4; (ii) **Figure 5.4** thus suggests that there are two reactions present, i.e, a fast reaction ($t_{1/2}$ <5 seconds), as observed from this chemical shift in the free ethylenediamine (en) ligand (δ = ~2.7 ppm) to ca δ = ~2.2 ppm and a second slow reaction ($t_{1/2}$ >4 hours) as manifested by the decrease in this signal at 2.2 ppm (peak 1) to finally yield the product and potential side products indicated with peak 2 and 4, shown in **Figure 5.4**. (iii) There is also another secondary reaction, denoted by the changes in peak 3 **(Figure 5.3** and **5.4)**, which currently is an unidentified process.

By carefully integrating the relevant peaks attributed to the coordinating ethylenediamine (en) and plotting it against time, the plot of integral intensities *vs* time is obtained **(Figure 5.5)** for the analysis of the formation reaction between ethylenediamine and ReAA at 25°C, where the rate constants (k_{obs}) were obtained from the appropriate fits to Eq 5.4.

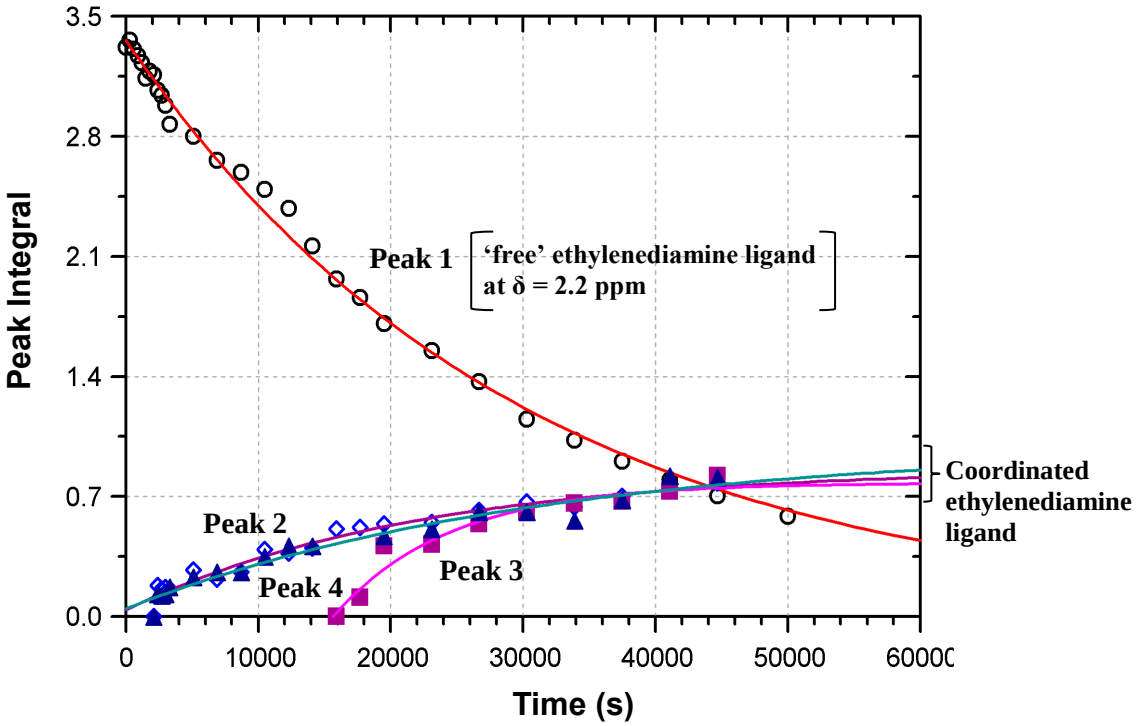

Figure 5.5: A plot of Integral intensites *vs* time of peak 1-4 (coordinated ethylenediamine) from the ^{1}H NMR analysis with [en] = 0.002 M and [ReAA] = 0.001 M in dry CD_3OD at 25°C.

Figure 5.5 clearly illustrates a decrease of the starting material and rapid formation of the intermediate (following the first fast reaction) (peak 1) and final product (peak 2 and 4). From **Figure 5.5**, rate constants are obtained from the disappearance/formation of the different peaks, peak 1 (k_{obs} = (3.38 ± 0.0007) x 10^{-5} s^{-1}), peak 2 (k_{obs} = (4.55 ± 0.0004) x 10^{-5} s^{-1}), peak 3 (k_{obs} = (1.13 ± 0.001) x 10^{-4} s^{-1}) and peak 4 (k_{obs} = (3.22 ± 0.0003) x 10^{-5} s^{-1}), an average of 3.72 x 10^{-5} s^{-1} is obtained from the rates values of peak 1, 2 and 4 (peak 3 is as indicated, a secondary reaction).

5.3.2.3 Preliminary UV/Vis Evaluation of the Formation Reaction

Since a ^{1}H NMR study requires much higher concentration of the metal complex, ReAA, this reaction was further investigated by UV/Vis measurements. A similar conclusion from the above ^{1}H NMR study is made when the UV/Vis spectra of the formation reaction is considered **(Figure 5.6)**, which clearly shows a fast reaction ($t_{1/2}$ = <5 seconds) and a slow reaction ($t_{1/2}$ > 4 hours) when the two reactants ([ReAA] = 1x10^{-4} M and ethylenediamine (en) [en] = 0.03 – 0.15 M) are mixed in a tandem cuvette.

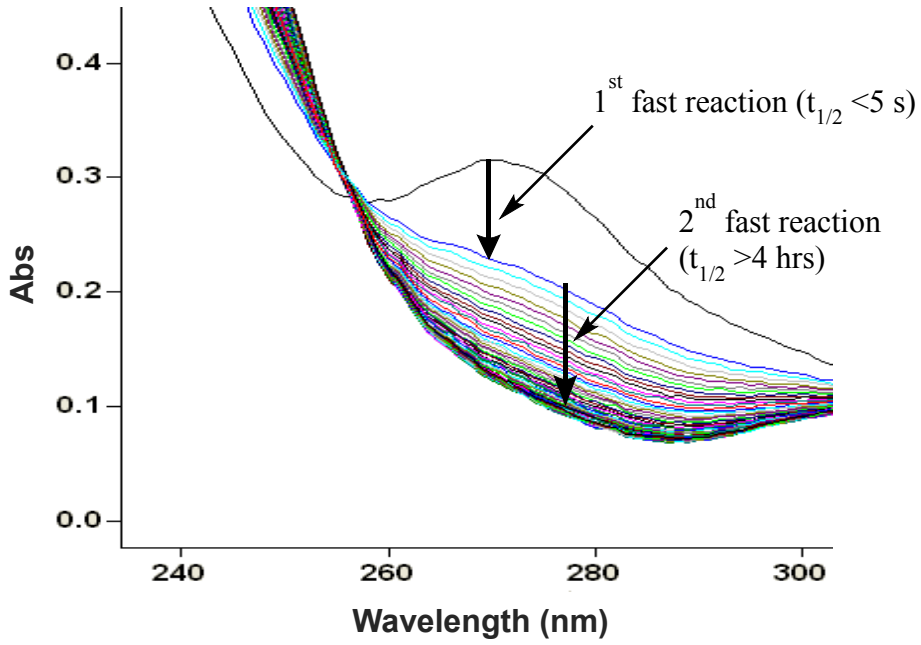

Figure 5.6: A typical characteristic UV-Vis spectrum change for the formation reaction *fac*-[Re(CO)$_3$(X)(en)] (X = Br, MeOH) with [ReAA] = 1x10^{-4} M and [en] = 0.03 M, λ = 280 nm at 25.2°C in dry methanol, clearly showing two reactions.

Preliminary evaluation of the first fast reaction was done, also attempting fast stopped flow measurements, but the reaction could not be studied in detail since it was quite fast ($t_{1/2}$ ~ milliseconds. It was therefore considered beyond the scope of this MSc study and was not investigated further.

5.3.2.4 Detailed Kinetic Study of the Second Slow Reaction between ethylenediamine (en) and ReAA

The second slower reaction between ethylenediamine and ReAA could be evaluated in more detail. The ligand (en) concentration and reaction temperature were consequently varied for the study of the second slow reaction and individual data points obtained for the *pseudo* first order rate constants (k_{obs}) from fits to Eq 5.4 are illustrated in **Figure 5.7**. The rate constants as obtained from fitting the k_{obs} values to Eq 5.7, yields the second order rate constants for the forward (k_1) and reverse reaction (k_{-1}) and are reported in **Table 5.1**.

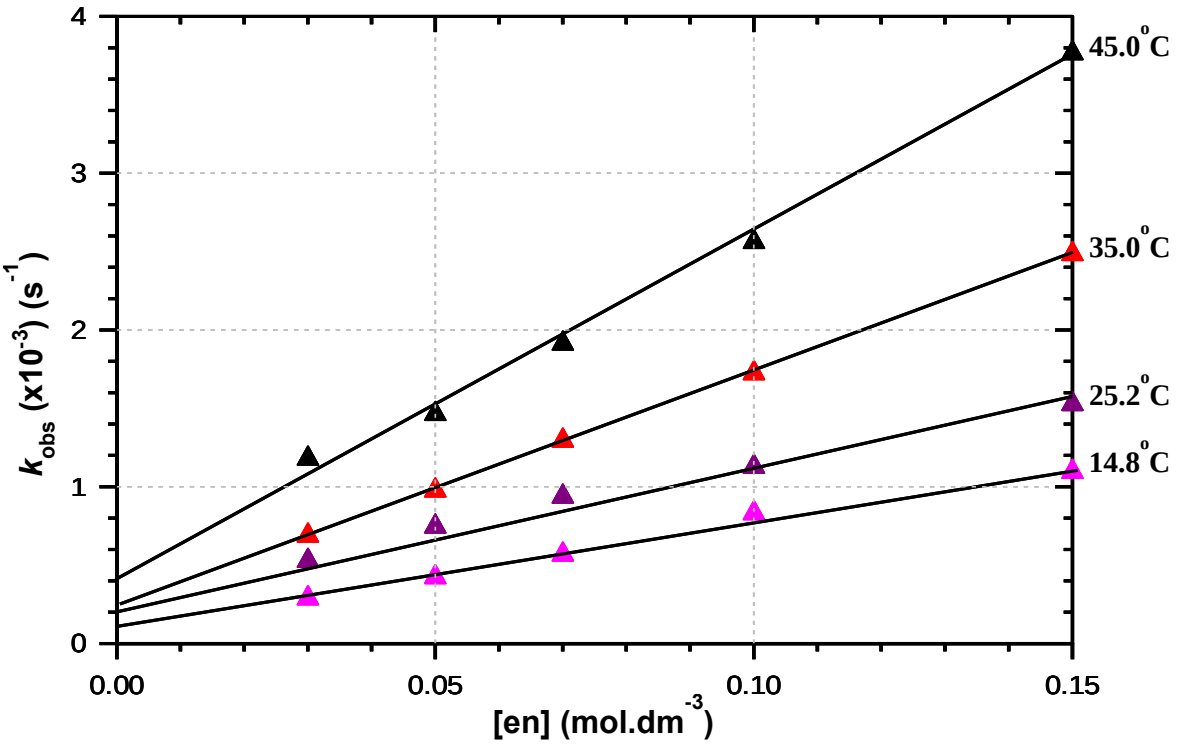

Figure 5.7: Graph of k_{obs} *vs.* time for the formation reaction of *fac*-[Re(CO)$_3$(X)(en)] (X = Br, MeOH) with [ReAA] = 1x10^{-4} M and [en] = 0.03-0.15 M, λ = 280 nm, at various temperatures in dry methanol.

Table 5.1: The summary of kinetic data of rate constants and parameters for the formation reaction of *fac*-[Re(CO)$_3$(X)(en)] (X = Br, MeOH), [ReAA] = 1x10^{-4} M and [en] = 0.03 – 0.15 M at various temperatures.

Rate constants and parameters	14.8°C	25.2°C	35.0°C	45.0°C
$(10)^3 k_1$ ($M^{-1}.s^{-1}$) $(10)^3 k_{-1}$ (s^{-1}) K_1 ($M^{-1}s^{-1}$)	6.88(3) 0.111(3) 62(19)	8.11(3) 0.344(3) 24(2)	14.97(1) 0.256(9) 59(2)	21.91(8) 0.444(7) 49(9)
$\Delta H^{\neq}_{(k1)}$ (kJ mol^{-1}) $\Delta S^{\neq}_{(k1)}$ (J K^{-1} mol^{-1})		28(5) -188(17)		

The activation parameters were obtained from Eq 5.5, as shown in **Figure 5.8** and are listed in **Table 5.1**. With the use of Eq. 5.4 (and the values obtained from **Figure 5.7**), the data was fitted to obtain the activation parameters of the formation reaction of *fac*-[Re(CO)$_3$(Br)(en)]. From the Eyring plot **(Figure 5.8)**, the standard enthalpy change of activation ($\Delta H^{\neq}_{(k1)}$) was calculated as 28(5) kJ mol^{-1} and the standard entropy change of activation ($\Delta S^{\neq}_{(k1)}$) was obtained as -188(17) J K^{-1} mol^{-1}.

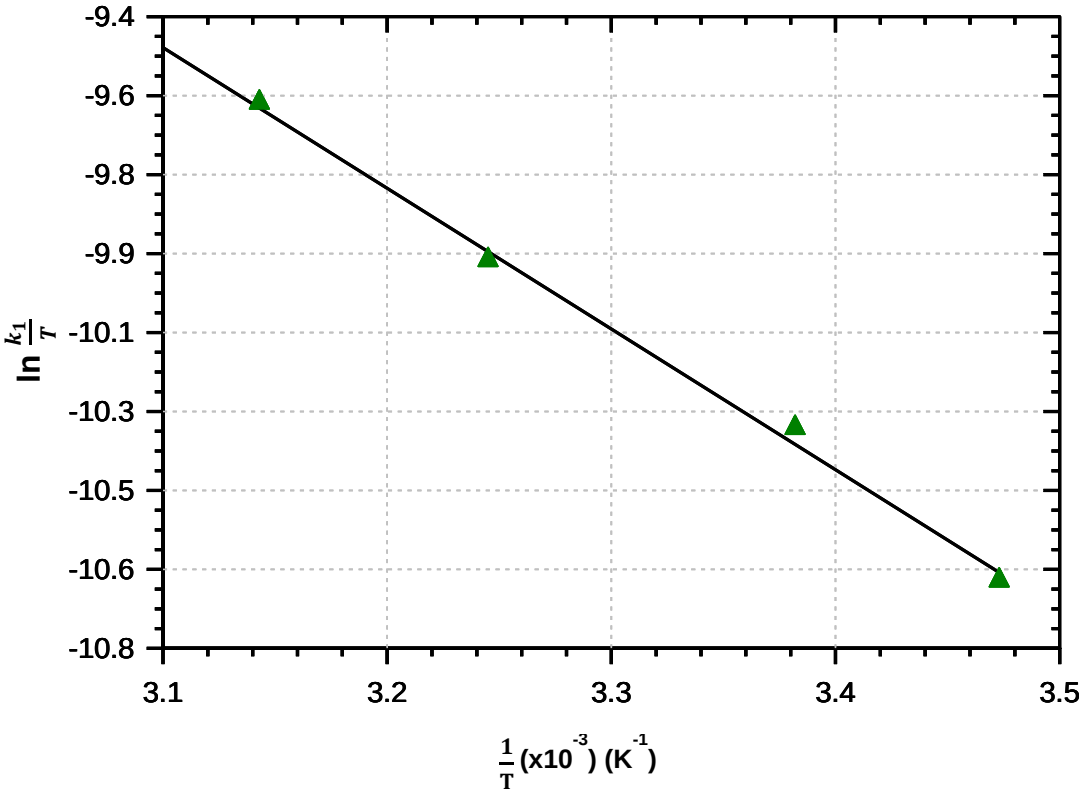

Figure 5.8: Eyring plot of ln(k_1/T) *vs* 1/T for the formation reaction *fac*-[Re(CO)$_3$(Br)(en)] in dry methanol.

5.4 DISCUSSION

The kinetic investigation of the reaction between *fac*-$[M(CO)_3]^+$ core and a Schiff base ligand (5Me-Sal-Cyhex) at 25.0^{o}C showed unsatisfactory results as indicated by **Figure 5.2**, with multiple reactions and small absorbance changes over time.[11] This formation reaction of the *fac*-$[M(CO)_3]^+$ core and Schiff base ligand with the ratio of [Re complex] : [Ligand] = 1 : 10, occur with the first ligand coordinating facially to the rhenium metal centre by removing the two bromide groups while the second ligand replace the monodentate ligand (Br^-/MeOH) on the sixth position, forming the Zwitterionic complex.[10] Also, with 10 time higher concentration of the ligand to the metal complex, multiple reactions occur accompanied with very small absorbance change as viewed by the spectroscopic data.

Since the formation reaction between the *fac*-$[M(CO)_3]^+$ core and the Schiff base ligand was complex and deemed beyond the scope of this current study, a symmetrical *N,N'*-bidentate ligand, ethylenediamine (en) was utilized for the investigation of the formation kinetics with postulation that the kinetics will be less complex. The formation kinetics of the reaction between ethylenediamine (en) and ReAA was conducted with the aid of ^{1}H NMR and UV/Vis analysis. From the ^{1}H NMR analysis, it is observed that there is a rapid chemical shift when ethylenediamine reacts with ReAA as it is shown from the comparison of the reaction product with starting materials (ethylenediamine and ReAA) **(Figure 5.3)**. The ^{1}H NMR investigation also revealed two reactions that occur in the formation reaction between ethylenediamine (en) and ReAA ([en] : [Re] = 2 : 1), i.e, i) first fast and ii) second slow reaction. **Figure 5.3** and **5.4** indicate the first fast reaction with the half-life, $t_{1/2}$ = <5 seconds and **Figure 5.4** illustrate the second slow reaction with the half-life, $t_{1/2}$ >4 hours and the formation of the products shown at peak 2 (k_{obs} = (4.55 ± 0.0004) x 10^{-5} s^{-1}), peak 3 (k_{obs} = (1.13 ± 0.001) x 10^{-4} s^{-1}) and peak 4 (k_{obs} = (3.22 ± 0.0003) x 10^{-5} s^{-1}).

The UV/Vis analysis also has a similar conclusion of the existence of two reactions that occur during the overall formation reaction. Since the first fast reaction has the half-life, $t_{1/2}$ = <5 seconds, a stopped flow kinetic investigation would be needed. The second slow reaction with half-life, $t_{1/2}$ >4 hours, was conducted via UV/Vis, as mentioned above and this analysis was performed at various temperatures. **Figure 5.6** illustrates the absorbance change which indicated that the reaction completed with at 25.2^{o}C. The value of the rate constants, k_1, acquired for the reaction between the *fac*-$[M(CO)_3]^+$ core and ethylenediamine at 14.8^{o}C,

[10] P.P. Mokolokolo, MSc Dissertation, University of the Free State, Bloemfontein, 2014.

25.2°C, 35.0°C and 45.0°C were k_1 = (6.88 ± 0.03) x 10^{-3}, (8.11 ± 0.03) x 10^{-3}, (1.5 ± 0.01) x 10^{-2} and (2.2 ± 0.08) x 10^{-2} $M^{-1}.s^{-1}$, respectively. When the average of the three rate constants (which are attributed to the disappearance of peak 1 and appearance of peaks 2 and 4, respectively (peak 3 not incorporated since it represent a follow-up reaction)) obtained, from the ^{1}H NMR experiment (see above), it yields a k_{obs} ~3.5 x 10^{-5} s^{-1}. Since this was performed at [en] = 0.002 M and consider (from Eq 5.8) that $k_{obs} \sim k_1$[en], thus $k_1 = \frac{k_{obs}}{[en]} = \frac{3.5 \times 10^{-5}}{0.002} =$ 1.75 x 10^{-2} $M^{-1}s^{-1}$ is obtained. This is in fair agreement with k_1 = 8 x 10^{-3} $M^{-1}s^{-1}$ which is obtained from the UV/Vis study. This indicates that the same reaction was studied by ^{1}H NMR and UV/Vis spectroscopy.

The activation parameters of the formation reaction of *fac*-$[M(CO)_3]^+$ core and ethylenediamine were obtained to be $\Delta H^{\neq}$ = 28 ± 0.05 kJ mol^{-1} and $\Delta S^{\neq}$ = -188 ± 0.17 J K^{-1} mol^{-1}. The significant negative value for $\Delta S^{\neq}$ suggests a process undergoing association by the ligand plays an important part. Since this second step might denote the ring closing of the ethylenediamine (en) ligand, this is difficult to imagine and is not currently further explained. However, further indepth investigations which must include the activation volume changes is required to confirm conclusively what the precise type is.[12,13]

5.5 CONCLUSION

The formation reaction between ReAA and a Schiff base ligand (5Me-Sal-Cyhex) could not be studied due to the complex reaction, small absorbance changes and large absorbance from the 'free' ligand.

The formation reaction between ethylenediamine (en) and ReAA was less complex and proceeded in two reactions, as shown above, with the aid of ^{1}H NMR and UV/Vis investigation and proved to be a first fast and a second slow reaction. The second slow reaction was successfully studied in fair detail by both ^{1}H NMR and UV/Vis spectroscopy.

The ^{1}H NMR analysis for the second slow was conducted at 25°C. This analysis illustrated how the reaction proceeded **(Figure 5.4)** and how the starting material (ethylenediamine) decreases as a new product forms. The quest for the analysis of first fast reaction was short

[12] J.G. Leipoldt, S.S. Basson, I.M. Potgieter, A. Roodt, *Inorg. Chem*, 1987, **26**, 57.
[13] M. Schutte, A. Roodt, H.G. Visser, *Inorg. Chem*, 2012, **51**, 11996.

lived since the first fast reaction could not be analysed at present as its half-life is quite small, $t_{1/2}$ = <5 seconds.

The UV/Vis analysis for the first fast reaction could not be studied and required a stopped flow analysis, while the second slow reaction was conducted at various temperatures (14.8^{o}C, 25.2^{o}C, 35.0^{o}C and 45.0^{o}C) with the obtained rate constants and activation parameters ($\Delta H^{\neq}$ = 28 ± 0.05 kJ mol^{-1} and $\Delta S^{\neq}$ = -188 ± 0.17 J K^{-1} mol^{-1}). This large negative $\Delta S^{\neq}$ value indicates a significant dependence of the reaction on association and suggests almost a pure association mechanism. More detailed future studies will shed more light on the overall reaction and will be the theme of the follow-up investigation.

6 EVALUATION OF THE STUDY AND FUTURE WORK

6.1 EVALUATION

This chapter summarizes the experimental work and results obtained during the course of this MSc study. Technetium(I) and rhenium(I) tricarbonyl complexes may be considered as strong candidates for potential radiopharmaceuticals used as diagnostic and therapeutic agents, respectively. The interest of this study was to gain an understanding of the coordination chemistry involving the use of bidentate ligands such as Schiff base ligands to the *fac*-$[M(CO)_3]^+$ (M = Tc or Re) metal centre and the kinetic behaviour of *fac*-$[M(CO)_3]^+$ (M = Tc or Re) complexes to determine how fast the formation reaction proceeds by determining the rate constant, activation parameters as well as rate law of the formation reaction between the Schiff base ligand, analogues thereof and *fac*-$[M(CO)_3]^+$ core.

The coordination of the *N,O*-bidentate ligand systems with *fac*-$[M(CO)_3]^+$ core was successfully achieved. The imino substituent on the Schiff base ligand consisted of aromatic and aliphatic substituents with various steric and electronic properties. The Schiff base ligand synthesized, 5-methyl-(2-cyclohexyliminomethyl)phenol **(5Me-Sal-Cyhex)**, was characterized by (^{1}H and ^{13}C) NMR and IR spectroscopy. Moreover, the single crystal X-ray diffraction investigation of this ligand is also reported in Chapter 4 which clearly illustrates the absolute configuration of the ligand system. The Schiff base ligand, **5Me-Sal-Cyhex** and the following metal complexes, *fac*-$[Re(CO)_3$(MeOH)(5Me-Sal-Cyhex)], *fac*-$[^{99}Tc(CO)_3$(MeOH)(5Me-Sal-Cyhex)], *fac*-$[Re(CO)_3$(Imid)(5Me-Sal-Cyhex)] (Imid = imidazole), *fac*-$[Re(CO)_3$(Pyrazole)(5Me-Sal-Cyhex)] and *fac*-$[Re(CO)_3$(Py)(5Me-Sal-Cyhex)] (Py = Pyridine), were successfully synthesized and fully characterized in liquid and solid state by Infrared (IR) and Nuclear Magnetic Resonance (NMR) spectroscopy. The IR spectra of all metal complexes indicated the stretching frequency of the carbonyl groups. Two compounds yielded crystals suitable for single crystal X-ray diffraction, namely *fac*-$[Re(CO)_3$(MeOH)(5Me-Sal-Cyhex)] and *fac*-$[Re(CO)_3$(Imid)(5Me-Sal-Cyhex)] and illustrates the coordination mode of 5Me-Sal-Cyhex in the solid state as described in Chapter

4. The bond distances and angles were comparable with similar compounds. The complexes crystalized in the monoclinic crystal system in the respective space groups of $C2/c$ and $P2_1/n$.

Additional bidentate ligands containing substituents such as furyl ligands were evaluated as potential ligand systems, however the synthetic procedure could not be fully optimised and resulted in inconsistent results and products. The coordination of furyl ligands with *fac*-$[M(CO)_3]^+$ core were unsuccessful, as observed from ^{1}H NMR spectra that the complexes were not successfully produced. At present the poor coordination of the furyl ligands to the tricarbonyl complexes is not fully understood, however the steric close proximity of the 5 membered ring may affect the coordinative capability of the ligand system. Future work of furyl ligands will consist of the purification of furyl ligands and complexes as well as ensuring successful coordination by extending the distance of the ring systems from the coordinating metal center.

The synthesis of *fac*-[^{99}Tc(CO)$_3$(MeOH)(5Me-Sal-Cyhex)] and *fac*-[^{99}Tc(CO)$_3$(MeCN)(5Me-Sal-Cyhex)] complexes were successful with the confirmation from HPLC. The synthesis of technetium(I) tricarbonyl complexes were complicated due to the appearance of pertechnetate, [^{99}TcO$_4$]$^-$, in the HPLC output graphs. For example, in the synthesis of *fac*-[^{99}Tc(CO)$_3$(MeOH)(5Me-Sal-Cyhex)], HPLC analysis showed the product as well as pertechnetate, [^{99}TcO$_4$]$^-$. To remove the pertechnetate, the complex *fac*-[^{99}Tc(CO)$_3$(MeCN)(5Me-Sal-Cyhex)] was stabilized by changing the solvent from methanol (MeOH) to acetonitrile (MeCN), leading to successful synthesis of the technetium(I) tricarbonyl complexes.

6.2 FORMATION KINETIC STUDY

The formation kinetics study of the tricarbonyl complexes was included in this work to understand the mechanistic parameters that may occur or affect during radiopharmaceutical ligand labelling. The formation kinetic study of the reaction between $[NEt_4]_2[Re(CO)_3(Br)_3]$ – **ReAA** and 5-methyl(2-cyclohexyliminomethyl)phenol – 5Me-Sal-Cyhex was attempted at 25.0^{o}C. $[NEt_4]_2[Re(CO)_3(Br)_3]$ and 5Me-Sal-Cyhex were stable in dry methanol, however, too small absorbance changes, when monitored by UV/Vis techniques, were observed for this reaction as shown in Chapter 5. Such small changes would not ensure proper accuracy of the results obtained and would lead to large experimental errors.

Therefore, due to the small absorbance changes, a symmetrical ligand was rather selected as a better kinetic candidate to evaluate the formation reaction. The coordination of the symmetric ligand such as ethylenediamine to the metal complex has been evaluated by a detailed kinetic study, as described in Chapter 5, involving the formation reaction between ReAA and ethylenediamine in dry methanol. The formation reaction between ethylenediamine and ReAA was analysed by ^{1}H NMR and UV/Vis kinetic investigation.

The UV/Vis analysis showed two reactions **(Figure 5.9)** that occur during the formation reaction between ethylenediamine and ReAA. Since the first fast reaction has the half-life, $t_{1/2}$ = <5 seconds, the stopped flow kinetic investigation is required. The second slow formation reaction between ethylenediamine and ReAA was monitored at 14.8^{o}C, 25.2^{o}C, 35.0^{o}C and 45.0^{o}C. The second order rate constants, k_1, increased with increase of temperatures. Dry solvents were used, to ensure that one reaction was followed and to eliminate the possibility and complexity of following the water exchange reaction, for all reactions performed in the UV-Vis spectroscopy. The rate constants and the rate law were successfully obtained as well as activation parameters ($\Delta H^{\neq}$ = 28 ± 0.05) kJ mol^{-1} and $\Delta S^{\neq}$ = -188 ± 0.17 JK^{-1} mol^{-1}) **(Table 5.1)**.

The formation kinetics was additionally monitored in a preliminary ^{1}H NMR study to evaluate carefully the reaction between ethylenediamine ([en] = 0.002 M) and ReAA ([ReAA] = 0.001 M) at 25^{o}C, where the ^{1}H NMR scans were repeatedly taken over a 15 hour period. The ^{1}H NMR results were virtually identical to that observed with UV/Vis as described above. The ^{1}H NMR scan taken for the product and product washed with THF obtained from the experimental reaction of ethylenediamine and ReAA in dry CD_3OD showed virtually identical ^{1}H NMR spectra. From the ^{1}H NMR investigation, it was observed that the formation reaction between ethylenediamine and ReAA occurs via two reactions, defined as a first fast and second slow reaction. The first fast reaction has a half-life, $t_{1/2}$ = <5 seconds, this reaction could not be analysed by UV/Vis or ^{1}H NMR investigation and required a stopped flow analysis. The second slow reaction has a half-life, $t_{1/2}$ = ~15 hours and this reaction yielded products, indicated by at peak 2 (k_{obs} = (4.55 ± 0.0004) x 10^{-5} s^{-1}), peak 3 (k_{obs} = (1.13 ± 0.001) x 10^{-4} s^{-1}) and peak 4 (k_{obs} = (3.22 ± 0.0003) x 10^{-5} s^{-1}) **(Figure 5.4)**.

6.3 CRYSTALLOGRAPHIC ANALYSIS

Three crystal structures were obtained from single X-ray structural analysis and fully characterized as described in Chapter 4. The crystals obtained had the following morphology: **1)** Cuboid colourless crystals of 5Me-Sal-Cyhex **(Compound 1)** crystallized in an orthorhombic crystal system in the $P2_12_12_1$ space group. The crystal of 5Me-Sal-Cyhex possessed the intermolecular hydrogen bond (C-H…Cg interaction) and packed with parallel overlapping of plates. **2)** Cuboid colourless crystals of *fac*-[$Re(CO)_3(HOCH_3)$(5Me-Sal-Cyhex)] **(Compound 2)** crystallized in the monoclinic crystal system in the *C*2/*c* space group. The crystal of compound **2** showed π-π interaction between two centroid rings (Cg) and possessed classic hydrogen bonds. This compound packed along *c*-axis showing π-π interaction between two centroid rings (Cg). **3)** Cuboid colourless crystals of *fac*-[$Re(CO)_3$(Imid)(5Me-Sal-Cyhex)] **(Compound 3)** crystallized in the monoclinic crystal system in the $P2_1/n$ space group. This crystal showed π-π interaction between two centroid rings (Cg) with intermolecular hydrogen bond, it also showed π-π interactions when packed along *b*,*c*-axis.

6.4 FUTURE WORK

The results described above illustrate the potential of developing the work further. The following potential work will be considered in future as listed below:

- Additional synthetic exploration to produce the furyl ligands, and to determine the methods in which they can be successfully synthesized and coordinated to *fac*-$[M(CO)_3]^+$ metal centre.

- This study is to be expanded by producing Schiff base ligands especially biologically active Schiff base ligands or biological *N*,*O*-bidentate ligands for further coordination to *fac*-$[M(CO)_3]^+$ metal centre (M = Tc or Re). The production of these complexes with a biological ligand to be coordinated to the metal complex in an aqueous medium, is to ensure improved *in vivo* application.

- Crystallographic investigation of complexes formed from biological bidentate ligands, particularly, Schiff base ligands coordinated to *fac*-$[M(CO)_3]^+$ metal centre to confirm complex conformation.

- Expand the kinetic investigation of the formation reaction between bidentate ligands (Schiff base ligands) or biological bidentate ligand and the *fac*-$[M(CO)_3]^+$ metal centre (M = Tc or Re). Conduct the formation kinetics of the reaction between ethylenediamine and ReAA via a stopped flow kinetic investigation in order to obtain the rate of the first fast reaction.

APPENDIX A: THEORY OF UV-Vis, INFRARED SPECTROSCOPY, NUCLEAR MAGNETIC RESONANCE, X-RAY DIFFRACTION and CHEMICAL KINETICS

A.1 INTRODUCTION

The rays of the sun are scattered by raindrops to produce a rainbow, thus the appearance of a colourful spectrum produced when a narrow beam of sunlight is passed through a triangular glass prism is an example of a white light formed into a visible spectrum of primary colors. The visible white light form part of the spectrum of the electromagnetic radiation and extends from radio waves to cosmic rays. The electromagnetic radiation travels at the same velocity but with different frequencies and wavelength. The electromagnetic radiation consists of electromagnetic waves, and the interaction of the radiation and matter are studied and researched as a spectroscopy. The recent methods of spectroscopy that resides in different regions of the electromagnetic radiation are significantly utilised in the analysis and investigation of the molecules. These methods of spectroscopy are used to study and characterise all products acquired in this work, and are Ultraviolet and Visible spectroscopy (UV-Vis), Infrared spectroscopy (IR), Nuclear Magnetic Resonance (NMR). In addition to methods of characterization, other methods were used such as X-ray diffraction (XRD) and Chemical Kinetics.[1]

[1] C.N.R. Rao, *Ultra-Violet and Visible Spectroscopy: Chemical Applications*, 2nd Ed, Butterworths, London, 1967, xii, 1-3.

A.1.1 ELECTROMAGNETIC RADIATION

The electromagnetic radiation illustrates a range of energies, frequencies and wavelengths. Important frequencies changes from $>10^{19}$ Hz which are gamma (γ) rays to 10^{3} Hz representing radio waves. Different types of radiation such as gamma (γ) rays and radio waves differ from visible light only in energy or frequency of their photons.[2]

Table A.1: Illustration of electromagnetic spectrum.[2]

	Type of Spectroscopy						
	NMR	ESR	Microwave	Infrared	Ultraviolet and Visible	X-ray	Gamma Rays
Energy, J/mol	10^{-3}	10^{-1}	10	10^{3}	10^{5}	10^{7}	10^{9}
Frequency, Hz	$3x10^{6}$	$3x10^{8}$	$3x10^{10}$	$3x10^{12}$	$3x10^{14}$	$3x10^{16}$	$3x10^{18}$
Wavelength	10 m	100 cm	1 cm	$100x10^{6}$ m	1000 nm	10 nm	100 pm
Wavenumber, cm^{-1}		10^{-2}	1	100	10^{4}	10^{6}	10^{8}

A.2 ULTRAVIOLET AND VISIBLE SPECTROSCOPY

Ultraviolet-visible spectroscopy is used as one of the characterization method for obtaining the extinction coefficient and maximum wavelength for all products obtained and it is used mostly in kinetic mechanistic analysis of the samples. The ultraviolet-visible spectroscopy uses the electromagnetic radiation in the region of 200 to 800 nm, where the radiation is divided into ultraviolet in the 200-400 nm region and visible in the 400-800 nm region. The unit used for wavelength is nanometer unit, nm, or it can be the milimicron, mμ. Also the wavenumber, $\bar{\upsilon} = 1/\lambda$, is used and its unit is the reciprocal of a centimetre, cm^{-1}. In ultraviolet or visible radiation, a molecule absorbs the radiation and this causes the molecule to transit

[2] D.A. Skoog, D.M. West, F.J. Holler, S.R. Crouch, *Fundamental of Analytical chemistry*, 8th Ed, Brooks/Cole Cengage Learning, Belmont, USA, 2004, 714.

among the electronic energy levels and this is called the electronic spectroscopy. The change in electronic energy of the molecule is caused by the energy absorbed in the ultraviolet region. In the transition, a molecule absorbs energy and the electron of the molecule is elevated from an occupied molecular orbital such as a non-bonding N or bonding π-orbital to an unoccupied orbital such as an antibonding π^* or σ^* orbital with higher potential energy. The σ orbitals are the lowest energy occupied molecular orbitals and corresponds to σ bonds, while the π orbitals are the higher energy orbitals than σ orbitals. The non-bonding orbitals that have unshared pairs of electrons resides at higher energies than π and σ orbitals, and the antibonding orbitals π^* and σ^* orbitals are of even higher energies.

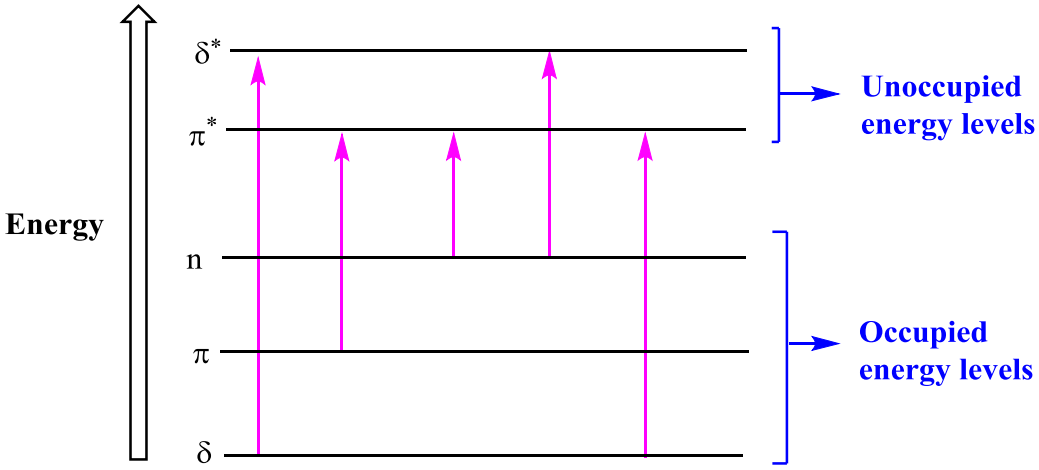

Figure A.1: A schematic illustration of the transition.

The transition of the saturated aliphatic hydrocarbons (alkanes) or compounds with single bonds shows only $\sigma \rightarrow \sigma^*$ transition, and the type of a functional group and organic molecules have the capacity to undergo several possible transitions which can be classified as $n \rightarrow \pi^*$ (double bond) < $n \rightarrow \sigma^*$ < $\pi \rightarrow \pi^*$ (double bond) < $\sigma \rightarrow \pi^*$ (compounds with lone pairs) < $\sigma \rightarrow \sigma^*$. The mostly likely transition involves absorption of energy by the molecules, and causes an electron to be promoted from highest occupied molecular orbital (HOMO) to the lowest unoccupied molecular orbital (LUMO). The molecule absorbs energy when subjected to an electromagnetic radiation, and their absorption can be explained in terms of absorption law called Beer's and Lambert's law.[1,3]

[3] D.L. Pavia, G.M. Lampman, G.S. Kritz, *Introduction to Spectroscopy*, 3rd Ed, Thomson Learning Inc, 2001, 15.

A.2.1 ABSORPTION LAW: BEER'S LAW

The Beer-Lambert's law or just Beer's law tells us that fraction of an incident radiation absorbed is proportional to the number of absorbing molecules in the light path, meaning, if a sample is dissolve in a solvent, the solution will absorb the radiation that is proportional to its molecular concentration, provided that the solvent itself does not have any absorbance capability in that specific wavelength region. As light passes through a medium containing an absorbing analyte, the complex is excited. In the analysis of a solution with a certain concentration, if the length of the medium which the light passes is long, absorption is higher. Beer's law describes the relationship between absorbance and concentration of the absorbing analyte. The transmittance of the absorbing analyte is a fraction of the incident radiation transmitted by the solution and is expressed in percentage. Transmittance is given by:

$$T = \frac{P}{P_o}$$

where the radiant power decreases from P_o to P.

Beer's law is elaborated further by stating that absorbance is directly proportional to the concentration of the solution c and path length b of the absorbing medium, and thus

$$A = \log \frac{P_o}{P} = abc$$

where a is a proportionality constant called absorptivity. Since the absorbance does not have any units, the absorptivity must have unit that cancels units of b (g) and c (cm), thus a has unit of $L.g^{-1}.cm^{-1}$ and if g is changed to mol, then absorptivity has unit of $L.mol^{-1}.cm^{-1}$. This absorptivity has a special symbol, ε, the proportionality constant called molar absorptivity. Therefore Beer's law becomes[1,3]

$$A = \varepsilon bc$$

A.3 INFRARED SPECTROSCOPY

Infrared spectroscopy is one of the most used methods of characterization and its great advantage is that any sample of any state can be analysed. Infrared spectrometers have existed since the 1940's. Infrared spectroscopy is a technique involving the vibrations of atoms of the sample examined and the infrared spectrum is obtained by infrared irradiation

through the sample to determine the fraction of the incident radiation absorbed at a particular energy. The energy at which the absorbance of the sample occurs relates to the frequency of vibrating atoms of a molecule. This appendix chapter discusses the vibrations of molecules as they take part in the interpretation of the infrared spectra. To broaden the understanding of infrared spectroscopy, electromagnetic radiation is discussed in detail.

A.3.1 ELECTROMAGNETIC RADIATION

The electromagnetic radiation has visible part that is visible to the human eye, but there are regions of the electromagnetic spectrum that are not visible to the human eye and are known as radio wave, microwave, ultraviolet, x-ray, γ-ray and infrared. Maxwell's theory of electro- and magneto-dynamics is based on the interpretation of the nature of various radiation, and lead to the term, electromagnetic radiation. Maxwell's theory describes how radiation is taken as two mutually perpendicular electric (E) and magnetic (M) fields that oscillates in single plane while making 90^{o} angle between each other.[4]

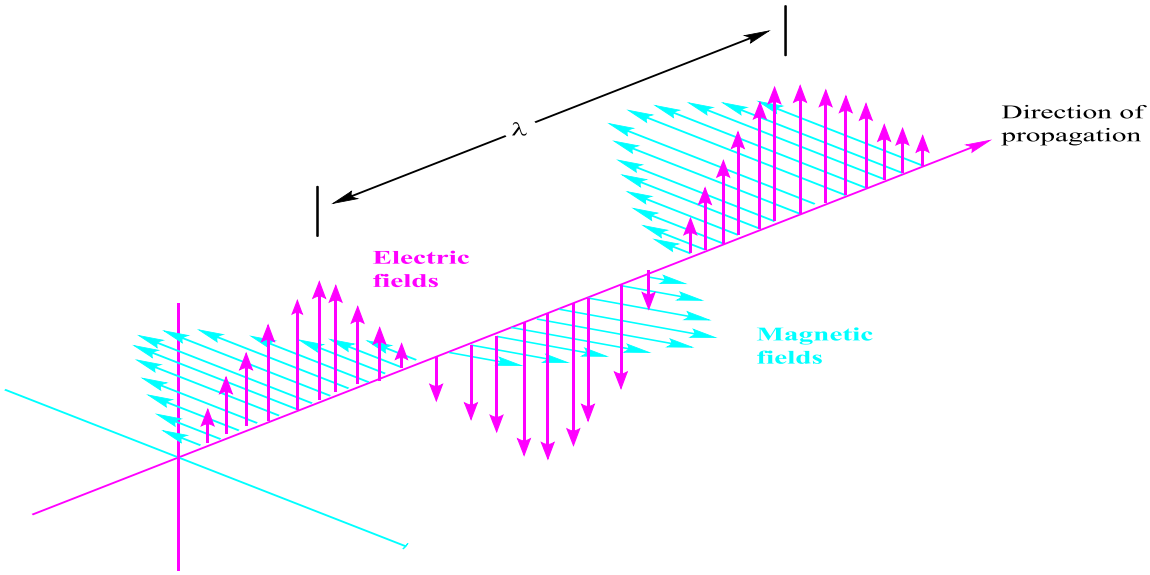

Figure A.2: A schematic illustration of an electromagnetic wave.[5]

The discovered aspect of electromagnetic radiation was that the velocity of propagation was constant in a vacuum throughout the spectrum and the velocity of light (c) has the value of 2.997 925 x 10^{8} m.s^{-1}. The velocity of one complete wave traveling at a fixed distance is the product of the wavelength (λ) and the frequency (υ). Hence,

[4] B. Stuart, *Infrared Spectroscopy: Fundamentals and Applications*, John Wile and Sons, Ltd, 2004, 1-27.
[5] www.nde-ed.org/EducationResources/CommunityCollege/RadiationSafety/theory/nature.htm

$$c = \lambda\upsilon$$

Also the unit used in infrared spectroscopy is called the wavenumber, $\bar{\upsilon}$, expressed in cm^{-1} and is given by

$$\bar{\upsilon} = 1/\lambda = \upsilon/c$$

The advantage of a wavenumber is that it has a linear relationship with energy.

A continuous interaction of matter with energy was observed to be inconsistent by scientists in the 19th century. Scientists like Einstein, Planck and Bohr showed that electromagnetic radiation could considered as quanta (stream of particles) for which energy, *E*, is given by Bohr equation as,

$$E = h\upsilon$$

where h is a Planck's constant ($h = 6.626 \times 10^{-3}$ J.s) and υ is a frequency.[4]

A.3.2 INFRARED ABSORPTION OF A MOLECULE

The molecule shows infrared absorptions if it has an electric dipole moment that changes during vibration, and this is called the selection rule for infrared spectroscopy. The heteronuclear diatomic or "infrared-active" molecule **(figure A.3)** has a dipole moment that change as the bond stretches out and compresses in. Unlike "infrared-active" molecule, an "infrared-inactive" molecule or homonuclear diatomic molecule has a dipole moment that remains zero despite the distance of the bond.[4]

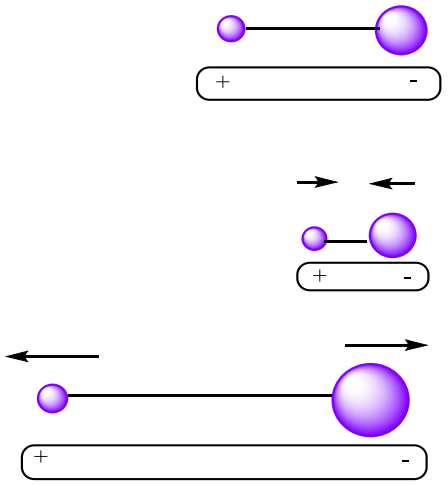

Figure A.3: A schematic illustration of "infrared-active" molecule.

A.3.3 THE NORMAL ABSORPTION MODES

The change in the dipole moment of molecules related to the vibrations and rotations can be used to better describe the interaction of infrared radiation with matter. Molecules can be studied as a system of masses that are joined by bonds having spring-like properties, for example, diatomic molecules. The diatomic molecules have two degrees of rotational freedom and three degrees of transitional freedom, and possess atoms that move in relation to one another. The stretching (change in bond length) and bending (change in bond angle) movements are referred to as vibrations. The diatomic molecule has one vibration movement that is related to the stretching and compression of the bond, and thus this molecule has one degree of vibrational freedom. However, the polyatomic molecules that contain many *N* atoms possess 3*N* degree of freedom.

Vibration involves stretching or bending. Other bonds stretch as (in-phase) symmetrical stretching and (out-of-phase) asymmetrical stretching shown in figure A.4[6]

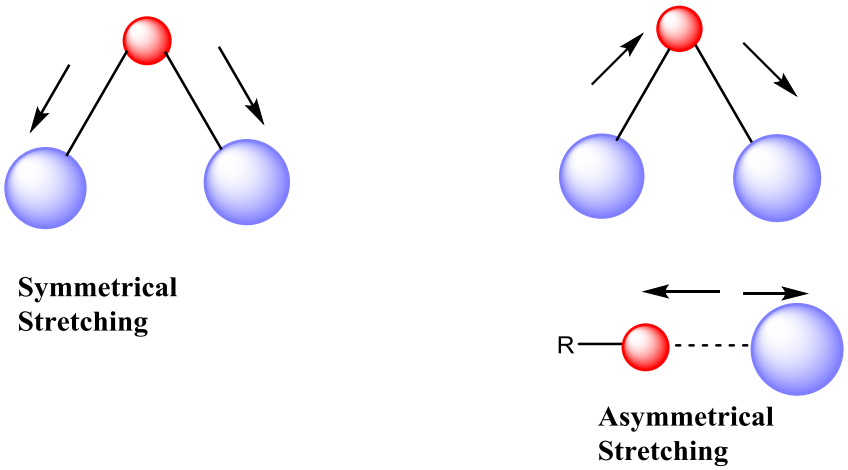

Figure A.4: A schematic illustration of symmetrical and asymmetrical stretching.

In bending vibrations, the molecule is cut by a plane through the hydrogen atoms and the carbon atom. In this plane, hydrogen atoms can move in the same or opposite directions shown in figure A.5.

[6] B. Stuart, *Modern Infrared Spectroscopy*, John Wiley and Sons, Ltd, 1996, 2

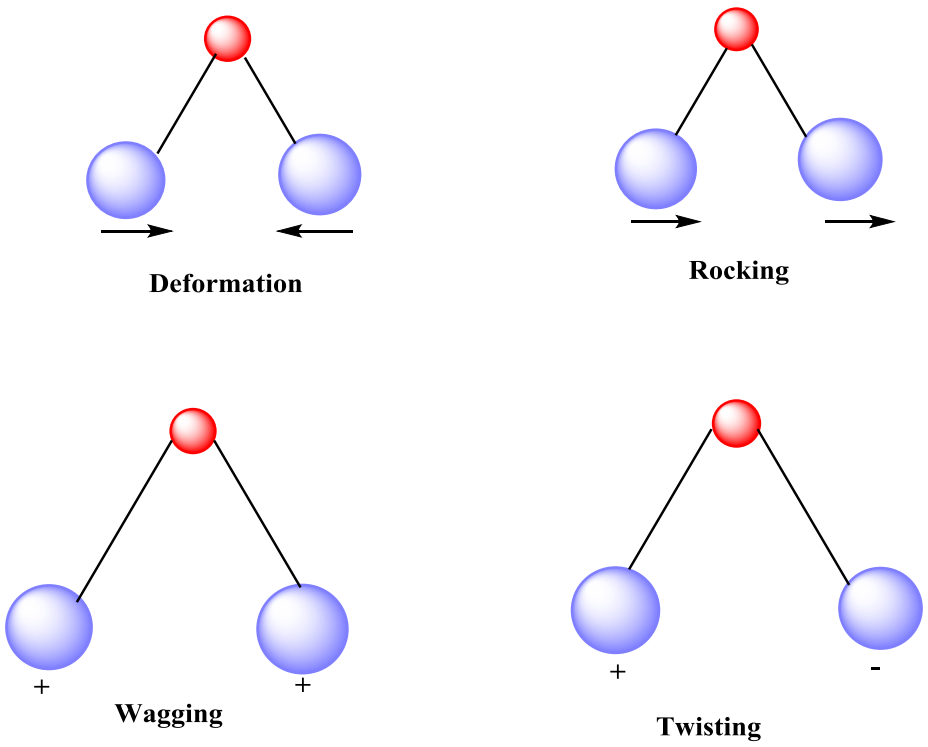

Figure A.5: A schematic illustration of bending vibrations.

As mentioned above, the absorption of infrared radiation produced by vibration which causes change in the dipole moment of the molecule. If the change in dipole moment is higher, the intensity of absorption will increase. Specifically, the carbonyl group is permanently polarized due to the variation of electronegativity between carbon and oxygen. If the carbonyl bond is stretched, the change in dipole moment increases, and thus carbonyl bond stretching has high intensity of absorption.[6]

A.3.4 FOURIER-TRANSFORM INFRARED SPECTROMETERS

Infrared spectroscopy is the mostly used technique for characterization of molecules or samples by obtaining spectra, and a variety of methods used for obtaining spectra requires instrumentation. The most significant instrument used in infrared spectroscopy is Fourier-Transform spectrometers. This instrument utilises an interferometer and exploits mathematical process of fourier-transformation. The fourier-transform infrared (FTIR) spectroscopy improved the time to collect data and the quality of infrared spectrum. The fourier-transform infrared (FTIR) spectroscopy involves the interference of radiation between beams to yield an interferogram. The interferogram is a signal considered as a function of the

change of path length between the two beams. The mathematical method called fourier-transform is used to interconvert the domains of distance and frequency.[4,6]

A.3.5 INFRARED SPECTRA

The result from the instrument used for infrared absorption analysis is called a spectrum, and the spectrum is presented with a wavenumber ($\bar{\upsilon}$) decreasing from left to right for many instruments. The infrared spectrum is divided in three main parts, namely, the far-infrared (<400 cm^{-1}), the mid-infrared (4000-400 cm^{-1}) and the near-infrared which in 13000-4000 cm^{-1} region. Many infrared spectrum are examined in the mid-infrared region, but the far- and near-infrared regions provided vital information for other compounds. It is common to present the infrared spectrum in absorbance or transmittance as a measure of band intensity, but the ordinary spectrum is presented in % transmittance in many cases. The transmittance is used for spectral interpretation and absorbance is used for quantitative analysis.[4,6]

A.4 NUCLEAR MAGNETIC RESONANCE

Nuclear magnetic resonance (NMR) spectra fall into the region of microwaves and radio waves in the electromagnetic spectrum. Nuclear magnetic resonance (NMR) spectroscopy was first developed in 1946, and it is used for identification of the structure of the sample analysed. The NMR phenomenon is based on the fact that nuclei of atoms have the magnetic properties used to provide chemical information. The NMR analysis involves nuclei with superimposed magnetic fields $\mathbf{B_o}$ irradiated by inducing transitions between energy levels. The nucleus of atom that is irradiated have an angular momentum, which is obtained from the spin and orbital angular momentum. Some atoms have spin quantum number of zero, for example, ^{12}C, ^{16}O and ^{32}S, as the spins are paired and they cancel each other out. Other atoms like ^{1}H, ^{13}C, ^{31}P, ^{15}N, etc have spin and spin quantum numbers. Several rules are considered towards determining the spin of a nucleus, and are as follows:[7]

a) No spin – Number of neutrons and protons are both even.
b) Half-integer spin (1/2, 3/2, 5/2) – Number of neutrons plus number of protons is odd.
c) Integer spin (1, 2, 3) – Number of neutrons and protons are both odd.

[7] P. Sohår, *Nuclear Magnetic Resonance*, CRC Press Inc, Boca Raton, Florida, 1983, **Vol I**, 1-7.

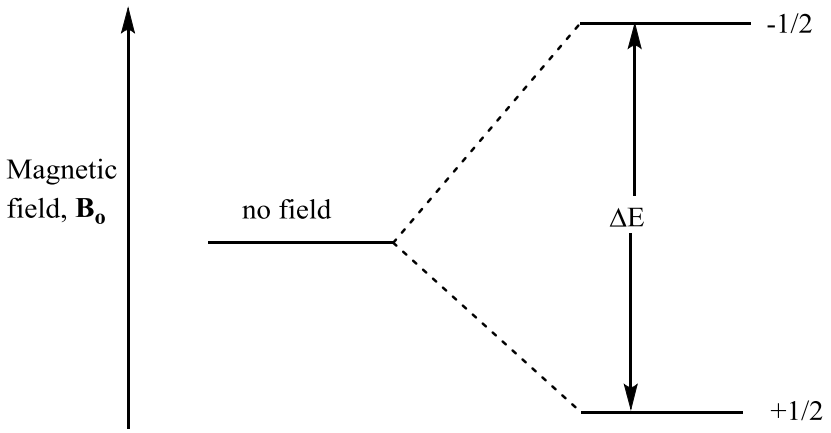

Figure A.6: Transition between energy levels.

Transition occurs from the lower to higher energy level as energy is absorbed and the energy is released when the transition is reversed. The nucleus with the spin quantum number of ½ has only one transition that occurs between energy levels. Any nucleus with nuclear magnetic moment associate with externally applied magnetic field $\mathbf{B_o}$ in quantum mechanics.

Nucleus in the rotational axis cannot be orientated parallel or antiparallel with the direction of applied magnetic fields, but can proceed about this field at an angle with angular velocity, this expressed as

$$\omega_o = \gamma \mathbf{B_o}$$

where ω_o is known as Lamor frequency. The transition from lower to higher energy level occurs when the frequency of electromagnetic radiation is related to Lamor frequency.[7]

A.4.1 CHEMICAL SHIFTS

Over the years NMR has been used to analyse samples. In an NMR experiment, the NMR scale need to be standardised at 0 reference, when all protons are compared. The most used standard reference is tetramethylsilane (TMS), and this molecule consists of four CH_3 methyl group single bonded to a silicon atom with highly shielded protons. This is used in small quantities and appears in NMR spectrum as a single peak that is separated from resonance on the spectrum. The position of the resonance is obtained by measuring frequency separated from the reference peak, and the difference of the frequency from reference peak is divided by frequency of the reference peak. Thus chemical shift, δ, is as follows

$$\delta\ (\text{ppm}) = 10^6 \times \frac{\upsilon - \upsilon_{ref}}{\upsilon_{ref}}$$

where υ is the frequency and υ_{ref} is the frequency of the internal standard. The chemical shift is defined for most electronegative atoms as "deshielded atoms" while atoms with nucleus opposing the magnetic field are "shielded". The chemical shifts can be defined in terms of spin quantum number as; if m = -1/2, the resonance is shifted to higher frequency, and thus deshielded. If m = +1/2, the proton resonance is shifted to lower frequency, and thus shielded.[8,9,10]

A.4.2 SPIN-SPIN COUPLING

Spin-spin coupling in NMR spectrum analysis is based on the NMR line being spilt with intensities and spacings or distance. In the molecule containing hydrogen atoms, hydrogens attached to an adjacent carbons can interact with each other, and they are defined by n + 1 rule. The n + 1 rule is utilised where protons with n equivalent adjacent protons show n + 1 peaks. ^{13}C nucleus has magnetic moment that splits the peaks of ^{1}H into two proton resonance. The distance between the peaks is called coupling constant and is measured in Hz. Coupling constant can either be positive or negative and are determined by band distances of protons, electronegative substituents and bond angles.[8,9,10]

A.5 X-RAY DIFFRACTION

The field of crystallography was explored extensively after the discovery of x-rays by Wilhelm Conrad Röntgen in 1895, and the first x-ray experiment was conducted by Max von Laue in 1912. It is evident that x-rays have high energy particles and x-rays might be considered to be waves. Von Laue's experiment proved the wave nature of x-rays by x-ray diffraction method. The x-ray diffraction provides information about the crystal structure, the shape, size of the unit cell and scattering of electron density throughout the unit cell. For x-ray diffraction to be implemented, crystalline solids need to be produced.[11]

[8] P.J. Hore, *Nuclear Magnetic Resonance*, Oxford University Press, 1995, 22.
[9] J. Clayden, N. Greeves, S. Warren, *Organic Chemistry*, 1st Ed, Oxford University Press, 2000.
[10] J. Keeler, *Understanding NMR Spectroscopy*, John Wiley and Sons Ltd, 2005,6.
[11] J.P. Glusker, K.N. Trueblood, *Crystal Structure Analysis : A Primer*, 3rd Ed, Oxford University Press, New York, 2010, 3-15.

A.5.1 CRYSTAL

A crystal is a solid material containing high degree of long-range three-dimensional internal order arrangement of atoms or ions. The ability of crystals to be diffracted was determined by Max von Laue in 1912. To produce or grow crystals, a great perseverance or patience is important as good quality of the crystal results in a clear crystal structure. Generally, crystals are grown from solution, cooling molten material or sublimation of material onto a surface. The basic building block of a crystal is an imaginary three-dimensional pattern called "unit cell" containing one unit of translational pattern. The unit cell of a crystal is defined by crystal axes such as *a*, *b*, *c*. The angles between the crystal axes are as follows; α between *b* and *c*, β between *a* and *c*, and γ between *a* and *b*. The unit cell direction are measured as x, y, z. With the use of a unit cell, the crystal faces are described. To characterise the crystal face or plane, the three integers are obtained in the process called "indexing". A crystal face or plane is indexed with three integer numbers, h, k and l and these three numbers are described in parentheses as (hkl). The concept of the crystal faces was introduced by William Whewell and William Hallowes Miller, and the three integers are referred to as miller indices.

A.5.2 BRAGG'S EQUATION

X-ray diffraction was utilised to illustrate the three-dimensional arrangement of atoms in a crystal by William Lawrence Bragg in 1913. If the x-rays beams are reflected from the planes passing through crystal lattice point, this reflection behaves like a mirror for which the angle of incidence of radiation is equal to the angle of reflection. The waves travels with an intergral multiple of the wavelength, nλ. Thus the Bragg's equation is expressed as

$$n\lambda = 2d\sin\theta$$

where λ is the wavelength, n is an integer, θ is the angle of incidence, and d is the distance between crystal lattice planes.[12]

[12] J.P Glusker, K.N. Trueblood, *Crystal Structure Analysis*, Oxford University Press, 1972, 32.
[13] R.J.D. Tilley, *Crystals and Crystal Structures*, John Wiley and Sons Ltd, 2006.

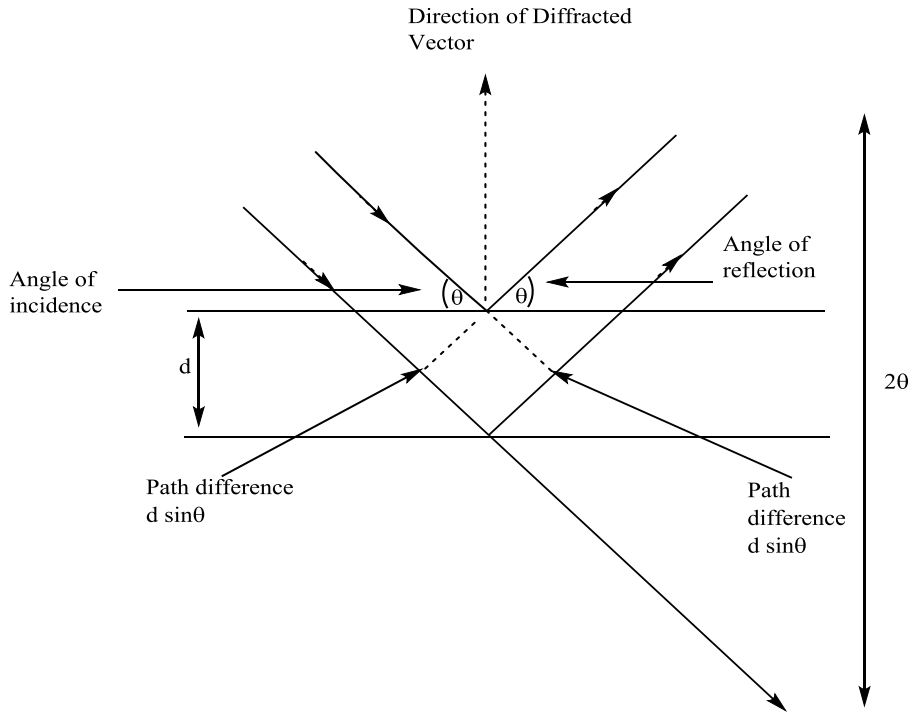

Figure A.7: Bragg's Law.

A.5.3 SCATTERING BY GROUP OF ATOMS – STRUCTURE FACTOR

The structure factor, F (hkl), is the X-ray radiation of waves scattered in the direction of the reflection hkl by j atoms in the unit cell. It is expressed as[13]

$$F(hkl) = F_{hkl} \exp(i\alpha_{hkl}) = \sum_i f_i \exp[2\pi i(hx_j + ky_j + lz_j)]$$

$$F(hkl) = F_{hkl} \exp(i\alpha_{hkl}) = \sum_j f_i \cos[2\pi(hx_j + ky_j + lz_j)] + i\sum_j f_i \sin[2\pi(hx_j + ky_j + lz_j)]$$

$$F_{hkl} = A_{hkl} + iB_{hkl}$$

where x_j, y_j and z_j are the positional coordinates of the j^{th} atom, f_j is the scattering factor of the j^{th} atom and α_{hkl} is the phase of diffracted beam. The scattering factor of the atom is the amplitude of the radiation scattered from the atom divided by the amplitude of the radiation scattered from a single.

The structure factor of the discrete atom summed is expressed as,

$$F(hkl) = \sum f_j e^{2\pi i(hxj + kyj + lzj)}$$

If the summation is replaced with an intergration and a cyclic electron density function, ρ with f_j, the structure factor is expressed in the form of Fourier transform as,

$$F\,(hkl) = \int \rho\,(x, y, z)\, e^{-2\pi i(hxj + kyj + lzj)}\, dV$$

This equation indicates that the cyclic electron density if the Fourier transform. Thus,

$$\rho\,(x, y, z) = \int F\,(hkl)\, e^{-2\pi i(hj + ky + lz)}\, dV$$

this equation is depicted as the relationship between electron density and the structure factor, and it is thus expressed in the form of summation as,

$$\rho\,(x, y, z) = \frac{1}{v} \sum \sum \sum F\,(hkl)\, e^{-2\pi i(hj + ky + lz)}$$

The above equation illustrates that electron density, ρ, can be calculated at any point (*x*, *y*, *z*) by making Fourier-series with coefficients that are equal to structure factors. This is considered to be the basic equation of crystallography. The symbol $I_o(hkl)$ can be utilised to represent the square of the structure factor, $|F\,(hkl)|^2$ and this symbol is called ideal intensity.[14]

$$I_o(hkl) \alpha |F\,(hkl)|^2$$

A.5.4 METHODS USED TO SOLVE PHASE PROBLEM

Phase problem is the circumstance where the data contains only the structure factor amplitude and not their phase angles. Two methods used for solving phase problem are, the Patterson method and direct method.[15]

A.5.4.1 Patterson Method

The Fourier transform $|F_o(hkl)|$ of the diffracted beam amplitides gives electron density and requires the position of the phase for determination of the structure factor F (hkl). The electron density at a certain point (*x*, *y*, *z*) is expressed as,[15]

$$P\,(x, y, z) = \frac{1}{Vc} \sum_h \sum_k \sum_l |F_o(hkl)|^2\, e^{-2\pi i(hj + ky + lz)}$$

[14] M.F.C Ladd, R.A. Palmer, *Structure Determination by X-ray Crystallography*, Plenum Press, 1993, 198.
[15] W. Clegg, *Crystal Structure Determination*, New York, Oxford University Press Inc, 1998.
[16] L.V. Azároff, *Elements of x-ray crystallography*, McGraw Hill, 1968, 323.

A.5.4.2 Direct Method

Direct methods are used to determine good phase information for structures consisting of no heavy atoms. Direct method has a common feature of the values for x-ray reflections derived from the structure factor calculated on parts of the structure.[15]

A.5.4.3 Least-Square Refinement

When the correct crystal structure is obtained, the diffraction pattern can be assessed. When atoms of the model structure correlate in correct position, then the calculated and observed structure factor should be similar. The least-square refinement shows the comparison of the calculated structure factor $|F_c|$ to the observed structure factor $|F_o|$. The difference between them, $||F_c| - |F_o||$ is described in terms of the residual index of R-factor as,

$$R = \frac{\sum ||F_c| - |F_o||}{\sum |F_o|}$$

where R is called R-factor for a set of structure factor magnitudes.

The equation of R-factor is varied with the use of F^2 instead of |F| values. Thus a residual factor used to determine the crystal structure is expressed as[15,16]

$$wR2 = \sqrt{\frac{\sum w(F_o^2 - F_c^2)^2}{\sum w(F_o^2)^2}}$$

With *w*R as weight of the reflection and this equation is useful in statistical study.

A.6 CHEMICAL KINETICS

Chemical kinetics is the branch of chemistry that deals with rates of chemical reactions and factors on which the rates depend. The chemical kinetics is used to analyse the mechanism of chemical reaction of a simple and complex chemical reaction involving only one step or several consecutive steps. The chemical reactions that proceeds in a single step are called elementary reactions and other reactions proceeding in more than one step are called composite, stepwise or complex reactions.

A.6.1 RATES OF CONSUMPTION AND FORMATION

Chemical kinetics deals with rate of concentration of reactants and products. Consider a chemical reaction,

$$X + 3Y \longrightarrow 2Z$$

If the mixture contains X and Y but no Z, the rate of consumption of X is given as,

$$V_x = -\frac{d[X]}{dt}$$

In the beginning of the reaction, the negative slope represent the initial rate of consumption of X. The rate of formation of Z is given as

$$V_z = \frac{d[Z]}{dt}$$

The chemical reactions with stoichiometric coefficient are different for the three material X, Y, Z, and the change in concentration will also differ. Hence, the rate of consumption of Y, V_y, will be three times the rate of consumption of X, V_x, while the rate of formation of Z, V_z, will be twice the rate of consumption of X.

$$V_x = \frac{1}{3}V_y = \frac{1}{2}V_Z$$

where V_x, V_y, and V_z are rates of reactions.[16]

A.6.2 RATE OF REACTION

Consider the chemical reaction,

$$xX + yY \longrightarrow zZ + aA$$

If the rate of a chemical reaction is defined in a constant volume, the rate of the change of concentrations of reactants and products is given by,

$$V = -\frac{1}{x}\frac{dx}{dt} = -\frac{1}{y}\frac{dy}{dt} = \frac{1}{z}\frac{dz}{dt} = \frac{1}{a}\frac{da}{dt}$$

The time derivative of the concentration are either the rates of consumption or formation, hence the rate of reaction can be defined by

[16] K.J. Laidler, J.H. Meiser, B.L. Sanctuary, *Physical Chemistry*, 4th Ed, Houghton Miffin Company, New York, 2003, 363.

$$V = \frac{V_X}{x} = \frac{V_Y}{y} = \frac{V_Z}{z} = \frac{V_A}{a}$$

A.6.3 EMPIRICAL RATE EQUATION – RATE LAW

The empirical rate equation is expressed as

$$V_x = k_x[X]^{\alpha}[Y]^{\beta}$$

where k_x, α, and β are independent of the concentration and time. The k_x is called the rate constant, while α and β are orders of the reaction.

A.6.4 *PSEUDO*-FIRST ORDER REACTION

Consider that concentration of one reactants is smaller than the other reactant. That is,

$$[X] >> [Y]$$

The empirical rate equation is expressed as

$$\text{Rate} = V = k_{obs}[Y]^n \text{ and } k_{obs}[X]^m$$

where k_{obs} is the pseudo-first order constant. The second order reactions are treated the same way. There are two possibilities that describes second order reaction, and are that the rate of reaction is proportional to the reactant with two equal concentrations or different concentration. For similar concentration, the chemical reaction is expressed as

$$2X \longrightarrow Z$$

Different concentration has the chemical reaction of

$$X + Y \longrightarrow Z$$

And the rate equation is expressed as

$$\text{Rate} = V = k_1[X][Y] + k_2[X]$$

If the reaction is the pseudo-first order reaction, the constant k_{obs} is expressed as

$$k_{obs} = k_1[Y] + k_2$$

k_1 is the forward reaction constant and k_2 is the reverse constant. From this we obtain the equilibrium constant as

$$K_{eq} = \frac{k_1}{k_2}$$

Integrating from t = 0 to t = t, the initial rate equation becomes

$$\ln\frac{[\Delta Y]_t}{[\Delta Y]_o} = k_{obs}$$

where $[\Delta Y]_t$ and $[\Delta Y]_o$ represent the change in concentration of reactants at the time t and 0. Using Beer's law, the concentration corresponds to absorbance and is given by

$$A_t = A_\infty - (A_\infty - A_o)\exp(k_{obs})t$$

Where A_t is the absorbance at time t, A_o is the absorbance at time 0 and A_∞ is the absorbance at time infinity, ∞.[17]

[17] J.H. Espenson, *Chemical Kinetics and Reaction Mechanism*, McGraw Hill, 1981, 1.

APPENDIX B

Table B.1: Atomic coordinates ($x10^4$) and equivalent isotropic displacement ($Å^2 \times 10^3$) for 5Me-Sal-Cyhex. $U_{(eq)}$ is defined as one third of the trace of the orthogonalized U^{ij} tensor.

Atom	x	y	z	$U_{(eq)}$
N(1)	533(3)	92(2)	854(7)	41(4)
O(1)	214(2)	255(2)	841(5)	54(5)
C(1)	524(3)	50(3)	800(8)	41(5)
C(11)	366(3)	100(2)	763(8)	37(5)
C(12)	211(3)	197(2)	785(8)	40(5)
C(13)	53(3)	234(3)	750(9)	43(5)
C(14)	43(3)	178(3)	693(9)	42(5)
C(15)	198(3)	87(3)	670(8)	44(5)
C(16)	356(3)	48(2)	705(8)	43(5)
C(21)	689(3)	28(2)	891(8)	41(5)
C(22)	602(4)	-83(3)	938(9)	51(6)
C(23)	757(3)	-143(3)	981(9)	53(6)
C(24)	867(4)	3(3)	1007(9)	55(7)
C(25)	954(4)	114(3)	960(1)	58(7)
C(26)	801(3)	174(2)	917(9)	48(6)
C(141)	132(4)	216(3)	657(1)	57(6)

Table B.2: Bond distances (Å) and angles (^{o}) for 5Me-Sal-Cyhex.

Bond	Bond distance	Bond	Bond angles
N1-C1	1.272(2)	C1-N1-C21	120.16(18)
N1-C21	1.457(2)	C12-O1-H2	109.5
O1-C12	1.354(2)	N1-C1-C11	122.44(19)
O1-H2	0.84	N1-C1-H1	118.8
C1-C11	1.447(3)	C11-C1-H1	118.8
C1-H1	0.95	C16-C11-C12	117.88(19)
C11-C16	1.395(3)	C16-C11-C1	121.54(19)
C11-C12	1.413(3)	C12-C11-C1	120.50(17)
C12-C13	1.380(3)	O1-C12-C13	118.84(19)
C13-C14	1.392(3)	O1-C12-C11	120.79(19)
C13-H13	0.95	C13-C12-C11	120.37(18)
C14-C15	1.394(3)	C12-C13-C14	121.3(2)
C14-C141	1.497(3)	C12-C13-H13	119.4
C15-C16	1.382(3)	C14-C13-H13	119.4

C15-H15	0.95	C13-C14-C15	118.4(2)
C16-H16	0.95	C13-C14-C141	120.3(2)
C21-C26	1.519(3)	C15-C14-C141	121.23(19)
C21-C22	1.526(3)	C16-C15-C14	120.74(17)
C21-H21	1	C16-C15-H15	119.6
C22-C23	1.530(3)	C14-C15-H15	119.6
C22-H22A	0.99	C15-C16-C11	121.2(2)
C22-H22B	0.99	C15-C16-H16	119.4
C23-C24	1.512(3)	C11-C16-H16	119.4
C23-H23A	0.99	N1-C21-C26	110.17(16)
C23-H23B	0.99	N1-C21-C22	108.78(17)
C24-C25	1.522(3)	C26-C21-C22	110.99(17)
C24-H24A	0.99	N1-C21-H21	109
C24-H24B	0.99	C26-C21-H21	109
C25-C26	1.524(3)	C22-C21-H21	109
C25-H25A	0.99	C21-C22-C23	111.36(19)
C25-H25B	0.99	C21-C22-H22A	109.4
C26-H26A	0.99	C23-C22-H22A	109.4
C26-H26B	0.99	C21-C22-H22B	109.4
C141-H14A	0.98	C23-C22-H22B	109.4
C141-H14B	0.98	H22A-C22-H22B	108
C141-H14C	0.98	C24-C23-C22	111.54(17)
		C24-C23-H23A	109.3
		C22-C23-H23A	109.3
		C24-C23-H23B	109.3
		C22-C23-H23B	109.3
		H23A-C23-H23B	108
		C23-C24-C25	110.73(18)
		C23-C24-H24A	109.5
		C25-C24-H24A	109.5
		C23-C24-H24B	109.5
		C25-C24-H24B	109.5
		H24A-C24-H24B	108.1
		C24-C25-C26	111.8(2)
		C24-C25-H25A	109.3
		C26-C25-H25A	109.3
		C24-C25-H25B	109.3
		C26-C25-H25B	109.3
		H25A-C25-H25B	107.9
		C21-C26-C25	111.72(17)
		C21-C26-H26A	109.3
		C25-C26-H26A	109.3

		C21-C26-H26B	109.3
		C25-C26-H26B	109.3
		H26A-C26-H26B	107.9
		C14-C141-H14A	109.5
		C14-C141-H14B	109.5
		H14A-C141-H14B	109.5
		C14-C141-H14C	109.5
		H14A-C141-H14C	109.5
		H14B-C141-H14C	109.5

Table B.3: Anisotropic displacement parameters ($Å^2$ x 10^3) for 5Me-Sal-Cyhex. The anisotropic displacement factor exponent takes the form: $-2\pi(h2^{*2}U^{11}+\ldots 2hka^{*}b^{*}U^{12})$.

Atom	U11	U22	U33	U12	U13	U23
N(1)	38(1)	43(9)	42(9)	4(8)	2(8)	38(8)
O(1)	48(1)	73(1)	41(8)	18(8)	2(8)	-78(7)
C(1)	37(1)	38(1)	48(1)	0(1)	7(1)	-0(1)
C(11)	36(1)	35(1)	42(1)	1(1)	6(9)	3(8)
C(12)	40(1)	42(1)	39(1)	2(1)	7(1)	1(9)
C(13)	37(1)	46(1)	46(1)	5(1)	7(1)	3(1)
C(14)	41(1)	39(1)	47(1)	-7(1)	1(1)	5(1)
C(15)	51(1)	41(1)	41(1)	-2(1)	3(1)	-1(9)
C(16)	46(1)	39(1)	45(1)	4(1)	8(1)	-4(9)
C(21)	38(1)	41(1)	43(1)	6(1)	2(1)	2(9)
C(22)	44(1)	50(1)	59(1)	-3(1)	-1(1)	13(1)
C(23)	50(2)	49(1)	59(1)	-2(1)	-1(1)	15(1)
C(24)	62(2)	55(1)	50(1)	10(1)	-8(1)	1(1)
C(25)	56(2)	51(1)	66(1)	-12(1)	-14(1)	3(1)
C(26)	50(1)	42(1)	53(1)	-4(1)	1(1)	6(1)
C(141)	49(2)	67(2)	54(1)	-4(1)	-7(1)	6(1)

Table B.4: Hydrogen coordinates (x10^4) and isotropic displacement parameters ($Å^2$ x 10^3) for 5Me-Sal-Cyhex.

Atom	x	y	z	$U_{(eq)}$
H(2)	309	213	858	81
H(1)	626	-17	784	49
H(13)	-50	299	766	52
H(15)	195	51	631	53
H(16)	459	-16	689	52

H(21)	779	-41	866	49
H(22A)	539	-181	920	61
H(22B)	502	-18	960	61
H(23A)	695	-209	1012	63
H(23B)	849	-218	960	63
H(24A)	971	-40	1033	66
H(24B)	778	71	1032	66
H(25A)	1054	49	939	70
H(25B)	1018	212	978	70
H(26A)	711	251	937	58
H(26B)	865	238	885	58
H(14A)	-114	323	636	85
H(14B)	-246	224	682	85
H(14C)	-151	126	628	85

Table B.5: Torsion angles (^{o}) for 5Me-Sal-Cyhex.

Bond	Angles
N1-N1-C1-C11	0.0(7)
C21-N1-C1-C11	175.84(17)
N1-C1-C11-C16	-177.7(2)
N1-C1-C11-C12	-0.9(3)
C16-C11-C12-O1	-178.6(2)
C1-C11-C12-O1	4.5(3)
C16-C11-C12-C13	1.6(3)
C1-C11-C12-C13	-175.29(18)
O1-C12-C13-C14	179.91(19)
C11-C12-C13-C14	-0.3(3)
C12-C13-C14-C15	-1.6(3)
C12-C13-C14-C141	178.23(19)
C13-C14-C15-C16	2.1(3)
C141-C14-C15-C16	-177.71(19)
C14-C15-C16-C11	-0.8(3)
C12-C11-C16-C15	-1.1(3)
C1-C11-C16-C15	175.77(18)
C1-N1-C21-C26	122.1(2)
N1-N1-C21-C22	0.0(8)
C1-N1-C21-C22	-116.0(2)
N1-C21-C22-C23	-175.93(17)
C26-C21-C22-C23	-54.6(2)
C21-C22-C23-C24	55.8(2)
C22-C23-C24-C25	-55.6(3)
C23-C24-C25-C26	55.2(3)

N1-C21-C26-C25	174.78(17)
C22-C21-C26-C25	54.2(2)
C24-C25-C26-C21	-54.9(3)

Table B.6: Hydrogen bond distances (Å) and angles (°) for 5Me-Sal-Cyhex.

D−H···*A*	D−H (Å)	H···*A* (Å)	*D*···*A* (Å)	*D*−H···*A* (°)
O1−H2···N1	0.84	1.82	2.517	147
C1-H1…Cg1 #1	0.95	2.98	3.806	147
C13-H13…Cg1#2	0.95	2.92	3.721	143

Symmetry codes and transformation used to generate equivalent atoms:
#1 2-x, 1/2+y, 1/2-z, #2 1-x, -1/2+y, 1/2-z.

Table B.7: Atomic coordinates (x10^4) and equivalent isotropic displacement (Å^2 x 10^3) for *fac*-[Re(CO)$_3$(HOCH$_3$)(5Me-Sal-Cyhex)]. $U_{(eq)}$ is defined as one third of the trace of the orthogonalized U^{ij} tensor.

Atom	x	y	z	$U_{(eq)}$
Re(1)	3571(1)	4491(1)	1458(1)	32(1)
O(1)	4480(2)	3789(3)	1353(3)	37(1)
C(24)	2832(4)	5210(5)	1656(5)	44(2)
C(25)	2978(4)	4310(5)	110(6)	43(2)
C(27)	3887(4)	5632(5)	1067(5)	44(2)
C(01)	4146(3)	2206(4)	1443(4)	36(1)
N(1)	3269(2)	3147(3)	1933(3)	35(1)
O(26)	4275(3)	4593(3)	3025(4)	41(1)
C(05)	5092(3)	2622(4)	800(4)	40(1)
C(25)	2614(3)	4192(4)	-721(4)	69(2)
C(08)	3574(3)	2384(4)	1839(5)	39(1)
C(12)	2740(4)	3588(5)	3265(5)	49(2)
C(14)	1398(5)	3642(7)	2816(7)	81(3)
C(06)	4561(3)	2890(4)	1198(4)	33(1)
O(24)	2390(3)	5695(4)	1760(5)	67(2)
C(03)	4833(4)	1030(5)	942(5)	55(2)
C(13)	2101(4)	3426(6)	3631(6)	66(2)
C(11)	2648(3)	3036(5)	2308(5)	46(2)
C(26)	4282(5)	5378(6)	3690(7)	75(3)
O(27)	4057(3)	6338(4)	841(4)	71(2)
C(16)	1941(3)	3223(5)	1483(5)	52(2)
C(15)	1316(4)	3082(7)	1871(6)	72(2)
C(02)	4304(4)	1265(5)	1311(5)	51(2)

C(04)	5237(3)	1700(5)	668(5)	44(2)
C(07)	5807(4)	1446(6)	222(7)	67(2)

Table B.8: Bond distances (Å) and angles (°) for *fac*-[Re(CO)$_3$(HOCH$_3$)(5Me-Sal-Cyhex)].

Bond	Bond distances	Bond	Bond angles
Re1-C25	1.883(8)	C25-Re1-C24	88.1(3)
Re1-C24	1.886(7)	C25-Re1-C27	89.3(3)
Re1-C27	1.906(7)	C24-Re1-C27	84.8(3)
Re1-O1	2.112(4)	C25-Re1-O1	97.3(2)
Re1-N1	2.198(5)	C24-Re1-O1	173.5(2)
O1-C06	1.335(7)	C27-Re1-O1	91.6(2)
C24-O24	1.168(8)	C25-Re1-O26	175.8(2)
C25-O25	1.162(8)	C24-Re1-O26	94.8(2)
C27-O27	1.151(8)	C27-Re1-O26	93.9(2)
C01-C06	1.398(8)	O1-Re1-O26	79.94(16)
C01-C02	1.421(9)	C25-Re1-N1	92.2(2)
N1-C08	1.284(8)	C24-Re1-N1	98.1(2)
N1-C11	1.495(8)	C27-Re1-N1	176.8(2)
O26-C26	1.464(9)	O1-Re1-N1	85.39(16)
C05-C04	1.388(9)	O26-Re1-N1	84.44(17)
C05-C06	1.396(8)	C06-O1-Re1	129.0(3)
C05-H05	0.93	O24-C24-Re1	176.4(6)
C08-H08	9300	O25-C25-Re1	179.6(7)
C12-C11	1.517(9)	O27-C27-Re1	177.4(7)
C12-C13	1.531(10)	C06-C01-C02	118.2(6)
C12-H12A	0.97	C06-C01-C08	124.7(5)
C12-H12B	0.97	C02-C01-C08	117.1(6)
C14-C15	1.512(12)	C08-N1-C11	114.3(5)
C14-C13	1.514(12)	C08-N1-Re1	122.9(4)
C14-H14A	0.97	C26-O26-Re1	124.1(4)
C14-H14B	0.97	C04-C05-C06	122.3(6)
C03-C02	1.355(10)	C04-C05-H05	118.8
C03-C04	1.387(10)	C06-C05-H05	118.8
C03-H03	0.93	N1-C08-C01	130.5(6)
C13-H13A	0.97	N1-C08-H08	114.8
C13-H13B	0.97	C01-C08-H08	114.8
C11-C16	1.517(9)	C11-C12-C13	110.0(6)
C11-H11	0.98	C11-C12-H12A	109.7
C26-H26A	0.96	C13-C12-H12A	109.7

C26-H26B	0.96	C11-C12-H12B	109.7
C26-H26C	0.96	C13-C12-H12B	109.7
C16-C15	1.519(10)	H12A-C12-H12B	108.2
C16-H16A	0.97	C15-C14-C13	110.9(7)
C16-H16B	0.97	C15-C14-H14A	109.5
C15-H15A	0.97	C13-C14-H14A	109.5
C15-H15B	0.97	C15-C14-H14B	109.5
C02-H02	0.93	C13-C14-H14B	109.5
C04-C07	1.504(10)	H14A-C14-H14B	108
C07-H07A	0.96	O1-C06-C05	118.8(5)
C07-H07B	0.96	O1-C06-C01	122.4(5)
C07-H07C	0.96	C05-C06-C01	118.8(6)
		C02-C03-C04	121.2(6)
		C02-C03-H03	119.4
		C04-C03-H03	119.4
		C14-C13-C12	111.8(6)
		C14-C13-H13A	109.3
		C12-C13-H13A	109.3
		C14-C13-H13B	109.3
		C12-C13-H13B	109.3
		H13A-C13-H13B	107.9
		N1-C11-C16	111.9(5)
		N1-C11-C12	112.3(5)
		C16-C11-C12	113.0(6)
		N1-C11-H11	106.4
		C16-C11-H11	106.4
		C12-C11-H11	106.4
		O26-C26-H26A	109.5
		O26-C26-H26B	109.5
		H26A-C26-H26B	109.5
		O26-C26-H26C	109.5
		H26A-C26-H26C	109.5
		H26B-C26-H26C	109.5
		C11-C16-C15	111.1(6)
		C11-C16-H16A	109.4
		C15-C16-H16A	109.4
		C11-C16-H16B	109.4
		C15-C16-H16B	109.4
		H16A-C16-H16B	108
		C14-C15-C16	112.0(6)
		C14-C15-H15A	109.2
		C16-C15-H15A	109.2

		C14-C15-H15B	109.2
		C16-C15-H15B	109.2
		H15A-C15-H15B	107.9
		C03-C02-C01	121.3(6)
		C03-C02-H02	119.3
		C01-C02-H02	119.3
		C03-C04-C05	118.1(6)
		C03-C04-C07	121.6(6)
		C05-C04-C07	120.4(6)
		C04-C07-H07A	109.5
		C04-C07-H07B	109.5
		H07A-C07-H07B	109.5
		C04-C07-H07C	109.5
		H07A-C07-H07C	109.5
		H07B-C07-H07C	109.5

Table B.9: Anisotropic displacement parameters ($Å^2$ x 10^3) for *fac*-[$Re(CO)_3(HOCH_3)$(5Me-Sal-Cyhex)]. The anisotropic displacement factor exponent takes the form: $-2\pi(h2^{*2}U^{11}+\ldots 2hka^{*}b^{*}U^{12})$.

Atom	U11	U22	U33	U13	U12	U23
Re(1)	31(1)	30(1)	34(1)	9(1)	1(1)	1(1)
O(1)	35(2)	29(2)	49(2)	16(2)	-2(2)	-3(2)
C(24)	40(4)	38(4)	51(4)	10(3)	0(3)	2(3)
C(25)	45(4)	44(4)	43(4)	19(3)	-3(3)	5(3)
C(27)	47(4)	39(4)	44(4)	15(3)	0(3)	6(3)
C(01)	37(3)	35(3)	33(3)	7(3)	-2(3)	-6(3)
N(1)	32(2)	38(3)	35(3)	11(2)	1(2)	-1(2)
O(26)	40(3)	44(3)	37(3)	8(2)	6(2)	-7(2)
C(05)	38(3)	42(4)	38(3)	11(3)	-6(3)	-9(3)
O(25)	70(4)	84(4)	40(3)	1(3)	-15(3)	-2(3)
C(08)	40(3)	38(4)	36(3)	9(3)	-11(3)	-3(3)
C(12)	53(4)	55(4)	42(4)	18(3)	-4(3)	-4(3)
C(14)	63(5)	105(7)	89(6)	44(5)	-4(5)	-3(5)
C(06)	34(3)	35(3)	28(3)	5(2)	0(3)	-6(3)
O(24)	56(3)	62(3)	86(4)	28(3)	26(3)	4(3)
C(03)	62(4)	35(4)	65(5)	18(4)	5(3)	-12(3)
C(13)	79(5)	71(5)	62(5)	40(4)	-13(4)	-9(4)
C(11)	46(4)	45(4)	51(4)	24(3)	-6(3)	2(3)
C(26)	68(6)	87(6)	63(6)	12(4)	14(4)	2(4)
O(27)	83(4)	48(3)	86(4)	33(3)	-11(3)	16(3)

C(16)	40(4)	64(5)	51(4)	14(3)	-7(3)	-11(3)
C(15)	41(4)	98(6)	77(5)	22(4)	-18(4)	-12(5)
C(02)	56(4)	37(4)	61(4)	21(3)	-7(3)	-7(3)
C(04)	38(3)	47(4)	44(4)	9(3)	6(3)	-13(3)
C(07)	57(4)	62(5)	89(6)	33(4)	10(4)	-19(4)

Table B.10: Hydrogen coordinates (x10^4) and isotropic displacement parameters (Å^2 x 10^3) for *fac*-[Re(CO)$_3$(HOCH$_3$)(5Me-Sal-Cyhex)].

Atom	x	y	z	U(eq)
H(05)	5358	3078	617	47
H(08)	3396	1861	2063	46
H(12A)	2777	4241	3131	59
H(12B)	3178	3400	3786	59
H(14A)	1006	3503	3063	98
H(14B)	1379	4296	2654	98
H(03)	4928	407	871	66
H(13A)	2100	2785	3838	80
H(13B)	2151	3813	4216	80
H(11)	2640	2382	2492	55
H(26A)	4453	5919	3445	112
H(26B)	4591	5240	4363	112
H(26C)	3805	5488	3699	112
H(16A)	1891	2810	918	62
H(16B)	1936	3854	1244	62
H(15A)	876	3260	1348	86
H(15B)	1281	2431	2017	86
H(02)	4038	801	1482	61
H(07A)	6018	865	498	100
H(07B)	6169	1917	383	100
H(07C)	5598	1393	-500	100

Table B.11: Torsion angles (^{o}) for *fac*-[Re(CO)$_3$(HOCH$_3$)(5Me-Sal-Cyhex)].

Bond	Angle
C(11)-N(1)-C(08)-C(01)	175.3(6)
Re(1)-N(1)-C(08)-C(01)	0.5(9)
C(06)-C(01)-C(08)-N(1)	9.6(10)
C(02)-C(01)-C(08)-N(1)	-171.7(6)
Re(1)-O(1)-C(06)-C(05)	157.2(4)

Re(1)-O(1)-C(06)-C(01)	-24.3(7)
C(04)-C(05)-C(06)-O(1)	176.5(5)
C(04)-C(05)-C(06)-C(01)	-2.1(8)
C(02)-C(01)-C(06)-O(1)	-176.0(5)
C(08)-C(01)-C(06)-O(1)	2.8(9)
C(02)-C(01)-C(06)-C(05)	2.5(8)
C(08)-C(01)-C(06)-C(05)	-178.7(6)
C(15)-C(14)-C(13)-C(12)	56.4(10)
C(11)-C(12)-C(13)-C(14)	-55.1(9)
C(08)-N(1)-C(11)-C(16)	-108.5(6)
Re(1)-N(1)-C(11)-C(16)	66.4(6)
C(08)-N(1)-C(11)-C(12)	123.2(6)
Re(1)-N(1)-C(11)-C(12)	-61.9(6)
C(13)-C(12)-C(11)-N(1)	-178.3(6)
C(13)-C(12)-C(11)-C(16)	54.0(8)
N(1)-C(11)-C(16)-C(15)	178.5(6)
C(12)-C(11)-C(16)-C(15)	-53.6(9)
C(13)-C(14)-C(15)-C(16)	-55.5(11)
C(11)-C(16)-C(15)-C(14)	53.8(10)
C(04)-C(03)-C(02)-C(01)	-0.7(11)
C(06)-C(01)-C(02)-C(03)	-1.2(9)
C(08)-C(01)-C(02)-C(03)	179.9(6)
C(02)-C(03)-C(04)-C(05)	1.2(10)
C(02)-C(03)-C(04)-C(07)	-177.7(7)
C(06)-C(05)-C(04)-C(03)	0.2(9)
C(06)-C(05)-C(04)-C(07)	179.1(6)

Table B.12: Hydrogen bond distances (Å) and angles (^{o}) for *fac*-[Re(CO)$_3$(HOCH$_3$)(5Me-Sal-Cyhex)].

O-H…O	d(O-H) (Å)	d(H…O) (Å)	d(O…O) (Å)	<(O-H…O) (^{o})
O26-H26D…O1#1	0.99	1.63	2.605	165

Symmetry codes and transformation used to generate equivalent atoms:
#1 1-x, y, ½-z

Table B.13: Atomic coordinates (x10^4) and equivalent isotropic displacement (Å^2 x 10^3) for *fac*-[Re(CO)$_3$(Imid)(5Me-Sal-Cyhex)]. U$_{(eq)}$ is defined as one third of the trace of the orthogonalized U^{ij} tensor.

Atom	x	y	z	U(eq)
C(01)	4584(3)	-1708(6)	6831(3)	41(1)
C(02)	5199(4)	-2913(8)	7164(4)	52(1)
C(03)	5598(4)	-2894(8)	7983(4)	56(1)
C(04)	5409(4)	-1693(9)	8511(4)	55(1)
C(05)	4817(4)	-489(8)	8204(3)	51(1)
C(06)	4391(3)	-452(6)	7357(3)	41(1)
C(07)	5861(6)	-1643(12)	9416(5)	88(3)
C(08)	4181(3)	-1888(6)	5959(3)	39(1)
C(11)	3305(3)	-1458(6)	4611(3)	39(1)
C(12)	3796(3)	-540(7)	4062(3)	44(1)
C(13)	3440(5)	-967(9)	3151(4)	62(2)
C(14)	3422(5)	-2816(10)	2990(3)	68(2)
C(15)	2928(5)	-3725(8)	3535(4)	62(2)
C(16)	3306(4)	-3329(7)	4453(3)	49(1)
C(018)	1334(4)	421(9)	6200(5)	77(2)
C(019)	2228(4)	-1508(7)	6626(4)	49(1)
C(020)	953(4)	-740(10)	6574(5)	77(2)
C(24)	2472(4)	1974(7)	4850(3)	51(1)
C(25)	4031(4)	2715(7)	5625(4)	53(1)
C(27)	2725(4)	3457(7)	6257(4)	55(1)
N(1)	3612(3)	-943(5)	5509(2)	36(1)
N(2)	2152(3)	-60(6)	6243(3)	45(1)
N(3)	1515(3)	-1975(7)	6823(3)	53(1)
O(1)	3824(2)	725(5)	7106(2)	49(1)
O(24)	2027(4)	2320(9)	4217(3)	88(2)
O(25)	4522(3)	3559(6)	5440(5)	88(2)
O(27)	2443(4)	4696(6)	6427(3)	83(2)
Re(1)	3147(1)	1417(1)	5898(1)	38(1)

Table B.14: Bond distances (Å) and angles (^{o}) for *fac*-[Re(CO)$_3$(Imid)(5Me-Sal-Cyhex)].

Bond	Bond distance	Bond	Bond angles
C(01)-C(06)	1.408(7)	C(06)-C(01)-C(02)	119.1(5)
C(01)-C(02)	1.410(7)	C(06)-C(01)-C(08)	124.6(5)
C(01)-C(08)	1.447(7)	C(02)-C(01)-C(08)	116.3(5)
C(02)-C(03)	1.361(8)	C(03)-C(02)-C(01)	121.2(5)
C(02)-H(02)	0.93	C(03)-C(02)-H(02)	119.4
C(03)-C(04)	1.376(10)	C(01)-C(02)-H(02)	119.4
C(03)-H(03)	0.93	C(02)-C(03)-C(04)	120.7(5)
C(04)-C(05)	1.376(8)	C(02)-C(03)-H(03)	119.7
C(04)-C(07)	1.509(9)	C(04)-C(03)-H(03)	119.7

C(05)-C(06)	1.413(7)	C(03)-C(04)-C(05)	119.6(5)
C(05)-H(05)	0.93	C(03)-C(04)-C(07)	120.9(6)
C(06)-O(1)	1.318(6)	C(05)-C(04)-C(07)	119.5(6)
C(07)-H(07A)	0.96	C(04)-C(05)-C(06)	121.8(5)
C(07)-H(07B)	0.96	C(04)-C(05)-H(05)	119.1
C(07)-H(07C)	0.96	C(06)-C(05)-H(05)	119.1
C(08)-N(1)	1.293(6)	O(1)-C(06)-C(01)	123.6(4)
C(08)-H(08)	0.93	O(1)-C(06)-C(05)	118.7(4)
C(11)-N(1)	1.509(6)	C(01)-C(06)-C(05)	117.7(5)
C(11)-C(16)	1.516(7)	C(04)-C(07)-H(07A)	109.5
C(11)-C(12)	1.524(7)	C(04)-C(07)-H(07B)	109.5
C(11)-H(11)	0.98	H(07A)-C(07)-H(07B)	109.5
C(12)-C(13)	1.523(8)	C(04)-C(07)-H(07C)	109.5
C(12)-H(12A)	0.97	H(07A)-C(07)-H(07C)	109.5
C(12)-H(12B)	0.97	H(07B)-C(07)-H(07C)	109.5
C(13)-C(14)	1.499(10)	N(1)-C(08)-C(01)	128.3(5)
C(13)-H(13D)	0.97	N(1)-C(08)-H(08)	115.8
C(13)-H(13E)	0.97	C(01)-C(08)-H(08)	115.8
C(14)-C(15)	1.519(10)	N(1)-C(11)-C(16)	115.1(4)
C(14)-H(14C)	0.97	N(1)-C(11)-C(12)	110.3(4)
C(14)-H(14D)	0.97	C(16)-C(11)-C(12)	110.6(4)
C(15)-C(16)	1.533(8)	N(1)-C(11)-H(11)	106.8
C(15)-H(15A)	0.97	C(16)-C(11)-H(11)	106.8
C(15)-H(15B)	0.97	C(12)-C(11)-H(11)	106.8
C(16)-H(16A)	0.97	C(13)-C(12)-C(11)	110.1(5)
C(16)-H(16B)	0.97	C(13)-C(12)-H(12A)	109.7
C(018)-C(020)	1.341(9)	C(11)-C(12)-H(12A)	109.7
C(018)-N(2)	1.377(7)	C(13)-C(12)-H(12B)	109.7
C(018)-H(018)	0.93	C(11)-C(12)-H(12B)	109.7
C(019)-N(2)	1.309(6)	H(12A)-C(12)-H(12B)	108.2
C(019)-N(3)	1.330(7)	C(14)-C(13)-C(12)	112.5(5)
C(019)-H(019)	0.93	C(14)-C(13)-H(13D)	109.1
C(020)-N(3)	1.347(8)	C(12)-C(13)-H(13D)	109.1
C(020)-H(020)	0.93	C(14)-C(13)-H(13E)	109.1
C(24)-O(24)	1.163(7)	C(12)-C(13)-H(13E)	109.1
C(24)-Re(1)	1.881(6)	H(13D)-C(13)-H(13E)	107.8
C(25)-O(25)	1.140(7)	C(13)-C(14)-C(15)	111.0(6)
C(25)-Re(1)	1.911(6)	C(13)-C(14)-H(14C)	109.4
C(27)-O(27)	1.153(7)	C(15)-C(14)-H(14C)	109.4
C(27)-Re(1)	1.913(6)	C(13)-C(14)-H(14D)	109.4
N(1)-Re(1)	2.181(4)	C(15)-C(14)-H(14D)	109.4
N(2)-Re(1)	2.184(4)	H(14C)-C(14)-H(14D)	108

O(1)-Re(1)	2.122(4)	C(14)-C(15)-C(16)	109.6(5)
		C(14)-C(15)-H(15A)	109.7
		C(16)-C(15)-H(15A)	109.7
		C(14)-C(15)-H(15B)	109.7
		C(16)-C(15)-H(15B)	109.7
		H(15A)-C(15)-H(15B)	108.2
		C(11)-C(16)-C(15)	110.9(5)
		C(11)-C(16)-H(16A)	109.5
		C(15)-C(16)-H(16A)	109.5
		C(11)-C(16)-H(16B)	109.5
		C(15)-C(16)-H(16B)	109.5
		H(16A)-C(16)-H(16B)	108.1
		C(020)-C(018)-N(2)	109.2(6)
		C(020)-C(018)-H(018)	125.4
		N(2)-C(018)-H(018)	125.4
		N(2)-C(019)-N(3)	111.9(5)
		N(2)-C(019)-H(019)	124.1
		N(3)-C(019)-H(019)	124.1
		C(018)-C(020)-N(3)	106.9(6)
		C(018)-C(020)-H(020)	126.5
		N(3)-C(020)-H(020)	126.5
		O(24)-C(24)-Re(1)	177.3(5)
		O(25)-C(25)-Re(1)	175.8(5)
		O(27)-C(27)-Re(1)	176.1(6)
		C(08)-N(1)-C(11)	116.2(4)
		C(08)-N(1)-Re(1)	126.0(3)
		C(11)-N(1)-Re(1)	117.6(3)
		C(019)-N(2)-C(018)	104.9(5)
		C(019)-N(2)-Re(1)	127.4(4)
		C(018)-N(2)-Re(1)	127.3(4)
		C(019)-N(3)-C(020)	107.1(5)
		C(06)-O(1)-Re(1)	131.4(3)
		C(24)-Re(1)-C(25)	88.5(3)
		C(24)-Re(1)-C(27)	84.6(3)
		C(25)-Re(1)-C(27)	87.4(2)
		C(24)-Re(1)-O(1)	175.6(2)
		C(25)-Re(1)-O(1)	95.8(2)
		C(27)-Re(1)-O(1)	94.5(2)
		C(24)-Re(1)-N(1)	96.0(2)
		C(25)-Re(1)-N(1)	93.87(19)
		C(27)-Re(1)-N(1)	178.6(2)
		O(1)-Re(1)-N(1)	84.76(14)

		C(24)-Re(1)-N(2)	92.9(2)
		C(25)-Re(1)-N(2)	178.6(2)
		C(27)-Re(1)-N(2)	92.2(2)
		O(1)-Re(1)-N(2)	82.88(16)
		N(1)-Re(1)-N(2)	86.50(15)

Table B.15: Anisotropic displacement parameters ($Å^2$ x 10^3) for *fac*-[$Re(CO)_3$(Imid)(5Me-Sal-Cyhex)]. The anisotropic displacement factor exponent takes the form: $-2\pi(h^2 a^{*2} U^{11} + \ldots 2hka^* b^* U^{12})$.

Atom	U11	U22	U33	U13	U12	U23
C(01)	48(3)	34(2)	41(2)	12(2)	5(2)	-1(2)
C(02)	51(3)	47(3)	54(3)	8(2)	7(2)	-3(3)
C(03)	52(3)	58(4)	53(3)	3(2)	9(3)	10(3)
C(04)	51(3)	65(4)	46(3)	5(2)	4(3)	6(3)
C(05)	58(3)	56(4)	39(2)	9(2)	5(3)	-3(2)
C(06)	49(3)	38(3)	39(2)	14(2)	0(2)	-1(2)
C(07)	91(6)	115(8)	48(4)	-6(4)	31(5)	1(4)
C(08)	46(3)	32(2)	41(2)	14(2)	5(2)	-2(2)
C(11)	44(3)	39(3)	37(2)	11(2)	2(2)	1(2)
C(12)	58(3)	38(3)	39(2)	19(2)	0(2)	6(2)
C(13)	81(4)	66(4)	42(3)	19(3)	6(3)	12(3)
C(14)	87(5)	78(5)	34(3)	7(3)	2(4)	-6(3)
C(15)	75(4)	60(4)	45(3)	1(3)	-6(3)	-12(3)
C(16)	61(3)	41(3)	41(3)	6(2)	-2(2)	2(2)
C(018)	69(4)	56(4)	116(6)	45(4)	18(3)	32(4)
C(019)	59(3)	37(3)	54(3)	16(3)	3(2)	11(2)
C(020)	65(4)	64(4)	116(6)	51(4)	10(3)	19(4)
C(24)	67(3)	39(3)	50(3)	21(3)	13(3)	7(2)
C(25)	55(3)	33(3)	75(4)	25(3)	11(2)	9(3)
C(27)	72(4)	36(3)	60(3)	23(3)	3(2)	1(2)
N(1)	45(2)	32(2)	35(2)	15(2)	1(2)	3(2)
N(2)	54(2)	37(2)	50(2)	24(2)	10(2)	10(2)
N(3)	59(3)	47(3)	57(3)	22(2)	-2(2)	11(2)
O(1)	65(2)	40(2)	41(2)	12(2)	14(2)	-2(2)
O(24)	100(4)	95(5)	62(3)	5(3)	36(3)	23(3)
O(25)	59(3)	53(3)	163(6)	49(4)	6(2)	32(3)
O(27)	121(4)	39(3)	96(4)	40(3)	28(3)	-1(2)
Re(1)	50(1)	27(1)	40(1)	18(1)	6(1)	4(1)

Table B.16: Hydrogen coordinates (x10^4) and isotropic displacement parameters (Å^2 x 10^3) for *fac*-[Re(CO)$_3$(Imid)(5Me-Sal-Cyhex)].

Atom	x	y	z	U(eq)
H(02)	5335	-3737	6817	62
H(03)	6003	-3700	8187	67
H(05)	4693	322	8564	61
H(07A)	5732	-2637	9690	132
H(07B)	5683	-676	9676	132
H(07C)	6456	-1585	9456	132
H(08)	4352	-2801	5688	47
H(11)	2720	-1084	4438	47
H(12A)	3761	658	4144	53
H(12B)	4384	-863	4218	53
H(13D)	2874	-526	2983	74
H(13E)	3779	-427	2812	74
H(14C)	3993	-3243	3103	81
H(14D)	3166	-3027	2409	81
H(15A)	2948	-4922	3443	74
H(15B)	2345	-3372	3390	74
H(16A)	2982	-3891	4799	58
H(16B)	3878	-3748	4604	58
H(018)	1085	1396	5951	92
H(019)	2721	-2133	6746	59
H(020)	405	-700	6647	93
H(020)	-2320(110)	-2300(200)	7540(110)	260(70)

Table B.17: Torsion angles (^{o}) for *fac*-[Re(CO)$_3$(Imid)(5Me-Sal-Cyhex)].

Bond	Angles
C(06)-C(01)-C(02)-C(03)	0.9(9)
C(08)-C(01)-C(02)-C(03)	-177.9(5)
C(01)-C(02)-C(03)-C(04)	0.2(10)
C(02)-C(03)-C(04)-C(05)	-0.8(10)
C(02)-C(03)-C(04)-C(07)	-178.7(7)
C(03)-C(04)-C(05)-C(06)	0.3(10)
C(07)-C(04)-C(05)-C(06)	178.3(7)
C(02)-C(01)-C(06)-O(1)	-179.8(5)
C(08)-C(01)-C(06)-O(1)	-1.1(8)
C(02)-C(01)-C(06)-C(05)	-1.3(8)
C(08)-C(01)-C(06)-C(05)	177.3(5)

C(04)-C(05)-C(06)-O(1)	179.3(6)
C(04)-C(05)-C(06)-C(01)	0.8(9)
C(06)-C(01)-C(08)-N(1)	2.5(9)
C(02)-C(01)-C(08)-N(1)	-178.8(5)
N(1)-C(11)-C(12)-C(13)	-175.8(5)
C(16)-C(11)-C(12)-C(13)	55.8(6)
C(11)-C(12)-C(13)-C(14)	-55.5(7)
C(12)-C(13)-C(14)-C(15)	56.3(8)
C(13)-C(14)-C(15)-C(16)	-56.5(8)
N(1)-C(11)-C(16)-C(15)	176.1(5)
C(12)-C(11)-C(16)-C(15)	-58.0(7)
C(14)-C(15)-C(16)-C(11)	57.9(8)
N(2)-C(018)-C(020)-N(3)	-2.3(10)
C(01)-C(08)-N(1)-C(11)	-179.7(5)
C(01)-C(08)-N(1)-Re(1)	6.0(8)
C(16)-C(11)-N(1)-C(08)	31.6(7)
C(12)-C(11)-N(1)-C(08)	-94.3(5)
C(16)-C(11)-N(1)-Re(1)	-153.6(4)
C(12)-C(11)-N(1)-Re(1)	80.5(4)
N(3)-C(019)-N(2)-C(018)	0.3(7)
N(3)-C(019)-N(2)-Re(1)	173.1(4)
C(020)-C(018)-N(2)-C(019)	1.2(9)
C(020)-C(018)-N(2)-Re(1)	-171.5(5)
N(2)-C(019)-N(3)-C(020)	-1.8(8)
C(018)-C(020)-N(3)-C(019)	2.4(9)
C(01)-C(06)-O(1)-Re(1)	-9.4(8)
C(05)-C(06)-O(1)-Re(1)	172.2(4)

APPENDIX C

The formation reaction between ethylenediamine and ReAA was performed at four different temperatures (14.8^{o}C, 25.2^{o}C, 35.0^{o}C and 45.0^{o}C) by the UV/Vis spectroscopy, supplementary data of the formation kinetics of ethylenediamine and ReAA in table C.1 and C.2.

Table C.1: Graph of k_{obs} *vs.* [en] for the formation reaction between ethylenediamine and ReAA at four temperatures in methanol, [Re complex] = 1 x 10^{-4} M, [en] = 0.03-0.15 M and λ = 280 nm.

	k_{obs}			
[en] (M)	**14.8^{o}C**	**25.2^{o}C**	**35.0^{o}C**	**45.0^{o}C**
0.03	0.000308±0.002	0.000547±0.003	0.000708±0.006	0.001199±0.01
0.05	0.000443±0.002	0.000766±0.005	0.000996±0.007	0.0014840.01
0.07	0.000587±0.002	0.000957±0.006	0.001314±0.07	0.001933±0.01
0.1	0.000851±0.006	0.001147±0.03	0.001744±0.01	0.002581±0.02
0.15	0.001115±0.02	0.001547±0.03	0.002504±0.09	0.003785±0.07

Table C.2: The Eyring graph of the rate constant for the formation reaction between ethylenediamine and ReAA.

$\frac{1}{T}$ (x10^{-3} K^{-1})	ln ($\frac{k_1}{T}$)
3.473	-10.643
3.382	-10.304
3.239	-9.934
3.143	-9.584

The formation reaction between ethylenediamine and ReAA was performed at 25^{o}C by the ^{1}H NMR kinetic investigation, supplementary NMR fits of peak integral vs time data of the formation kinetics of ethylenediamine and ReAA in table C.3.

Table C.3: A plot of Integral vs time of peak 1-4 (coordinated ethylenediamine) from the ^{1}H NMR analysis with [en] = 0.002 M and [ReAA] = 0.001 M in dry CD_3OD at 25^{o}C.

Peak integral				
Time (s)	**Peak 1**	**Peak 2**	**Peak 3**	**Peak 4**
0	3.32	0	0	0

300	3.36	0	0	0
600	3.31	0	0	0
900	3.27	0	0	0
1200	3.23	0	0	0
1500	3.14	0	0	0
1800	3.18	0	0	0
2100	3.16	0	0	0
2400	3.07	0.18	0	0.13
2700	3.04	0.16	0	0.12
3000	2.98	0.17	0	0.13
3300	2.87	0.16	0	0.17
5100	2.8	0.27	0	0.23
6900	2.66	0.22	0	0.26
8700	2.59	0.26	0	0.26
10500	2.49	0.39	0	0.35
12300	2.38	0.37	0	0.41
14100	2.16	0.4	0	0.41
15900	1.97	0.51	0	0.71
17700	1.86	0.52	0.11	0.87
19500	1.71	0.54	0.41	0.47
23100	1.55	0.55	0.42	0.51
26700	1.37	0.62	0.54	0.61
30300	1.15	0.67	0.61	0.61
33900	0.91	0.64	0.66	0.56
37500	0.78	0.7	0.67	0.68
41100	0.71	0.75	0.73	0.82
44700	0.52	0.78	0.82	0.81